Spring 5-31-1997

Multi-wavelength infrared imaging computer systems and applications

Jun Li
New Jersey Institute of Technology

ABSTRACT

MULTI-WAVELENGTH INFRARED IMAGING COMPUTER SYSTEMS AND APPLICATIONS

by
Jun Li

This dissertation presents the development of three computer systems for multi-wavelength thermal imaging.

Two computer systems were developed for the multi-wavelength imaging pyrometers (M-WIPs) that yield non-contact temperature measurements by remotely sensing the surface of objects with unknown wavelength-dependent emissivity. These M-WIP computer systems represent the state-of-art development in remote temperature measurement system based on the multi-wavelength approach. The dissertation research includes M-WIP computer system integration, software development, performance evaluation, and also applications in monitoring and control of temperature distribution of silicon wafers in a rapid thermal process system.

The two M-WIPs are capable of data acquisition, signal processing, system calibration, radiometric measurement, parallel processing and process control. Temperature measurement experiments demonstrated the accuracy of $\pm 1^\circ C$ against blackbody and $\pm 4^\circ C$ for colorbody objects. Various algorithms were developed and implemented, including real-time two-point non-uniformity correction, thermal image pseudocoloring, PC to SUN workstation data transfer, automatic IR camera integration time control, and radiometric measurement parallel processing.

A third computer system was developed for the demonstration of a 3-color InGaAs FPA which can provide images with information in three different IR wavelength range simultaneously. Numbers of functions were developed to demonstrate and characterize 3-color FPAs, and the system was delivered to be used by the 3-color FPA manufacturer.

MULTI-WAVELENGTH INFRARED IMAGING COMPUTER SYSTEMS AND APPLICATIONS

by
Jun Li

A Dissertation
Submitted to Faculty of
New Jersey Institute of Technology
in Partial Fulfillment of the Requirements for the Degree of
Doctor of Philosophy

Department of Computer and Information Science

May 1997

APPROVAL PAGE

MULTI-WAVELENGTH INFRARED IMAGING COMPUTER SYSTEMS AND APPLICATIONS

Jun Li

Dr. Edwin Hou, Dissertation Advisor   Date
Associate Professor of Computer and Information Science
Associate Professor of Electrical and Computer Engineering, NJIT

Dr. Peter A. Ng, Committee Member   Date
Chairman and Professor of Computer and Information Science, NJIT

Dr. Yun-Qing Shi, Committee Member   Date
Associate Professor of Electrical and Computer Engineering, NJIT

Dr. Douglas Hung, Committee Member   Date
Associate Professor of Computer and Information Science, NJIT

Dr. Timothy Chang, Committee Member   Date
Associate Professor of Electrical and Computer Engineering, NJIT

BIOGRAPHICAL SKETCH

Author: Jun Li

Degree: Doctor of Philosophy

Date: May 1997

Undergraduate and Graduate Education:

- Doctor of Philosophy in Computer and Information Science,
  New Jersey Institute of Technology,
  Newark, New Jersey, 1997

- Master of Engineering in Pattern Recognition and Intelligence Control,
  Tsinghua University,
  Beijing, China, 1988

- Bachelor of Engineering in Industrial Instrumentation and Automation,
  Tsinghua University,
  Beijing, China, 1985

Major: Computer Science

Presentations and Publications:

J. Li, T. Fukaya, W.F. Kosonocky, G.H. Olsen, M.J. Cohen, and M.J. Lange, "Development of 3-Color InGaAs FPA Demonstration System," accepted to the 5th Annual Conference of the Society for Imaging Science and Technology, 18-23 May, 1997, Cambridge, MA.

J. Li, and E. Hou, "Parallel Processing for Multi-Wavelength Imaging Pyrometer," accepted to the 1997 SPIE AeroSense Symposium, 20-25 April, 1997, Orlando, FL.

J. Li, E. Hou, and W.F. Kosonocky, "Signal Processing Computer System for Multi-Wavelength Imaging Pyrometer," *Proceedings of IEEE International Conference on Systems, Man and Cybernetics*, Vol. 1, 456-460, 1996.

M.B. Kaplinsky, J. Li, N.J. McCaffrey, E.S.H. Hou, and W.F. Kosonocky, "Experimental Multi-Wavelength Pyrometer for Remote Sensing of Temperature Profiles on Surfaces with Unknown Emissivity," *International Archives of Photogrammetry and Remote Sensing*, Vol. XXXI, Part B1, 78-83, 1996.

M.B. Kaplinsky, J. Li, N.J. McCaffrey, E.S.H. Hou, and W.F. Kosonocky, "Progress on the Development of Multi-Wavelength Imaging Pyrometer," *SPIE Proceedings*, Vol. 2746, 178-189, 1996.

J. Li, E.S. Hou, M.B. Kaplinsky, N.J. McCaffrey, and W.F. Kosonocky, "M-WIP Workstation for RTP Monitoring and Control," *Transient Thermal Processing Techniques in Electronic Materials*, N. M. Ravindra, and R. K. Singh, eds., 147-150, TMS, 1996.

M.B. Kaplinsky, J. Li, N.J. McCaffrey, W.F. Kosonocky, E.S. Hou, and N.M. Ravindra, "Multi-Wavelength Imaging Pyrometer for Non-Contact Temperature Measurement," *Transient Thermal Processing Techniques in Electronic Materials*, N.M. Ravindra, and R.K. Singh, eds., 125-132. TMS, 1996.

J. Li, and E. Hou, "Pseudocoloring Schemes for Thermal Imaging," *SPIE Proceedings*, Vol. 2656, 77-83, 1995.

E.S.H. Hou, J. Li, and W.F. Kosonocky, "Real-Time Implementation of Two Point Non-Uniformity Correction for IR-CCD Camera," *SPIE Proceedings*, Vol. 2598, 44-50, 1995.

M. Kaplinsky, W.F. Kosonocky, N.J. McCaffrey, J. Li, E.S. Hou, C.N. Manikopoulos, and N.M. Ravindra, "Multi-Wavelength Imaging Pyrometer for Non-Contact Temperature Sensing," *Proceedings of the IEEE International Symposium on Industrial Electronics*, 199-204, 1995.

W.F. Kosonocky, M. Kaplinsky, N.J. McCaffrey, E.S. Hou, C.N. Manikopoulos, N.M. Ravindra, S. Belikov, J. Li, and P. Vapel, "Multi-Wavelength Imaging Pyrometer," *SPIE Proceedings*, Vol. 2225, 26-43, 1994.

This work is dedicated to
my family

ACKNOWLEDGMENT

TABLE OF CONTENTS

LIST OF TABLES

LIST OF FIGURES

CHAPTER 1

INTRODUCTION

The infrared imaging commercial market has grown significantly with the advances in the development of lower-cost infrared focal-plane-array (FPA) cameras and other thermal imaging instruments [1]. Thermal imaging offers advantages, such as non-contact temperature measurement by remote sensing and two-dimensional temperature measurement with high spatial resolution, that makes imaging pyrometers unique temperature measurement instruments which can be used in numerous industrial applications.

The major contribution of this dissertation is the development of computer systems for the multi-wavelength imaging pyrometers (M-WIPs). M-WIPs can overcome the spatial resolution limitation of conventional pyrometers and provide surface temperature profiles of distant objects under study. Using infrared (IR) imagers and radiometric models, M-WIPs yield non-contact thermographic measurements by remotely sensing the surface of objects with unknown wavelength-dependent emissivity.

Two M-WIP computer systems were investigated to perform data acquisition, signal processing, and to provide functions for data analysis, system calibration, temperature measurement, and process control. One of the computer system is named as SUN M-WIP which is developed based on a SUN workstation system and the other is a PC based computer system referred as PC M-WIP.

The dissertation research includes integration of the M-WIP computer systems, development of the M-WIP software, the evaluation of the M-WIP performance, and also applications of M-WIP for monitoring and control of temperature distribution of silicon wafers in a rapid thermal process (RTP) system.

1

In addition, a third computer system is also developed for the demonstration of a 3-Color InGaAs FPA which can provide images with information in three different IR wavelength range simultaneously.

The dissertation is organized into eight chapters.

Chapter 1 provides the background and objectives of the dissertation research. The designed feathers of the target M-WIP systems are described in detail. Hardware and software requirements are also introduced in this chapter.

Chapter 2 describes the electronic imaging subsystem developed for the SUN M-WIP. In addition, novel non-uniformity correction and pseudocoloring algorithms are also discussed.

Chapter 3 describes the radiometric calibration subsystem and the parallel processing subsystem for M-WIP computation. The feedback control subsystem for controlling a rapid thermal process system is also discussed.

Chapter 4 describes the software development for the SUN M-WIP, including user interface, data acquisition, parallel processing, and M-WIP computations. Experimental results that demonstrate the SUN M-WIP performance are also presented.

Chapter 5 describes the hardware aspects of the PC M-WIP. This includes the frame grabber, data acquisition, parallel processing, and filter-wheel.

Chapter 6 describes the software development for the PC M-WIP. This includes user interface, filter-wheel control, parallel processing, and M-WIP computations. Experimental results that demonstrate the PC M-WIP performance are also presented.

Chapter 7 describes the development of a PC based system for the demonstration of the 3-Color InGaAs FPA.

Finally the conclusions of this research are presented in Chapter 8.

In this chapter, basic concepts of thermal imaging and M-WIP non-contact temperature measurement are reviewed as the background of the dissertation research. System configurations of the M-WIP computer systems are also introduced.

1.1 Thermal Radiation Principles

All objects at temperatures above absolute zero emit electromagnetic radiation as a function of temperature in accordance with the Planck Equation, first formulated by the great physicist Max Planck about 100 years ago [2]. Planck's Law (Eq 1.1) establishes the dependency of *blackbody* thermal radiance energy on wavelength and temperature.

$$L(\lambda, T) = \frac{C_1}{\lambda^5 \pi [exp(\frac{C_2}{\lambda T}) - 1]} \qquad (1.1)$$

where

L: blackbody radiance ($Wcm^{-2}sr^{-1}\mu m^{-1}$);

λ: wavelength of narrow band channel (μm);

T: temperature of blackbody (K);

$C_1 = 3.74151 \times 10^4$ ($Wcm^{-2}sr^{-1}\mu m^4$);

$C_2 = 1.43879 \times 10^4$ ($\mu m K$).

Figure 1.1 shows the Planck's curves [2].

Wien's Approximation (Eq 1.2) makes it possible to linearize the approximation with logarithms.

$$L(\lambda, T) = \frac{C_1}{\lambda^5 \pi exp(\frac{C_2}{\lambda T})} \qquad (1.2)$$

Whenever $\lambda T < 3125$ $\mu m K$, this approximation gives a deviation of less than 1% from the Planck's Law.

The physical quantity measured remotely by an infrared camera is the directional spectral radiance reaching the sensor. Based upon the relationship given above, the temperature of an object may be determined by measuring the radiation it emitted. However, most surface materials do not emit radiance like a blackbody,
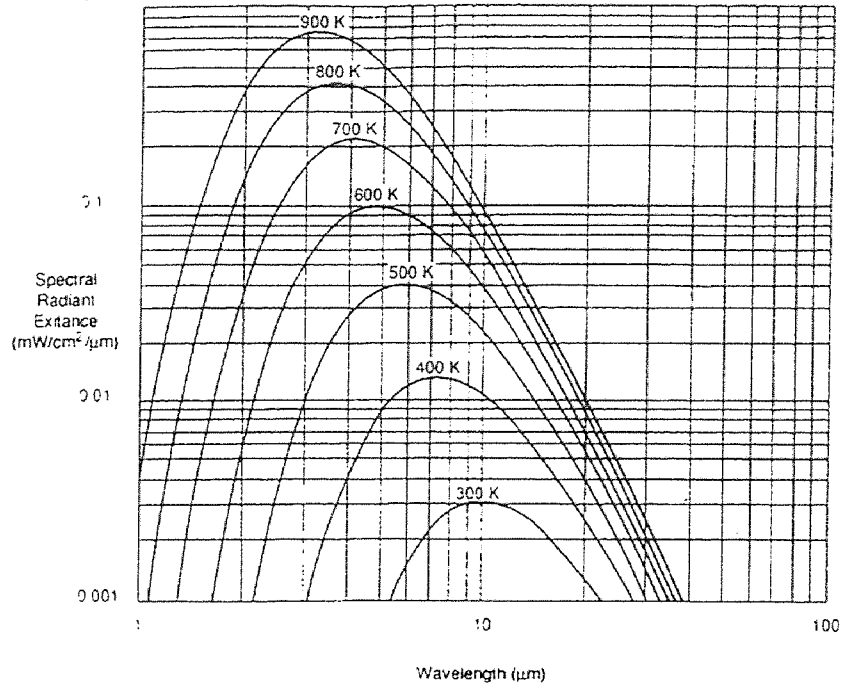
Figure 1.1 Planck's Curves

which is a perfect emitter. The *spectral emissivity* ε, $0 < \varepsilon \leq 1$, is a measure of a material's ability to emit radiation compared to a blackbody where both are at the same temperature.

$$\tilde{L}(\lambda, T) = \varepsilon(\lambda, T) L(\lambda, T) \tag{1.3}$$

where

$\tilde{L}$: body radiance ($W\,cm^{-2}sr^{-1}\mu m^{-1}$);

ε: spectral emissivity.

The emissivity of an actual object is a function of wavelength, temperature, and surface condition. In most of the cases, the surface condition can be considered to be time invariant (assuming no oxidation or other coatings), thus the spectral emissivity at certain temperature can be modeled by polynomials or exponentials of wavelength.

For example,

$$\varepsilon(\lambda) \;\; = \;\; \varepsilon_{01} + \varepsilon_{11}\lambda + \varepsilon_{21}\lambda^2 \tag{1.4}$$

$$\varepsilon(\lambda) = \varepsilon_{02} + \varepsilon_{12}\lambda^{-1} + \varepsilon_{22}\lambda^{-2} \tag{1.5}$$

$$\varepsilon(\lambda) = exp(\varepsilon_{03} + \varepsilon_{13}\lambda) \tag{1.6}$$

Effects other than emissivity can be removed by using radiative transfer models of the optical and electronic path.

1.2 Conventional Imaging Pyrometer

In industrial applications and scientific research, it is often necessary to measure the temperature of an object from a distance, without making contact. For example, a moving object on an assembly line, or a very hot object in a furnace, or an inaccessible object in a high-vacuum chamber. The method used for making these non-contacting temperature measurements is known as *radiation pyrometry*.

The feasibility of using infrared imaging technologies in remote target non-contact surface temperature measurement has been investigated for a long time [3]. Using thermal imagery, measurement and control of temperature can be achieved for material manufacturing and processing applications where physical contact is not desirable or impractical.

Several detection mechanisms can be used in infrared imaging and they fall into three broad classes: photon, thermal and wave interaction [4]. The first two mechanisms will be examined by using example detector arrays introduced in the later chapters.

Narrow band optical filters are often used in the IR imaging system to obtain signal at certain wavelength. The passbands of the filters can be located in long-wave infrared (LWIR, 8-12 μm), mid-wave infrared (MWIR, 3-5 μm), short-wave infrared (SWIR, 1-3 μm), and near infrared (NIR, 0.7-1 μm).

- In the case of blackbody target with known unit emissivity, given the wavelength (by using a narrow passband optical filter) and incident radiance

(by calibration), temperature can be easily calculated by solving the following equation derived from the Planck's Law.

$$T = \frac{C_2}{\lambda ln(\frac{C_1}{\lambda^5 \pi L(\lambda,T)} + 1)} \tag{1.7}$$

- The existence of non-unity emissivity raises the difficulty in the measurement of graybody and colorbody. *Graybody* has constant emissivity for all the wavelengths, while *colorbody* has emissivity that varies with wavelength changes. To measure the temperature of graybody or colorbody, multi-wavelength (multispectral) imaging technologies have to be employed, where more than one narrow bandpass filters are used to obtain radiance responses of the sensor for each narrow band channel.

According to the Planck's Law, the radiance corresponding to the target in each of the N wavelengths is a function of the unknown emissivity of the target at that wavelength and the unknown surface temperature of the target. This results in a set of N equations with $N + 1$ unknowns, including N emissivities and 1 temperature. Theoretically, there exists an infinite combination of values of emissivity and temperature that can be used to solve this set of under-determined equations. However, whenever the value of one of these $N + 1$ variables is known, all the other N values can be obtained by simple computation.

In the case of graybody, applying logarithm to the radiance ratio of two different wavelength channels (corresponding to two narrow bandpass optical filters with their center wavelength away from each other), temperature can be calculated by solving the following equation derived from Equation 1.7.

$$T = \frac{C_2(\lambda_2 - \lambda_1)}{\lambda_1 \lambda_2 [5 ln(\frac{\lambda_2}{\lambda_1}) - ln(\frac{L(\lambda_1,T)}{L(\lambda_2,T)})]} \tag{1.8}$$

This method is called *ratio method.*

• The ratio method has been extended to measure temperature of colorbodies. There were several multi-wavelength ratio methods proposed other than the two channel technique described above. For example, the three channel method and the four channel method make the following assumptions.

$$\varepsilon(\lambda_1)\varepsilon(\lambda_3) = [\varepsilon(\lambda_2)]^2 \tag{1.9}$$

$$\varepsilon(\lambda_1)[\varepsilon(\lambda_3)]^2 = [\varepsilon(\lambda_2)]^2\varepsilon(\lambda_4) \tag{1.10}$$

Although ratio methods have been used in many applications, including medical imaging [5] and environment sensing [6], it has been demonstrated that these techniques cannot adequately provide accurate temperature estimates [7].

• An algorithm was developed to refine the upper and lower bounds of surface temperature using realistic bounds of emissivities [8]. The bounds on the temperature are then used to estimate a tighter bound on the emissivity.

The algorithm is based on a bandpass radiance model given by Equation 1.11. The model gives a 1.5×10^{-7} $Wcm^{-2}sr^{-1}\mu m^{-1}$ deviation away from actual radiance. This regressed radiance error corresponds to 0.03 K between estimated and actual temperature.

$$L_\lambda(T) = a_\lambda + b_\lambda T + c_\lambda T^2 \tag{1.11}$$

where

L_λ: blackbody radiance at wavelength λ;

$a_\lambda, b_\lambda, c_\lambda$: constant coefficients at wavelength λ.

The algorithm was applied to identify water temperatures for the detection of underwater thermal, saline, and fresh water thermal springs. Although it cannot be used directly to measure temperature, the algorithm can provide

reasonable bounds on temperature and emissivity that can be used to reduce the computational load of other measurement algorithms.

Broadband signal is also used in many applications providing the target surface emissivity will not change from time to time during the calibration and measurement. In this case, a lookup table and a interpolation procedure will be sufficient to resolve the temperature.

1.3 Multi-Wavelength Imaging Pyrometer

It has been proved by experiments that the *least-squares based method* is the most accurate multi-wavelength technique [9].

Using adapted commercial instrument, measurement using least-squares implementation gave 0.5% absolute temperature accuracy on a number of radiating sources in the temperature range of 900 to 2300°C. However, the experimental results had been unsatisfactory with some materials. It was assumed that the unsatisfactory results were due to incorrect form (or lack of function) for emissivity model and correlation effects (inability of curve-fitting routines to distinguish changes in emissivity and temperature in certain circumstances) [10].

- If the emissivity is a linear exponential function of the wavelength, linear least-squares method can be used.

  Assuming perfect measurements, the following equation can be derived from Wien's Approximation,

$$\tilde{L}_i = \varepsilon(\lambda_i) \frac{C_1}{\lambda_i^5 \pi \, exp(\frac{C_2}{\lambda_i T})} \qquad (1.12)$$

where

$\tilde{L}_i$: measured radiance energy;

λ_i: the ith wavelength.

Taking the natural logs, then

$$ln(C_1^{-1}F_i\lambda_i^5\pi) = ln(\varepsilon(\lambda_i)) - C_2\lambda_i^{-1}T^{-1} \qquad (1.13)$$

All the quantities on the left side of the equation are known and the unknowns are $\varepsilon(\lambda_i)$ and the temperature T.

Let $\alpha_{m-1} = -C_2T^{-1}$, $N_i = ln(C_1^{-1}\tilde{L}_i\lambda_i^5\pi)$ and model the emissivity by

$$\varepsilon(\lambda_i) = exp(\sum_{j=0}^{m-2}\alpha_j\lambda_i^j) \qquad (1.14)$$

A set of linear equations can be obtained in the form of $AX = B$, where

$$B = [N_1\,N_2\,\cdots\,N_n]^T \qquad (1.15)$$

$$X = [\alpha_0\,\alpha_1\,\cdots\,\alpha_{m-1}]^T \qquad (1.16)$$

and

$$A = \begin{bmatrix} 1 & \lambda_1 & \lambda_1^2 & \cdot & \cdot & \cdot & \lambda_1^{m-2} & \lambda_1^{-1} \\ 1 & \lambda_2 & \lambda_2^2 & \cdot & \cdot & \cdot & \lambda_2^{m-2} & \lambda_2^{-1} \\ \cdot & \cdot & \cdot & & & & \cdot & \cdot \\ \cdot & \cdot & \cdot & & & & \cdot & \cdot \\ \cdot & \cdot & \cdot & & & & \cdot & \cdot \\ 1 & \lambda_n & \lambda_n^2 & \cdot & \cdot & \cdot & \lambda_n^{m-2} & \lambda_n^{-1} \end{bmatrix} \qquad (1.17)$$

where

n: number of passband wavelength;

m: $n-1$.

Then X can be solved by using the least-squares method to minimize the error E [11].

$$E^2 = ||AX - B||^2 \qquad (1.18)$$

When X becomes known, emissivity and temperature values can be easily calculated.

- If the emissivity is not a linear exponential function of the wavelength, non-linear least-squares method can be used.

In this case, the cost function is given by

$$\chi^2(\alpha_j) = \sum_{i=1}^{n} \{ \frac{1}{\sigma_i^2} [S_i(\alpha_j, \lambda_i) - \dot{S}_i]^2 \}, (j = 0, 1, ..., m - 1) \qquad (1.19)$$

where

S_i: theoretical signal at λ_i;

$\dot{S}_i$: detected signal at λ_i;

σ_i: rms (root-mean-square) noise of detected signal at λ_i;

α_j: unknowns including temperature and emissivity coefficients.

The objective is to solve for α_j at the minimum of χ^2. Since N_i is nonlinear in α_j, linear techniques such as Gaussian elimination cannot be used to solve the equations. However, some iterative solution techniques can be used to solve them. [12].

- The Legendre polynomials and the Chebyshev polynomials can be used in least-squares based method [13]. For example, given

$$\varepsilon(\lambda) = \sum_{j=0}^{N-1} \alpha_j P_j(\lambda) \qquad (1.20)$$

then the first few Legendre polynomials are

$$P_0 = 1 \qquad (1.21)$$

$$P_1 = \lambda \qquad (1.22)$$

$$P_2 = 0.5(3\lambda^2 - 1) \qquad (1.23)$$

$$P_3 = 0.5(5\lambda^3 - 3\lambda) \qquad (1.24)$$

and the first few Chebyshev polynomials are

$$P_0 = 1 \qquad (1.25)$$

$$P_1 = \lambda \qquad (1.26)$$

$$P_2 = 2\lambda^2 - 1 \tag{1.27}$$

$$P_3 = 4\lambda^3 - 3\lambda \tag{1.28}$$

These orthogonal sets of basic functions are especially useful for high order emissivity expansions since any least-squares estimation techniques eventually reduces to the problem of inverting a large matrix to obtain the values of the parameters that minimize the cost function. Using orthogonal polynomials tends to reduce the numerical value of the off-diagonal elements in the matrix that needs to be inverted, thus avoiding the ill-conditioned problem that often plague high order expansions.

1.4   SUN M-WIP System Configuration

Using the least-squares technique, NJIT's M-WIPs are designed to demonstrate temperature measurement by remotely sensing the surface of objects with unknown wavelength-dependent emissivity.

The first experimental M-WIP system, the SUN M-WIP is developed as a general purpose imaging pyrometry computer system. In the SUN M-WIP system, an IR-CCD camera is employed as a radiometer to detect the radiation emitted from the surface of the measured object [14]. It works in the IR wavelength range from 1.5 μm to 5.5 μm.

1.4.1   Schottky Barrier Imager

In the evolution of modern thermal imaging systems, photon detection played a major role. It is still the leading technique in infrared detection mechanisms. Many photon detectors were developed for infrared detection, such as (Hg,Cd)Te, InSb, PbSe, AlGaAs/GaAs and PtSi. These photon detectors offer both broad spectral bandwidth and fast response but cryogenic operation is required. The imager used

(a) SBD Operation   (b) SBD Structure
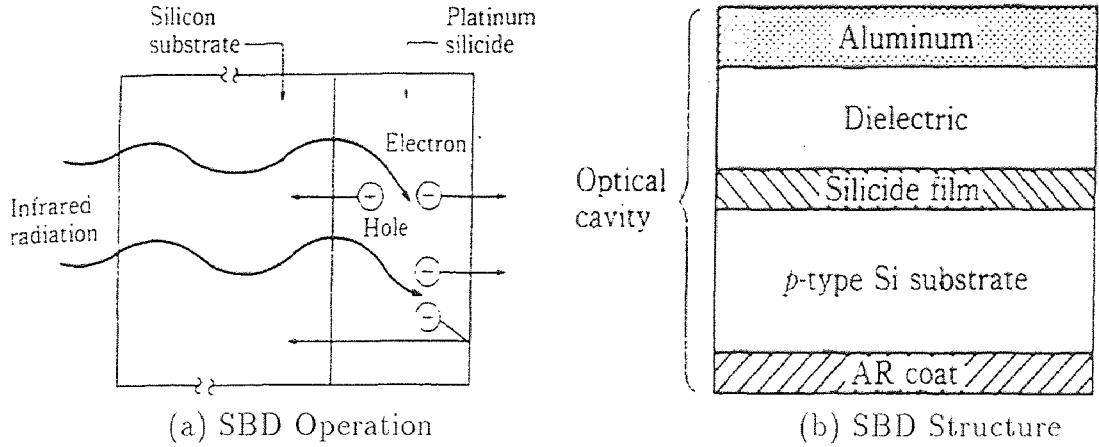
Figure 1.2 Schottcky Barrier Detector

in the SUN M-WIP is a Schottky barrier detector (SBD) FPA produced by David Sarnoff Research Center [15].

When an intimate contact of a metal and a semiconductor is formed, the separation of charges at the interface generates an internal energy barrier (*Schottky barrier*) devoid of mobile carriers in the semiconductor. Nearly all silicide exhibit metallic conductivity so that silicide-silicon conjunction behaves like a metal-semiconductor contact. Usually, silicide-silicon contact gives lower barrier (0.12 to 0.48 eV reported [16]) comparing to the barrier of metal-semiconductor contact (0.7 to 0.9 eV [17]).

The mechanism of a SBD can be described by an example. In the case of a *PtSi* and *p*-type *Si* detector, when incident infrared radiation is absorbed in the silicide of the diode, and holes are excited from states near the Fermi energy. The "hot" holes which have sufficient momentum can pass across the internal energy barrier into the semiconductor of the diode where they collapse the depletion region, and signal is detected as electrons left behind contributes to a net negative charge in the silicide. Figure 1.2 (a) sketches the SBD operation [16].

For the optimized SBD structure, the IR radiation is introduced from the bottom side of the "optical cavity" as shown in Figure 1.2 (b). The Anti-Reflective

(AR) coat, deposited on the back side of the silicon substrate, increases the coupling of IR radiation into the SBD by about 30%. The SiO or SiO_2 dielectric layer separates an aluminium reflector and the silicide layer by about quarter-wave to maximize the optical absorption by setting up a peak of an optical standing wave at the thin silicide film. In this back-illuminated case, the photon energy of the incident infrared radiation must be less than the bandgap of silicon to allow itself to be transmitted through the silicon substrate and greater than the Schottky barrier formed between p-type silicon and silicide to generate hot holes which have sufficient kinetic energy to surpass the barrier. This can be described by

$$\psi < h\upsilon < Eg \qquad (1.29)$$

where

ψ: the height of Schottky-barrier;

$h\upsilon$: photon energy;

Eg: silicon bandgap energy (1.1 eV).

IR signal detected can be readout by two different structures. In the *monolithic structure*, the charge transfer readout channel and the actual IR sensitive detector are formed within the same substrate. In the *hybrid structure*, the array of IR sensitive detectors is interfaced with the charge transfer readout channels. Figure 1.3 gives one example for each of the readout structures [16]. The imager in the SUN M-WIP uses monolithic structure with charge couple devices (CCD) readout.

1.4.2   PtSi IR-CCD Camera

The $320X244$ IR-CCD imager used in the SUN M-WIP has a pixel size of $40X40$ μm^2 and its fill factor is 43%. The imager is designed as an interline transfer (IT) CCD with two vertical detectors interlaced to the same vertical channel. The operation of the two interlaced fields represents frame integration which makes the display less

(a) SBD with CCD monolithic readout   (b) SBD with hybrid readout
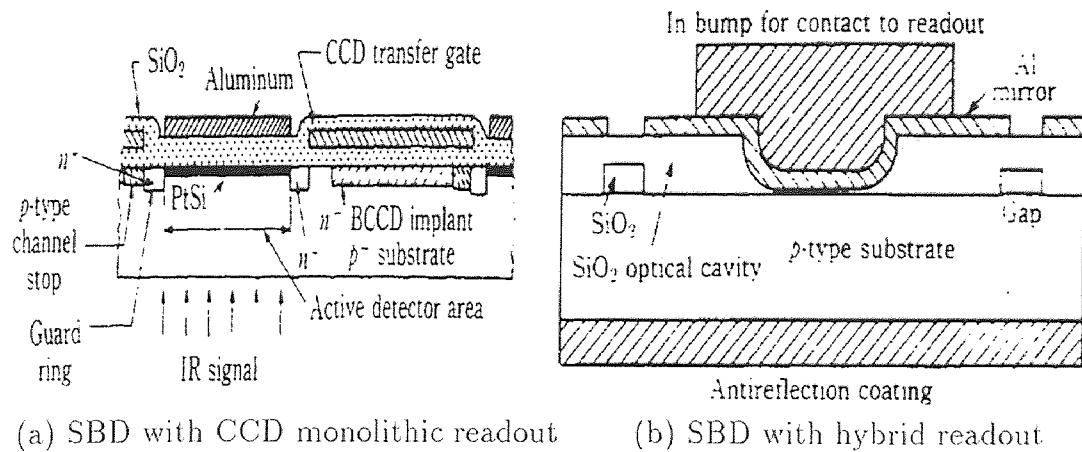
Figure 1.3 SBD Readout Structures

flicker. In the SUN M-WIP, the imager is operated with the frame made up of only one field, and this realize $320X122$ non-interlaced frame transfer (FT).

To facilitate variable integration time control and frame counter, the camera has built-in circuits which embed critical information in the video signal for radiometric processing [18]. Due to the residual charge from inefficient sweep procedure, the first 10 lines of video are ignored and they are used to carry the embedded integration time and frame count information. The information are formatted into two 12-bit pixels. The highest 8 bits of the first and second pixels are filled by the MSB and LSB of the frame count value respectively, while the lowest 4 bits in each of the two pixels are duplicated with the integration time code. The two information carrying pixels are followed by two synchronization pixels: the third pixel has all ones in its 12 bits and the fourth all zeros. All four pixels are repeated 80 times (4 pixels X 80 = 320 pixels = 1 line) to form an information carrying line, and this line is duplicated 3 times. This redundancy is designed to insure that the radiometric information of a frame can be guaranteed in the event of corrupted pixels due to noise.

A line-sensing filter assembly is installed in the SUN M-WIP. Its seven narrow-band filters "spreads" the image of one line on the target surface across a number of
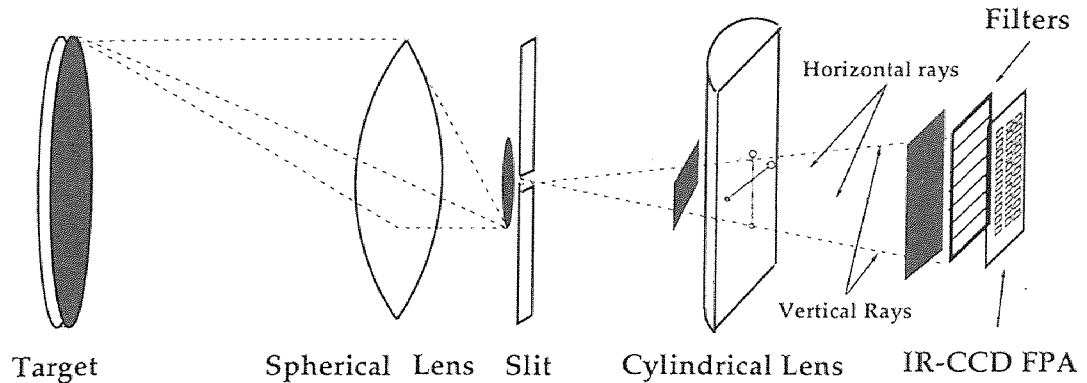
Figure 1.4 SUN M-WIP Filter Optics

horizontal stripes of filters. Figure 1.4 sketches the filter optics of the SUN M-WIP [19].

The 12-bit digital video signal from the IR-CCD camera is fed into the real-time image processing system for data acquisition and pre-processing.

1.4.3 SUN M-WIP System Integration

As shown in Figure 1.5, the SUN M-WIP computer system contains five major components:

1. **Host computer** SUN SPARCstation;

2. **Electronic imaging subsystem** 320X122 PtSi IR-CCD camera with seven narrow band filters; MaxVideo (Datacube, Inc.) system which captures images from the IR camera and performs real-time image processing, such as frame averaging, pseudocoloring display, and non-uniformity correction.

3. **Radiometric calibration subsystem** LabTech (Laboratory Technologies, Co.) system which acquires thermocouple readouts and transfer it to the host computer. Working as a stand-alone system for RTP system testing and modeling, the LabTech PC system performs data acquisition, signal processing, and feedback control. Integrated to the SUN workstation, it acts as a data acquisition subsystem and also a backup control system for the SUN M-WIP.
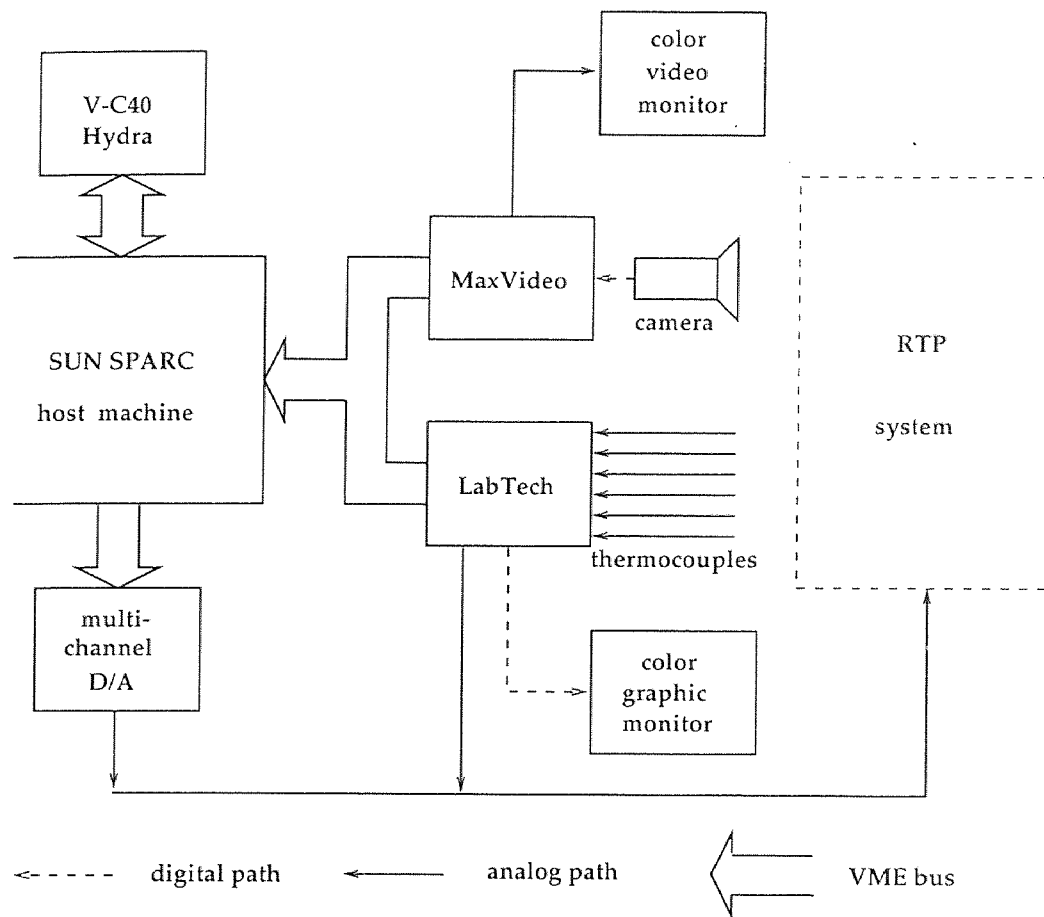
Figure 1.5 SUN M-WIP Configuration

4. **Parallel processing subsystem** V-C40 Hydra (Ariel, Inc.) board with multiple digital signal processing (DSP) chips for parallel processing.

5. **Feedback control subsystem** D/A boards which provide analog control signals to the RTP system.

1.5 PC M-WIP System Configuration

The second experimental M-WIP system, the PC M-WIP is developed as a cost effective M-WIP system. In the PC M-WIP, an uncooled microbolometer IR camera plays the role of a radiometer which detects the radiation emitted from the surface of object being studied.

1.5.1 Uncooled Microbolometer FPA

The earliest thermal imaging systems employed single detector and two-dimensional scanning techniques. Later approaches used linear arrays and one-dimensional scanning mechanisms. Only photon detectors could meet both the sensitivity and response speed requirement in these systems. In recent years, with the advent of two-dimensional arrays, the response speed requirement is reduced and thereby uncooled IR FPAs employing thermal detection mechanisms emerge. These mechanisms depend on the change in the property of a material due to a change in temperature of the material when electromagnetic radiation is absorbed. No cryogenic operation is required.

The three most popular thermal detection mechanisms are resistive bolometers, pyroelectric detectors, and thermoelectric detectors. The microbolometer array described in this chapter is an example of the first technique. The thermoelectric array which will be introduced later in Chapter 5 is an instance of the last approach.

The imager used in the PC M-WIP is designed to be an uncooled FPA (UFPA) developed by Honeywell Technology Center [20] and Rockwell Research Center [21]. It works in the LWIR wavelength range from 8 μm to 12 μm.

The UFPA is a monolithic resistive bolometer array manufactured from standard silicon wafers using a standard silicon process line. It requires no cooling for sensitive operation. In the resistive bolometer, incident IR radiation absorbed by a sensing material causes temperature change in the material and in turn changes the electrical resistance. The changes is then detected by the readout electronics in the same detector structure. The UFPA detectors are formed from semiconductor film with high thermal coefficient of resistance (TCR), providing maximum sensitivity to the thermal variation in the detector.

In the microbolometer array, each pixel consists of a 0.5-μm-thick plate suspended clear of the underlying silicon substrate by two legs. The legs provide high thermal resistance between the suspended plate and its surroundings, allowing the plate to respond to incident IR radiation by being heated or cooled. The thermal isolation is achieved by a microbridge structure formed by silicon etching, and the low thermal conductance between the bolometer and the substrate contributes directly to the high sensitivity in the microbolometer array. Virtually no thermal crosstalk exists between pixels. Figure 1.6 shows one example of the detector and readout structures [22], and this kind of imager has been applied to some applications such as battlefield surveillance [23].

The temperature changes in the suspended plate cause changes in the electrical resistance, which are sensed by readout circuitry that is monolithically integrated into the underlying silicon and connected to the suspended plate by thin-film metallizations on the legs. A monolithic multiplexer on the array periphery allows random access addressing of any pixel in the array.

(a) Conceptual Schematic   (b) Implemented Schematic
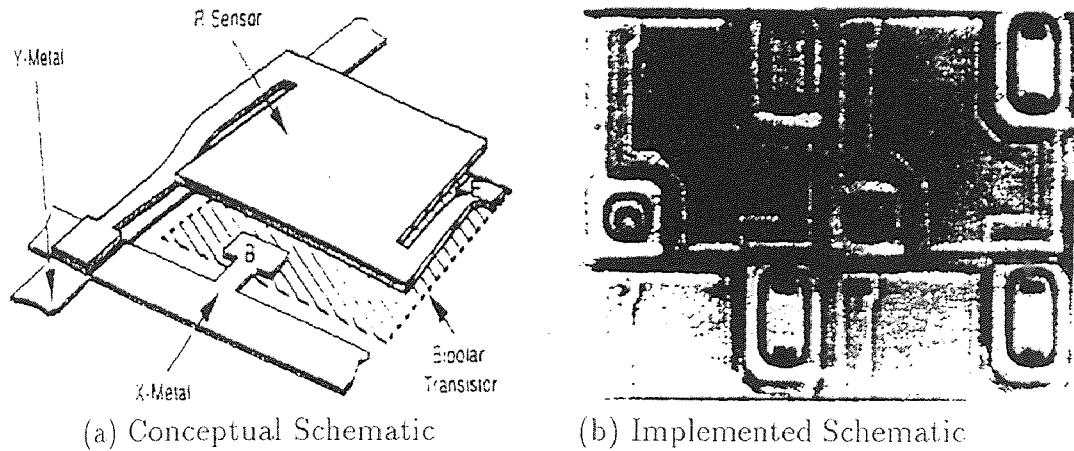
Figure 1.6 Silicon Microbolometer

1.5.2 Microbolometer Infrared Camera

The monolithic UFPA imager of the PC M-WIP has a fill factor of 50% with $50 X 50$ μm^2 pixels. It consists of a $320 X 240$ detector array and the detector selection switch transistors. During operation at a frame rate of at least 60 Hz, array rows are selected sequentially, from top to bottom, to produce a normal raster formatted readout [24]. The integration time is controlled by varying externally the LSync to extend the dynamic range.

The camera digitizes the array output and presents the resultant information to the scan converter to match the array readout frame rate with the standard video output field rate. It also performs video processing, including non-uniformity correction and integration time control. The output of the camera is 12-bit digital video.

In the PC M-WIP, a filter wheel will be used instead of the line-sensing filter assembly. Figure 1.7 sketches the filter optics of the PC M-WIP.

1.5.3 PC M-WIP System Integration

The basic components of the PC M-WIP is a host PC with data acquisition board, frame grabber, and parallel processing board installed. For high speed computation, a Pentium 166 MHz CPU and a PC-Hydra board with 4 TMS320C40 DSPs are used
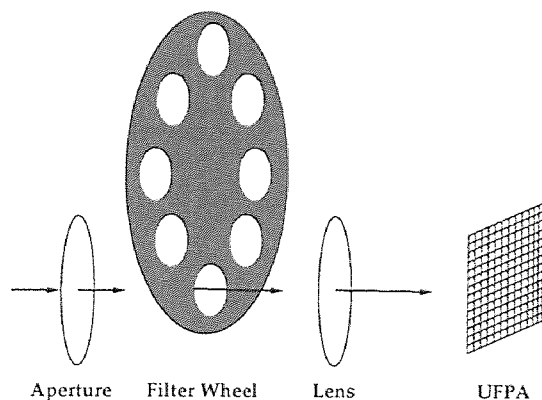
Figure 1.7 PC M-WIP Filter Optics

in the system. Figure 1.8 shows a block diagram of the PC M-WIP computer system without the filter wheel.

The frame grabber used in the PC M-WIP is IC-PCI (Imaging Technology, Inc.), a PCI bus image capture card, together with the AM-DIG, a digital acquisition model. The AM-DIG acquisition module has up to 16-bit differential digital input that can be acquired at up to 20 MHz. IC-PCI features fast image data transfer rates to PC memory (up to 132 MB/sec to the PCI bus and 120 MB/sec to the host memory). Capture and transfer rate much faster than real-time allows the maximum use of the Pentium CPU for host side processing since the CPU is not tied up arbitrating bus operations.

A Multifunction Board PCI-20428W-1 board (Intelligent Instrumentation, Inc.) is installed in an ISA slot of the PC. It provides eight 12-bit differential A/D input at 100 KHz, two 12-bit D/A output, and also 8-bit digital input, 8-bit digital output.

The PC-Hydra (Ariel, Co.) with 4 TMS320C40 DSPs built-in is the PC version of the V-C40 Hydra board used in the SUN M-WIP. It runs at 200 MFLOPS in a single ISA slot.

The filter-wheel's rotation and positioning is controlled by PC's via a serial communication port interfeced to the indexer and the encoder.
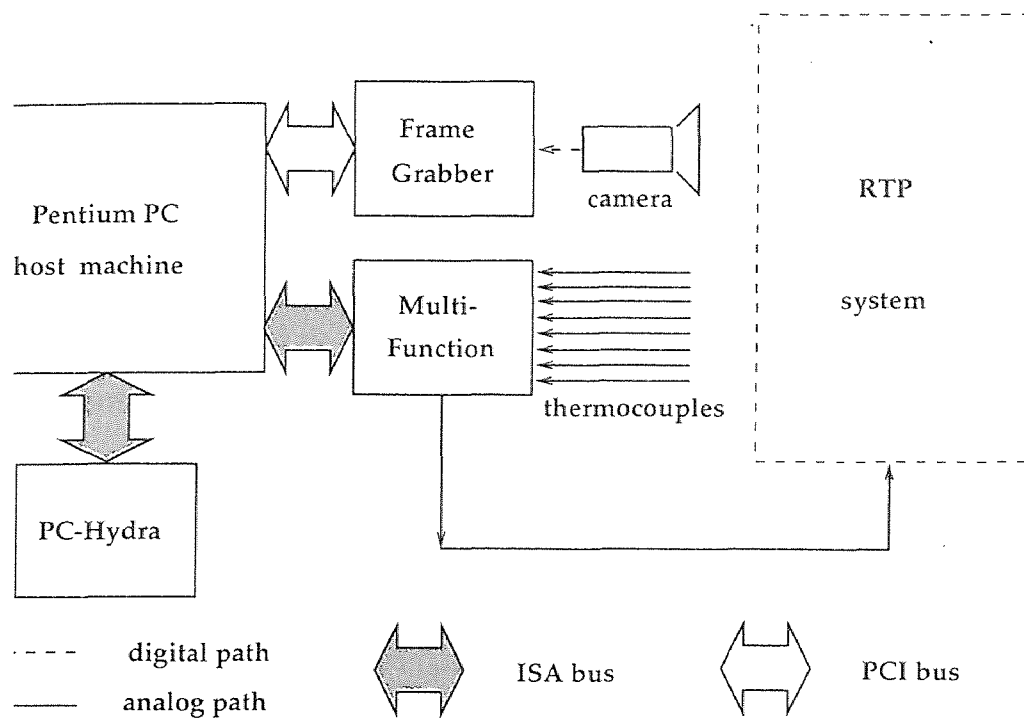
Figure 1.8 PC M-WIP Configuration

CHAPTER 2

SUN M-WIP: ELECTRONIC IMAGING SUBSYSTEM

2.1 MaxVideo System

The MaxVideo system (Datacube, Inc.) is a custom configurable real-time image acquisition and processing system which can operate at a maximum data rate of 10 MHz. It consists of a number of boards that can be interconnected to suit the image processing task at hand. The boards are housed in the MAX-BOX and the development software for the MaxVideo system is Datacube's ImageFlow·which is a set of C-callable libraries.

An interactive user interface was developed for system operation. Developed in C and Xlib, the image processing options of the menu-driven interface can be easily extended by using image processing libraries.

2.1.1 Equipment Descriptions

The MAX-BOX is a 20 slots expansion chassis which holds all the VME bus based boards in the SUN M-WIP system. A high speed VME bus to VME bus transparent repeater system, REPEATER 2000 (HVE Engineering, Inc.), is installed to expand the SUN workstation. The "primary card" is installed at the end of the IACKIN*/IACKOUT* daisy chain in the primary chassis of the SUN workstation, and the chain is intact to the repeater card. The "expansion card" is installed in the slot 1 of the expansion chassis (MAX-BOX) and 19 more slots are available for the VME boards including the following MaxVideo boards.

- The MAX-SCAN is a rate programmable, asynchronous image capturing board which supports standard and non-standard, analog and digital video input. The input bandwidth cannot exceed 20 MHz at 8-bit and 10 MHz at 16-bit.

22

- The ROI-STORE board with 512K bytes of memory can be configured to any size (512K 8-bit, 256K 16-bit, etc.) by the user. It supports region of interest (ROI) processing and can perform multiple ROI transfers.

- The MAX-SP is a general purpose signal processing board which can perform logic and arithmetic operations at 100 ns/pixel. Single point FIR (Finite Impulse Response) or IIR (Infinite Impulse Response) filters, image merging (addition, subtraction, logical operation), and minimum or maximum comparisons can be performed in a single frame time. Multiple point filters can be performed in multiple frame times.

- The MAX-GRAPH is a video and graphics display board with separate red, green, and blue outputs for simultaneous display of 256 colors from a palette of 16.8 million. It also supports light pen and up to 2 serial pointer devices, such as mouse. In the SUN M-WIP system, a color monitor connected to the MAX-GRAPH displays the live video output of the MaxVideo system.

Unlike general purpose processors, MaxVideo devices are pipeline image processors. General purpose processors have a control process which is synchronous with the flow of data. Data is processed one batch at a time and output is available only upon the conclusion of processing of each batch. MaxVideo devices operate on a continuous flow of pixel data. At any given instant, an operand pixel is input to, and a resultant pixel is output from, the processing pipeline. The control processes are asynchronous with the flow of data.

MaxVideo devices are modeled as collections of 35 different modular pipeline IP (Image Processing) elements [25]. Pipelines can be software configured by virtually connecting the appropriate IP elements provided by the MaxVideo devices, and physically connecting the appropriate ports on the devices with ribbon cables.
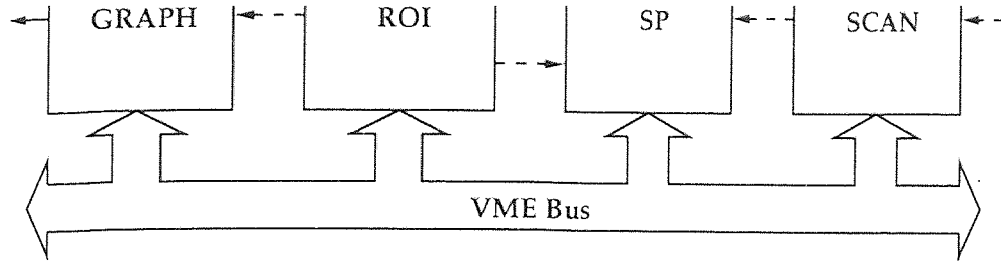
Figure 2.1 MaxVideo Setup

2.1.2 Basic Setup

Figure 2.1 sketches the basic arrangement of the MaxVideo boards in the MAX-BOX.

MAX-SCAN can act as a pixel clock master or slave. When it is the master, it generates pixel clock signal and transmits the signal out to a sensor. When it operates as a slave, it receives a pixel clock signal generated by a sensor. MAX-SCAN can also receive and/or transmit Hsync and Vsync as a Hsync/Vsync slave or master. In the SUN M-WIP, MAX-SCAN is set up to use sync signals (Hsync, Vsync) and pixel clock signal provided by the camera on separate cables.

There are some hardware settings and also several timing switches that determine the configuration of the MAX-SCAN. They are summarized in Appendix A.

In the basic setup, the MAX-SP and ROI-STORE perform IIR filtering to reduce the shot noise and other temporal noise. The general equation of the IIR filter is

$$Accum = ((2^n - 1) * Accum + NewFrame)/2^n \qquad (2.1)$$

Since the input video resolution is 12-bit and the MaxVideo system can handle up to 16-bit, n can be as large as 4. The built-in multiplier of MAX-SP cannot be used to implement IIR for the 12-bit video data since its operands cannot be more than 8 bits. Therefore, the 12X16 LUT of MAX-SP is used.

The MAX-GRAPH is set up to display the filtered live video which is captured by MAX-SCAN, processed by MAX-SP and saved in ROI-STORE. It also performs pseudocoloring and graphics overlay generation. Since MAX-SCAN and MAX-GRAPH have different timing bus requirements, ROI-STORE also plays the role of "timing translation". The MAX-SCAN's SC_XMT gateway must use a PR (Processing Rectangle) timing bus, while MAX-GRAPH's GH_RCV gateway will always use the SPC (System Pixel Clock) timing bus. Thus, two separate pipes must be created for the acquisition (SC_XMT to RS_RCV) and display (RS_XMT to GH_RCV), respectively.

2.2 Non-Uniformity Correction

Due to the inherent anomalies in the process of imaging chip fabricating, the photo-detector response of the staring IR-CCD camera contains non-uniformity. The non-uniformity may arise from the variations in

1. cutoff wavelength,

2. detector quantum efficiency,

3. detector dark current,

4. detector area,

5. threshold voltage,

6. transfer inefficiency, and

7. cold-shield shading.

Several theoretical modeling approaches and analytical results have been published for the evaluation and improvement of the IR-CCD camera performance [26, 27].

As a result of the spatial variations, the uncompensated imagery of area sensing IR-CCD camera usually exhibits an embedded fixed pattern noise which obscures low contrast details and limits camera sensitivity. It has been shown that the spatial noise is the dominant factor in high background environments (3 to 5 μm or 8 to 12 μm imagery at background temperature greater than 0°C). For high flux levels, the fixed pattern noise in the uncorrected image is proportional to I^2 while the shot noise is proportional to I, where I is the spatial averaged input signal level. Furthermore, to preserve radiometric correct performance, the noise must be compensated. .

The *non-uniformity* u is defined explicitly by the expression

$$< \sigma >= u < \mu > \tag{2.2}$$

where $<>$ denotes spatial average, $< \sigma^2 >=< (\mu- < \mu >)^2 >$ and μ is the mean value for one pixel obtained by averaging a number of consecutive frames.

In this section, a real-time implementation of the two-point non-uniformity correction algorithm based on commercial image processing equipment is presented. Experimental results that demonstrate the performance of the non-uniformity correction procedure are based on images captured by the IR-CCD camera.

2.2.1 Correction Algorithm

Within many non-uniformity correction methods which have been proposed [28], the two-point (offset and gain) correction is preferred in practical IR camera systems. For most cases, the residual error after applying this method is so small that the corrected image becomes shot noise dominated.

The two-point model for the non-uniformity correction is shown in Figure 2.2.

1. Figure 2.2 (a) shows the response $s(i, j, T)$ of an arbitrary uncorrected pixel at position (i, j) in the acquired image at temperature T. The spatial averaged response of all image pixels between the two given reference temperatures T_1 and T_2 is shown as $\bar{s}(T)$.
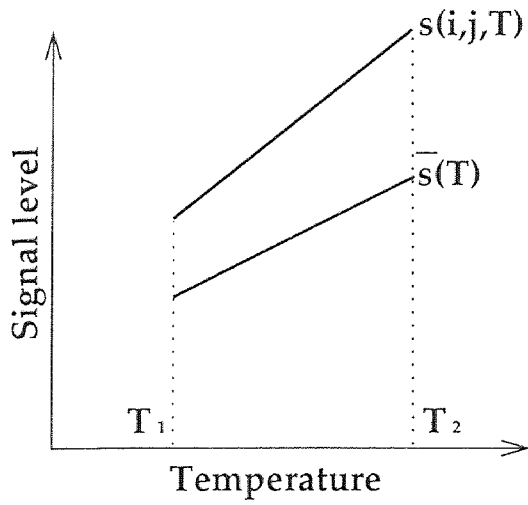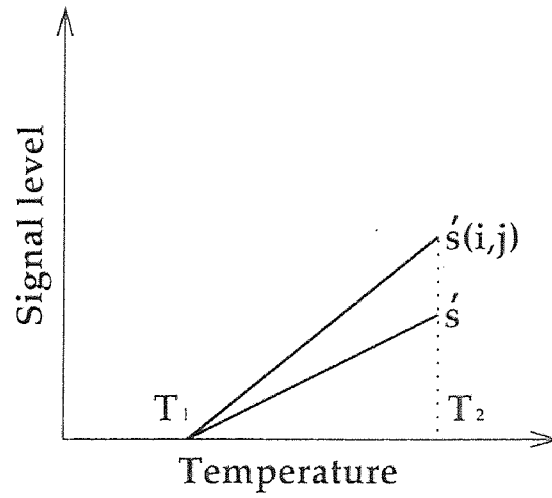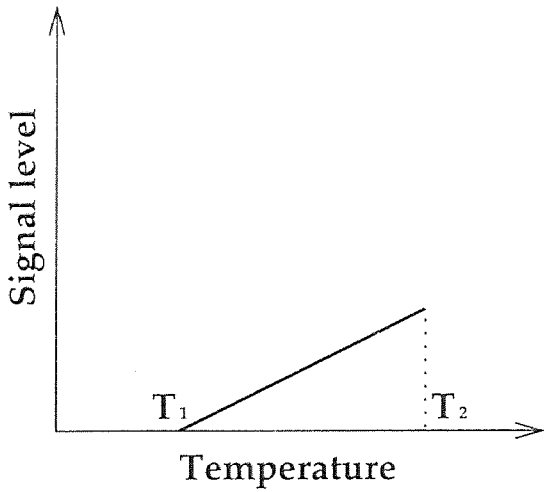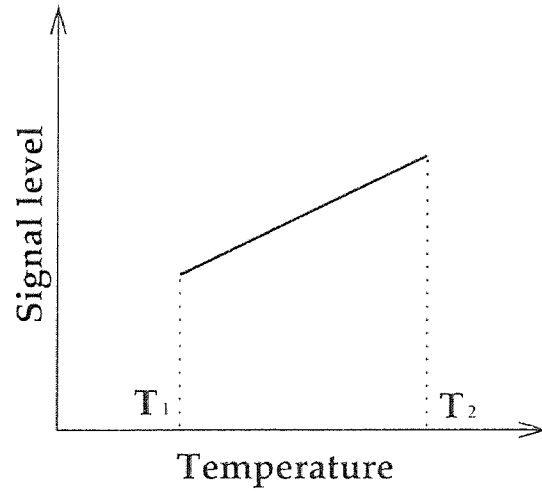
Figure 2.2 Non-Uniformity Correction Model

2. Figure 2.2 (b) is obtained from Figure 2.2 (a) with offset correction, that is, subtract the offset $\bar{s}(T_1)$ from $\bar{s}(T)$ and $s(i,j,T_1)$ from $s(i,j,T)$. The only difference between the two response curves within the temperature range defined by T_1 and T_2 is now their slopes. The gain coefficients for each pixel $gain(i,j)$ is calculated as

$$gain(i,j) = \frac{\acute{s}}{\acute{s}(i,j)} \qquad (2.3)$$

where $\acute{s} = \bar{s}(T_2) - \bar{s}(T_1)$, $\acute{s}(i,j) = s(i,j,T_2) - s(i,j,T_1)$.

3. Figure 2.2 (c) is obtained from Figure 2.2 (b) with gain correction, that is, multiply $s(i,j,T) - s(i,j,T_1)$ by the gain coefficients. The two response curves are identical now.

4. To obtain the corrected signal $\hat{s}(i,j,T)$, reinsert $\bar{s}(T_1)$ to preserve the radiometric information.

$$\hat{s}(i,j,t) = gain(i,j)(s(i,j,t) - s(i,j,T_1)) + \bar{s}(T_1) \qquad (2.4)$$

Using this model, the two-point non-uniformity correction algorithm can be described by the following three step procedure.

1. For two given reference temperatures, T_1 and T_2, $(T_2 > T_1)$, the spatial average value of all pixel response $\bar{s}(T_1)$ and $\bar{s}(T_2)$ are calculated from the gray level signal of each pixel $s(i,j,T_1)$ and $s(i,j,T_2)$. $s(i,j,T_1)$ is called $offset(i,j)$.

2. The gain coefficient of each pixel $gain(i,j)$ is calculated by

$$gain(i,j) = \frac{\bar{s}(T_2) - \bar{s}(T_1)}{s(i,j,T_2) - s(i,j,T_1)} \qquad (2.5)$$

where $s(i,j,T_2) > s(i,j,T_1)$ for $T_2 > T_1$.

3. For an image acquired at temperature T, $(T_1 \leq T \leq T_2)$, using the offset, the gain and the uncorrected signal $s(i,j,T)$, the corrected signal $\hat{s}(i,j,T)$ is

calculated as

$$\hat{s}(i,j,t) = gain(i,j)(s(i,j,t) - offset(i,j)) + \bar{s}(T_1) \qquad (2.6)$$

In the non-uniformity correction procedure, there are some noteworthy considerations:

1. Instead of using a single frame to calculate $\bar{s}(T_1)$ and $\bar{s}(T_2)$, the average of several frames acquired at temperature T_1 and T_2 can be used to reduce the random temporal noise [29]. In practice, 16 frame averaging is sufficient to reduce the temporal noise by a factor of 4.

2. Unless dark current (the signal response of leakage current) is very low within the measuring temperature range T_1 and T_2, the dark current compensation should be performed for all the input signals. This is particularly important where radiometric accuracy is required.

3. To ensure $s(i,j,T_2) > s(i,j,T_1)$ for $T_2 > T_1$, temperature difference $T_2 - T_1$ should be large enough to keep the signal difference much higher than noise level.

4. Since the non-uniformity also includes the effects such as COS^4 shading, the stability of the optical system must be ensured [30].

2.2.2   Real-Time Implementation

The experimental system used to implement the non-uniformity correction algorithm consists of three major components: the SUN workstation host computer, the IR-CCD camera, and the MaxVideo system. Figure 2.3 shows a block diagram of the computer system.

One MAX-SCAN (SC) board is used to acquire digital image with 12-bit resolution, four MAX-SP (SP) boards and three ROI-STORE (RS) boards are used to
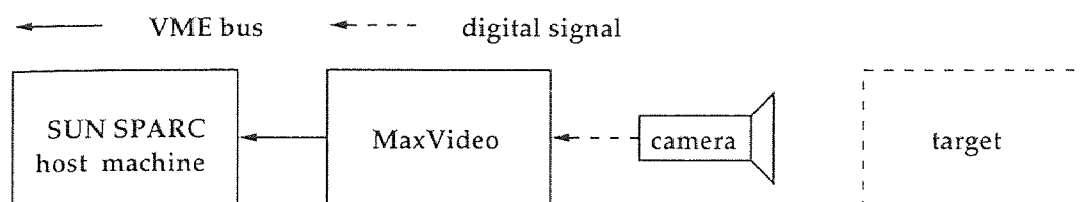
Figure 2.3 SUN M-WIP System Configuration

perform image pre-processing, including low-pass filtering and two-point correction. Figure 2.4 illustrates the data flow for the real-time implementation and the calculation of the 16-bit output.

Within the system, the SC00, RS00, and SP00 performs real-time IIR filtering instead of the averaging of consecutive frames to reduce temporal noise.

The SP01 subtracts the offset pre-stored in RS01 from the input provided by the IIR filter, $s(i, j, T) - offset(i, j)$. The 12-bit data subtraction for offset correction can be easily implemented by using SP01's ALU element.

The SP02 multiplies the gain pre-stored in RS02 with the offset correction result provided by SP01, $gain(i, j)(s(i, j, T) - offset(i, j))$. Since the MAX-SP only allows 8-bit by 8-bit multiplication using its multiplier element, a special implementation is designed to realize 12-bit (offset correction result) by 8-bit (gain coefficients) multiplication in MAX-SP. SP02's LUT element, a hardware lookup table, is used to map the 4-bit least significant nibble of the partial result and the 8-bit gain to the most significant 8-bit of their corresponding multiplication result. At the same time, SP02's MULT element is used to obtain the multiplication result of the most significant 8-bit of the partial result and the 8-bit gain. The final result of non-uniformity correction is converted to 12-bit data using the shifter element embedded in SP02. If needed, the 16-bit data can be kept to provide more precise result.
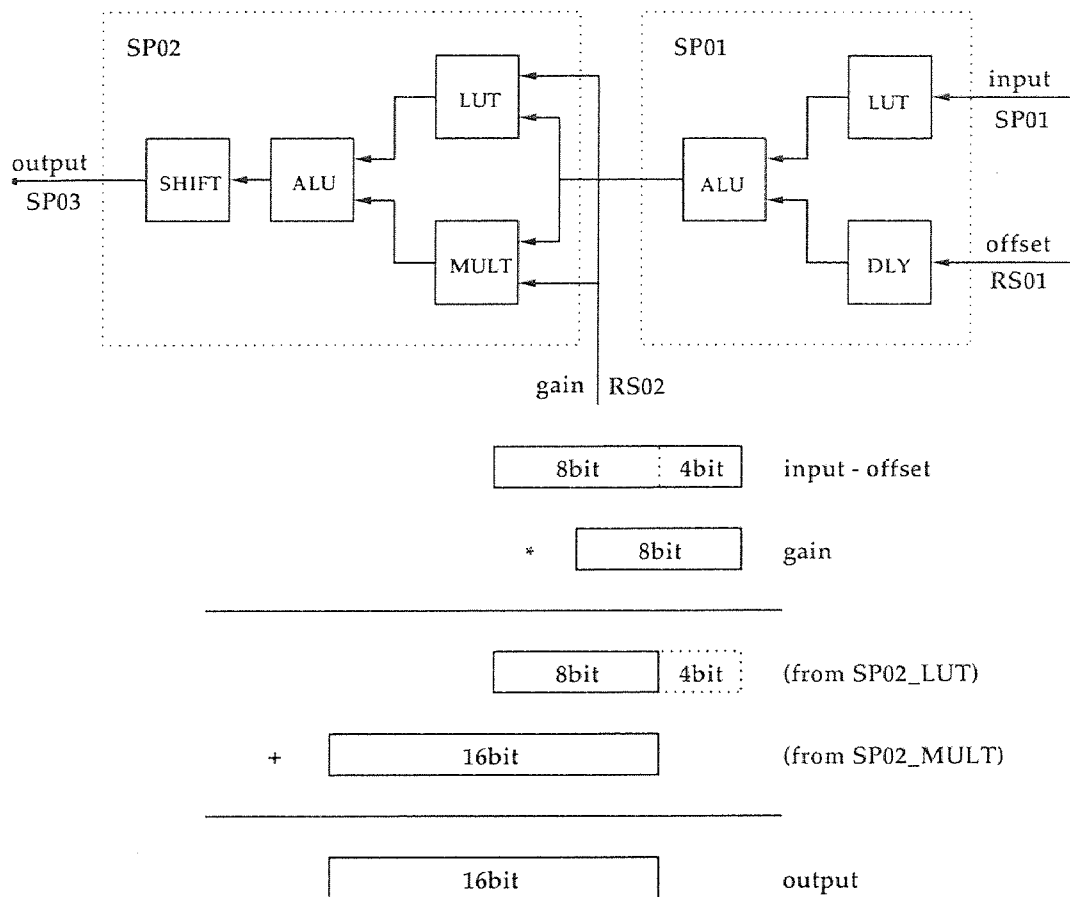
Figure 2.4 Real-Time Implementation

The gain correction result is then sent to SP03 to reinsert the $\bar{s}(T_1)$. The reinsertion of the spatial averaged offset can be easily implemented by using SP03's ALU element.

2.2.3 Experimental Results

In the experiments described below, two spatial averaged offset images are recorded at blackbody temperature of 25°C and 55°C. The images for testing the non-uniformity correction procedure are recorded at blackbody temperature of 35°C and 45°C.

Figure 2.5 and Figure 2.6 respectively show the images at blackbody temperature 35°C and 45°C with and without non-uniformity correction. Images are displayed after histogram equalization for contrast enhancement.

The non-uniformity in the 35°C case is 1.80022% before correction and 0.267749% after correction. In the case of 45°C, the non-uniformity is 1.80356% before correction and 0.229691% after correction. In both cases, the non-uniformity correction results in at least six fold improvement.

The defects in a detector array that introduce bad pixels can be

1. *black pixels*, also called *cold pixels*, which are non-functioning, corresponding to crack detectors,

2. *white pixels*, also called *hot pixels*, which are always in saturation, imposed by strong system noise, such as excessive dark current, and

3. dead columns, etc.

The two-point non-uniformity correction can partially fix the bad pixels. When the difference for one pixel between the two offset images is very small or even zero, the gain value is forced to be 1.0 and this will set the gray level (intensity value) of the pixel to the spatial average at the lower offset point. This can improve the cosmetic appearance of the displayed image by eliminating the visual distraction of
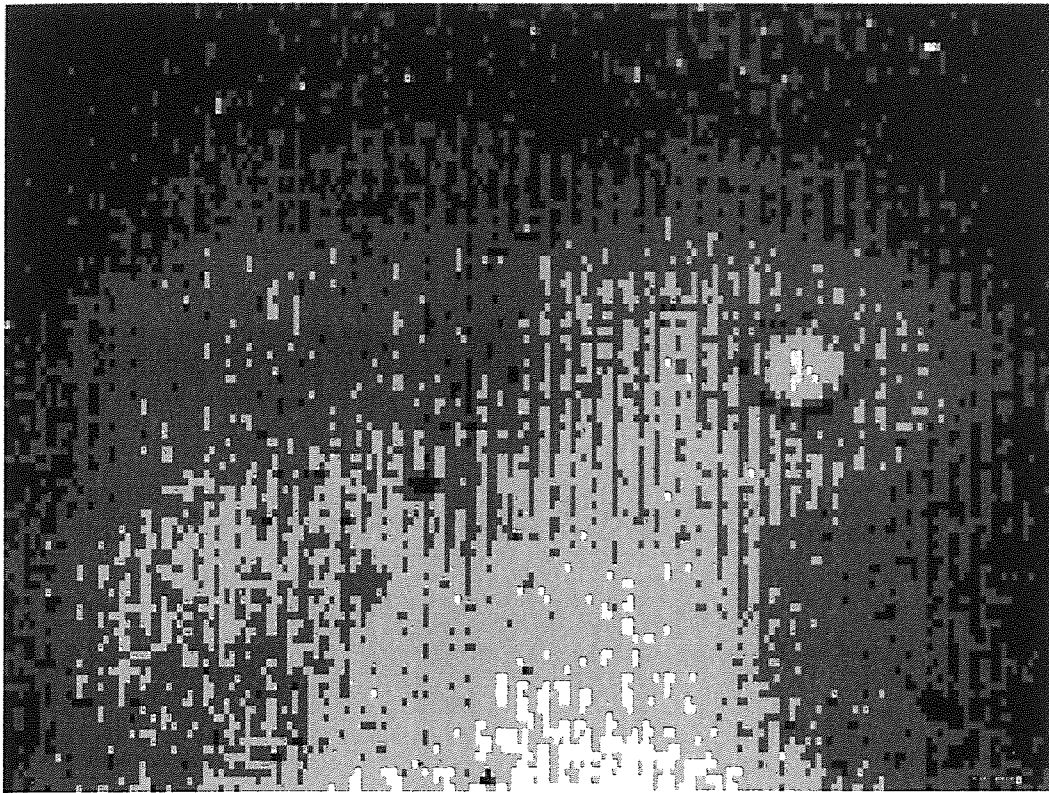
(a) Before Correction
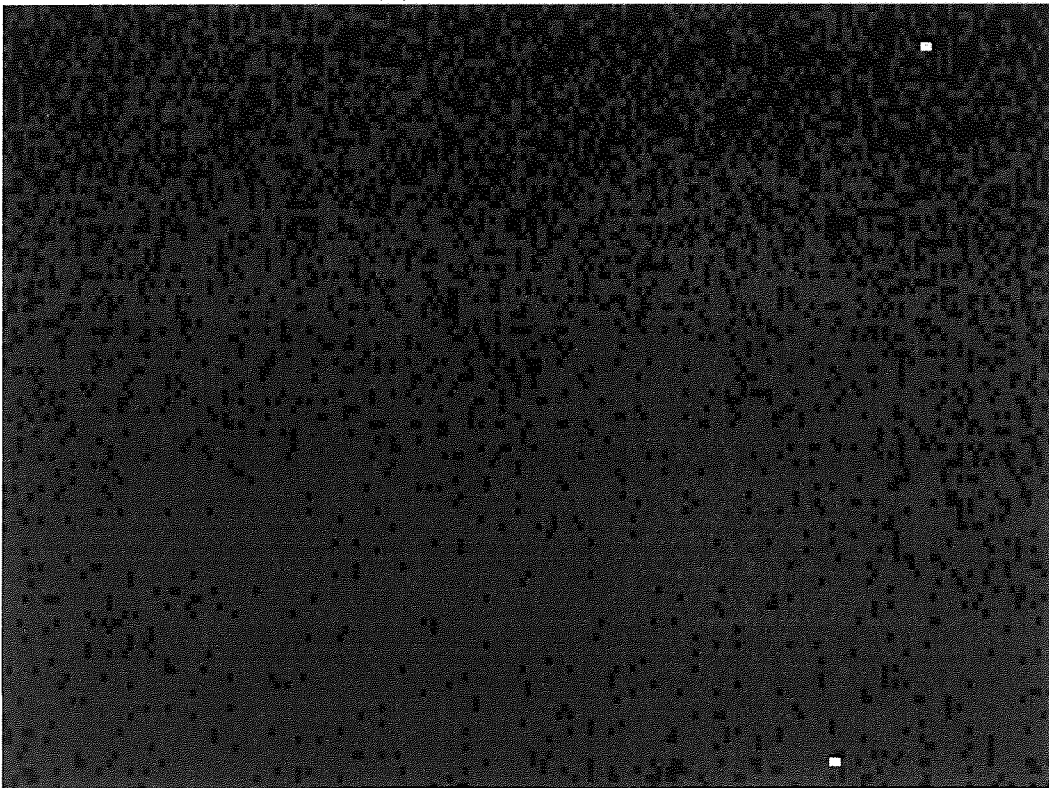
(b) After Correction

Figure 2.5 Correction Result at 35° C
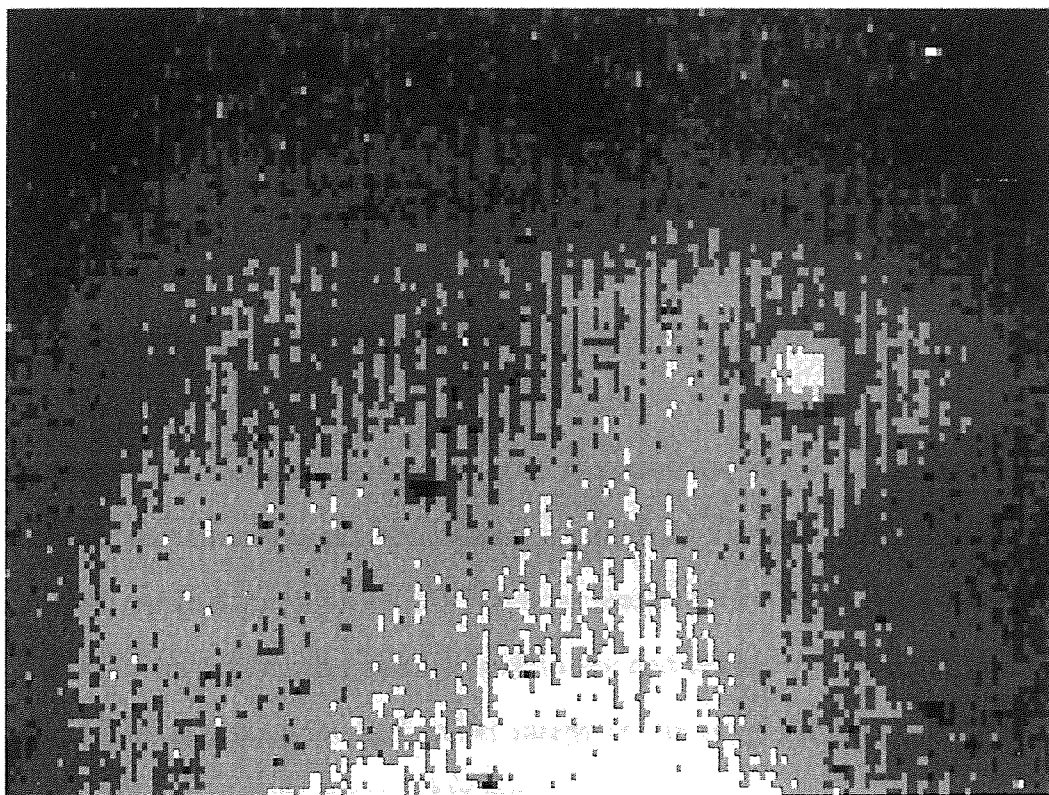
(a) Before Correction
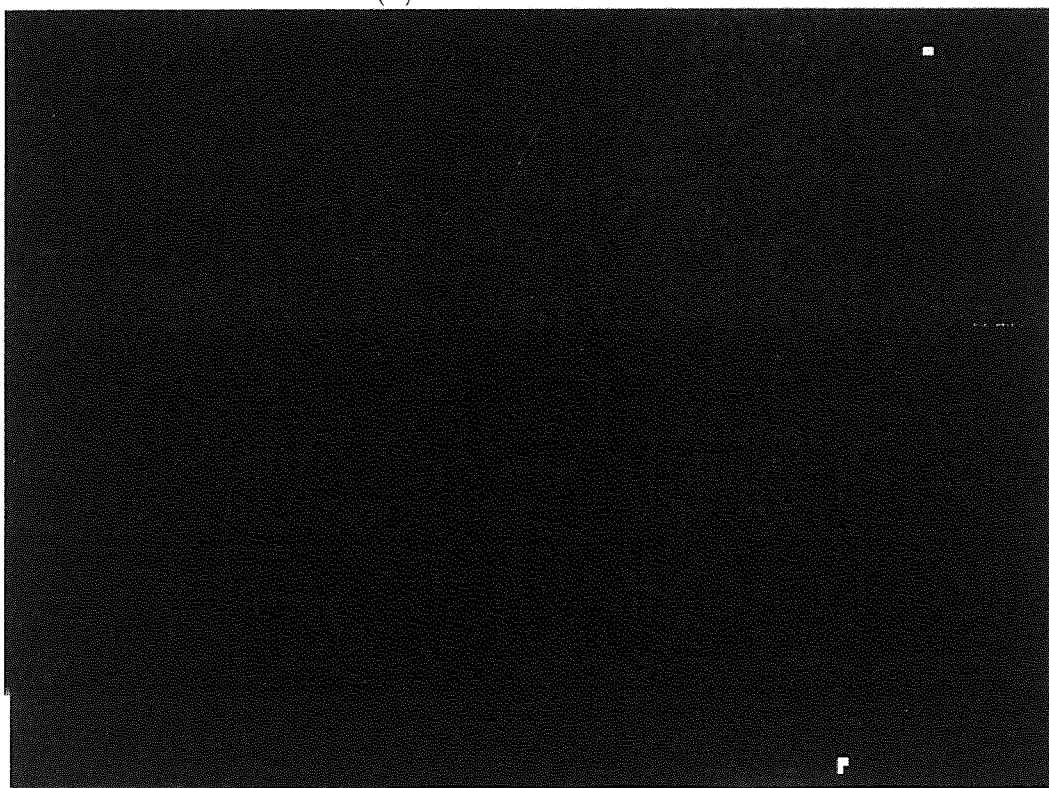
(b) After Correction

Figure 2.6 Correction Result at 45° C

the defective pixels, especially when the two offset points are close to each other. However, for radiometric measurement purpose, the bad pixels should be flagged by generating a bad pixel mask [31]. Defect eliminator [32] can also be used to replace the bad pixels.

The median of the pixel values can be used to obtain offset images instead of the spatial average to preserve the correct mean values which are used to calculate the gain and offset values. By manually imposing 1% black pixels in the example images shown above, the median method obtained the same mean values as the original one, but the average method gave more than 1% error in the mean values. The median method can also obtain more accurate result when certain area of the pixels presents very different response level to the rest of the pixels. Since the median filter is applied only once for each offset image at the time of calibration, its higher computational complexity is not a big issue.

When there are embedded information in the input video, such as integration time code, neither median method or average method is suitable. In this case, a known normal area (sub-image) must be present to obtain the spatial average value or the median of the data.

2.3 Pseudocoloring Display

It is well known that human eyes perceive both brightness and color information, and human visual system is much more sensitive to color differences than brightness variations.

The image processing method which involves the use of color in the representation of intensity images is named as "pseudocoloring." Using the technique of pseudocoloring by assigning a color to a gray level in an image according to a mapping scheme, an observer can see much clearly the differences of pixels in the image. Pseudocoloring techniques have been widely applied in image processing

and computer graphics. Some digital or optical pseudocoloring methods have been implemented in many special applications.

In some industrial applications, such as semiconductor process monitoring and control, thermal infrared radiance mainly corresponds to the surface temperature of the target under study (in the case that the emissivity of the target, say a wafer, is of spatially uniform). Since the contrast of an infrared image is usually much lower than that of a visible image, pseudocoloring techniques is often used in thermal image display. In this case, the grayscale images captured by the IR camera are converted to pseudocolored images to make different temperature levels more distinguishable.

In this section, pseudocoloring schemes are sketched by the mapping curves which are used to convert input gray levels (horizontal axis) to corresponding output RGB color intensities (vertical axis). Gray level and the intensities of each color primaries are normalized to the range of [0, 1].

2.3.1 Conventional Scheme

In daily life, red is usually used to indicate "hot" or high temperature and blue to represent "cold" or low temperature. The "conventional" pseudocoloring scheme fits this common sense [33]. Figure 2.7 (a) shows the scheme of the conventional pseudocoloring.

The features of the conventional scheme are obvious.

1. The pure primaries (R, G, B) occur only at the extreme ends (blue corresponding to the lowest input gray level, and red the highest) and the exact center of the input intensity (green).

2. The output brightness (the total intensity of R, G, B) is not uniform. Its profile shown in Figure 2.7 (b) has two peaks.
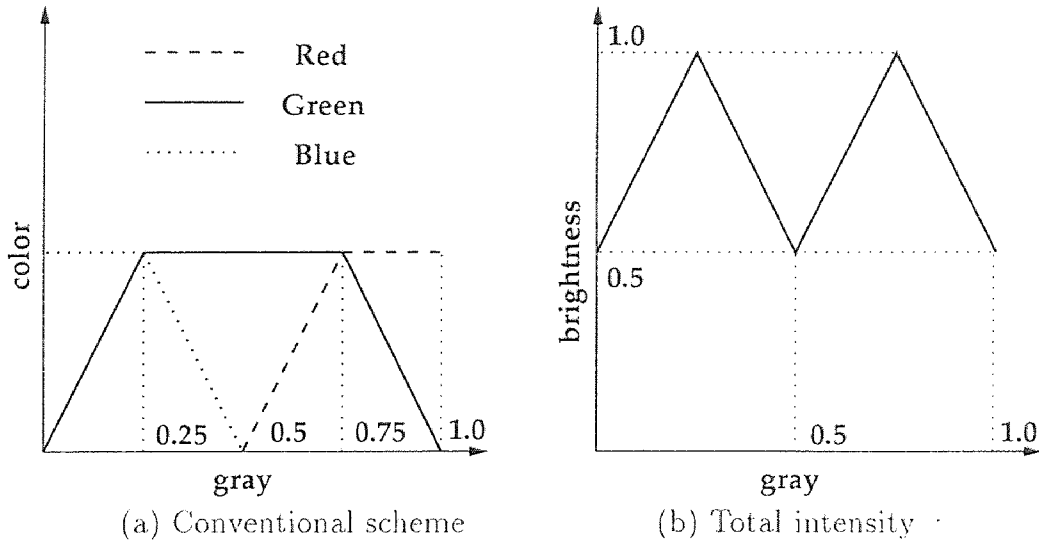
Figure 2.7 Schematic Diagram of Conventional Pseudocoloring

3. The green primary effects the whole image except the pixels with the two end gray levels (highest and lowest gray levels), while red and blue primaries effect only those pixels whose gray levels fell in half of the input gray levels. Thus the scheme is "green preferred in color".

2.3.2 Modified Conventional Scheme

Considering the second feature of the conventional pseudocoloring technique described above, this scheme is not adequate for temperature distribution monitoring. Generally, using both color and brightness can make the differences in grayscale easier to be discerned. However, for continuous temperature representation, uniform brightness is more preferable because large scale brightness variation may confuse the observer about the relative temperature differences. First of all, in daily life, brighter usually means hotter. Also, brightness variance can disturb the interception of color by human beings. For example, the same color in different brightness levels "looks like" different colors.

The conventional scheme is modified to realize uniform brightness color output. Figure 2.8 (a) shows the scheme of the modified conventional pseudocoloring.

(a) Modified scheme   (b) Total intensity
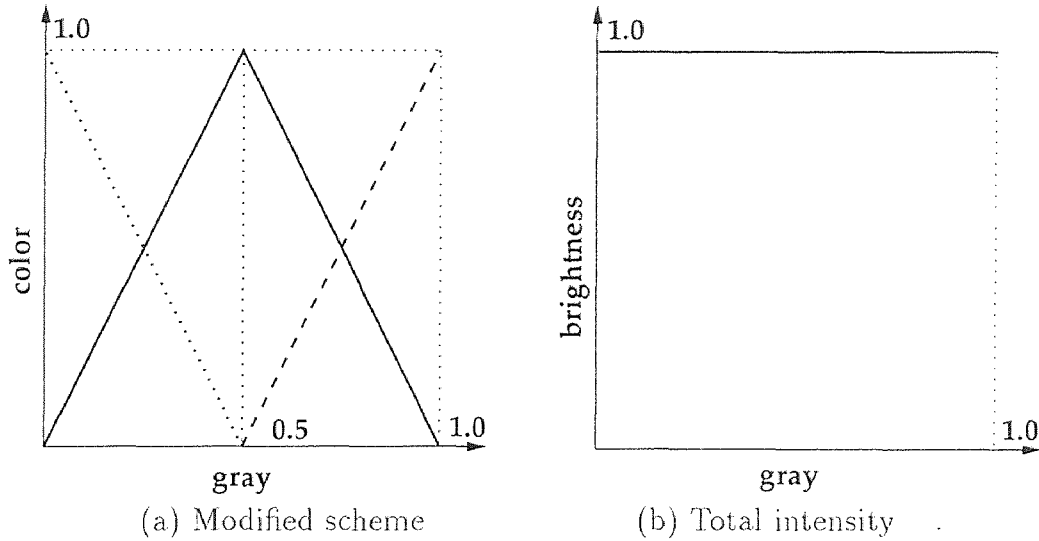
Figure 2.8 Schematic Diagram of Modified Conventional Pseudocoloring

This modified scheme retains the first feature and the third feature of the original conventional scheme but with uniform brightness color output, as shown in Figure 2.8 (b).

2.3.3 HSI Model Based Scheme

In color image processing, the HSI model is an ideal tool for developing image processing algorithms based on the color sensing properties of the human visual system. In the HSI model, H stands for hue (attribute that describes a pure color), S for saturation (degree to which a pure color is diluted by white light), and I for intensity. Since the intensity is decoupled from the color information in the image, the HSI model can be easily employed to establish a pseudocoloring scheme of uniform brightness.

To obtain the HSI model based scheme, first the features of the scheme with a HSI model is determined, and the HSI model is then converted to its corresponding RGB model for implementation.

For the uniform brightness feature, the I component in the HSI model is set to be constant 1. The S component is also set to constant 1 so that only pure

color is used. Thus, the only variable component is H. To keep the feature 1 of the conventional scheme, H is allowed to change from 240°C (pure blue) through 120°C (pure green) to 0°C (pure red), corresponding to grayscale changes from lowest to highest.

Let $I = 1$, and $S = 1$, the following equations can be derived from the HSI to RGB conversion formulas [34],

GB section ($120 \leq H \leq 240$, $H' = H - 120$):

$$Red \;=\; 0 \tag{2.7}$$

$$Green \;=\; \frac{1}{3}\left[1 + \frac{cos(H')}{cos(60 - H')}\right] \tag{2.8}$$

$$Blue \;=\; 1 - Green \tag{2.9}$$

RG section ($0 \leq H \leq 120$):

$$Red \;=\; \frac{1}{3}\left[1 + \frac{cos(H)}{cos(60 - H)}\right] \tag{2.10}$$

$$Green \;=\; 1 - Red \tag{2.11}$$

$$Blue \;=\; 0 \tag{2.12}$$

In both sections, $Red + Green + Blue \equiv 1$.

Simply let $H = 240(1 - Gray)$, where $0 \leq Gray \leq 1$, gray level (Gray) can be mapped to RGB color intensities (Red, Green, Blue).

Figure 2.9 (a) shows the scheme diagram of the HSI model based pseudo-coloring.

2.3.4 Bézier Function Based Scheme

Bézier/Bernstein blending function is the basis of the widely used Bézier curve technique [35] in the field of computer graphics. Here it is used to derive another new pseudocoloring scheme.

(a) HSI model based scheme   (b) Bézier function based scheme
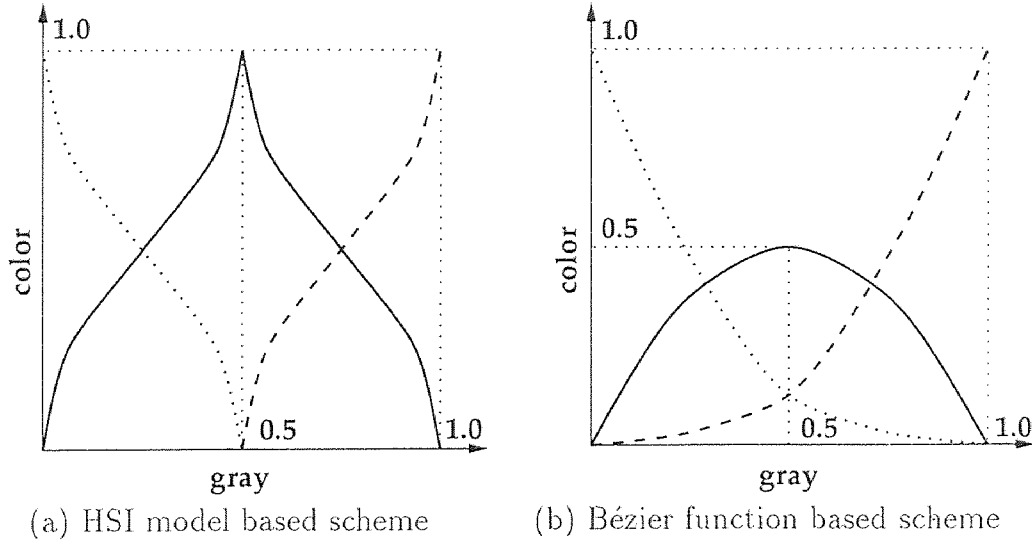
Figure 2.9 Schematic Diagrams of New Pseudocoloring Techniques

Given the following Bézier function $0 \leq t \leq 1$,

$$B_{n,i}(t) = \begin{pmatrix} n \\ i \end{pmatrix} t^i (1-t)^{n-i} \tag{2.13}$$

where

$$\begin{pmatrix} n \\ i \end{pmatrix} = \frac{i!}{n!(n-i)!} \tag{2.14}$$

Let $n = 2$, and $t = Gray$, $B_{2,0} = Red$, $B_{2,1} = Green$, $B_{2,2} = Blue$, then

$$Red = Gray^2 \tag{2.15}$$

$$Green = 2Gray(1 - Gray) \tag{2.16}$$

$$Blue = (1 - Gray)^2 \tag{2.17}$$

It is easy to prove that $Red + Green + Blue \equiv 1$, and this ensures that the Bézier function based scheme, as shown in Figure 2.9 (b), has the property of uniform brightness.

2.3.5 Scheme Comparison

Although all of the four schemes have similar colormaps, they are different theoretically and practically.

1. The conventional pseudocoloring scheme changes not only the color (hue and saturation) but also brightness (intensity), while the other three schemes only change the color (or even only the hue) but leave the brightness uniform;

2. The Bézier function based scheme uses all the three primaries to assign the RGB values for the pixels in the entire gray level range, but the other three schemes use red or blue primaries only when the gray level of a pixel falls in the upper or lower half of the gray level range;

3. The Bézier function based scheme does not give the pure green as the other schemes do at the exact center of the gray level range.

All of the four pseudocoloring schemes were implemented in the SUN M-WIP [1]. The main equipment used to realize the real-time thermal video pseudocoloring are a host machine (a SUN workstation with MAX-BOX), a MaxVideo system (a MAX-SCAN and a MAX-GRAPH), and a TRINITRON monitor (a RGB video monitor). The pseudocoloring schemes are implemented by setting up their corresponding colormap lookup table in the RGB LUT of the MAX-GRAPH board.

Experimental results of the schemes demonstrated that

1. The conventional pseudocoloring scheme gives significant brightness changes. Temperature differences are not distinguishable especially in the subranges where the secondary colors occur (highest brightness shown at pure yellow and pure cyan);

2. The modified conventional scheme and the HSI model based scheme have no major difference. As their schematic diagrams showed, the only difference between the two schemes is that the color of the HSI model based scheme changes faster in the pure red, green and blue dominated subranges but

[1]Gamma correction should be performed when necessary.

smoother in the pure yellow and cyan dominated subranges. Therefore, the modified conventional scheme can be regarded as a linear approximation of the HSI model based scheme. Although there is no brightness changes theoretically, one can still see from the colormap of the schemes that the pure green appears brighter than the colors close to it. This can be explained by the shape of the mapping curves of the two schemes. In fact, at the subrange around the pure green, although the intensities of both green and blue (or both green and red) are changing, the intensity of green is so high comparing to the other primary that the effect of the other primary cannot be seen. Therefore, the fast decreases in green intensity around the exact center of the input intensity gives the impression that the green "looks" brighter at the exact center of input intensity [2].

3. The Bézier function based scheme does not give any misleading color changes. Firstly, around the exact center of the input intensity, not only two primaries but three of them are changing. Secondly, the green intensity is the same as the sum of red and blue intensities so that the green is not bright enough to shadow the other two. Third, the first order derivative of the mapping curves for Bézier function based scheme is linear in the entire input range, but that of the conventional schemes are discontinued and that of the HSI model based scheme is non-linear and discontinued. Figure 2.10 shows the normalized absolute value of the first order derivatives of the HSI model based mapping curve and the Bézier function based mapping curve. (The first order derivative for the HSI model based scheme shows only the derivative of the green component since the normalized absolute derivative values of red and blue are overlapped on it.)

---

[2]The brightness perception characteristic of vision should also be considered. Since luminous efficiency peaks at about 555nm, the green will appear the brightest of the three primaries at the same intensity level.

(a) Derivative of HSI scheme   (b) Derivative of Bézier scheme
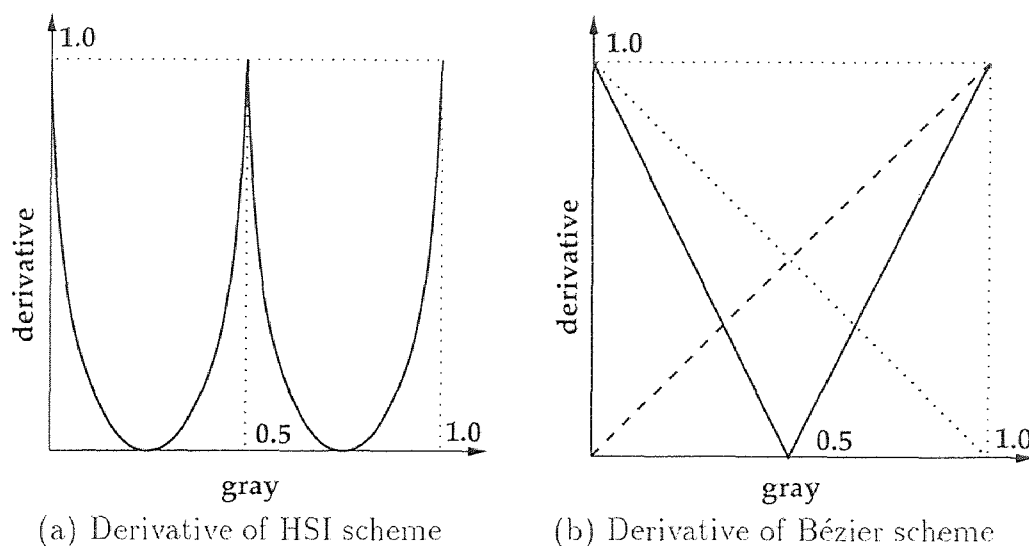
Figure 2.10 First-Order Derivatives of New Pseudocoloring Techniques

Experimental results showed that the Bézier/Bernstein blending function based pseudocoloring scheme gives the smoothest mapping among the four schemes and there is neither visible brightness changes nor the reason to raise the impression.

Compared with other schemes, the Bézier/Bernstein blending function based pseudocoloring scheme gives the best performance. The Bézier function based scheme is the default scheme employed in the SUN M-WIP.

Besides thermal imaging, the new schemes can be used in other applications where pseudocoloring of continuous distribution is required. For example, they can provide better magnitude visualization for geometric objects. They can also improve the display of volumetric data, radiometric data, and data for spectral analysis.

CHAPTER 3

SUN M-WIP: OTHER SUBSYSTEMS

3.1 Radiometric Calibration Subsystem

In the M-WIP systems, the least-squares method produces the result by fitting the simulation result signal from the radiometric model to the on-line thermal imaging data. To accurately measure the target surface temperature and emissivity, the radiometric model of the optoelectronic system needs to be precisely calibrated. The calibration is performed using a commercial blackbody M360 (Mikron Instrument Company, Inc.) which provides known temperature and close to unity emissivity. The radiometric calibration system can also be used to verify the performance of the M-WIP system.

3.1.1 LabTech System

A PC-based thermocouple data acquisition and communication system is setup to acquire contact temperature measurements at up to six points on the surface of the target for system calibration and performance evaluation. The thermocouple readouts are acquired into a PC-based LabTech system (Laboratory Technologies, Co.) which consists of 6 DCP5B47 modules, one LSDAS-12 board and one PDIO-96 board. The data is then transferred to the host computer via two DATEL-660 boards installed in the MAX-BOX. Figure 3.1 illustrates the arrangement of these modules.
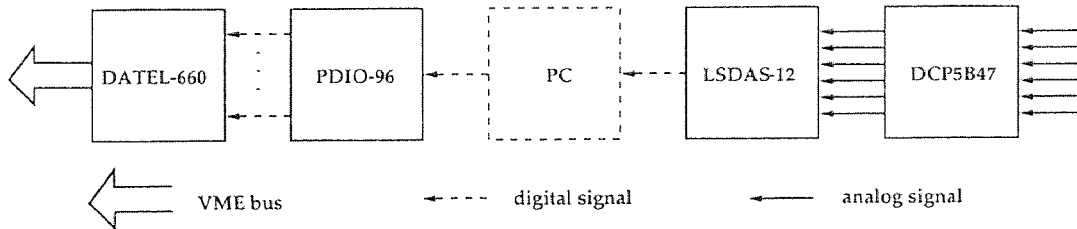
Figure 3.1 Calibration Subsystem

44

- The DCP5B47 module is an interface to several types of thermocouples including J, K, T, E, R, S, and B types. It filters, isolates, amplifies, linearizes the thermocouple signal and converts it to a high level analog voltage output.

- The LSDAS-12 is a data acquisition board, and the PDIO-96 is a 96-bit parallel digital I/O board. These two boards are programmed using LabTech's NoteBook to obtain the 12-bit temperature data from each thermocouple channel. It is then split to two bytes and sent to the host computer. The host computer will merge the two bytes to recover the temperature values with 12-bit resolution.

- The DATEL-660 is a 48-bit parallel I/O board (Datel, Inc.) which allows data from three thermocouple channels to be transferred.

3.1.2 Data Acquisition

The multi-channel temperature values are obtained by setting up an appropriate equation in the LabTech's "analog input block" to convert the input voltage to its corresponding temperature value and then transferred from the PC to the SUN workstation. The sender (PC) and the receiver (SUN) are synchronized to ensure the reliability of the data communication.

To send the 12-bit resolution data from PC to SUN, 12-bit or 16-bit parallel digital I/O cannot be used directly, because LabTech'ssoftware only support 8-bit I/O channels. Using the "calculated block" that LabTech provided, a split-merge method is employed to achieve the 12-bit I/O. Figure 3.2 shows the basic flowchart of the data path.

Three calculated blocks are used: block 1 amplified the temperature value ranging in [0.0, 999.9] by 10 to obtain the scaled temperature value ranging in [0000, 9999], and sends the result to block 2 and block 3; block 2 divides its input by 100 and send the remainders (the two least significant digits of the scaled temperature
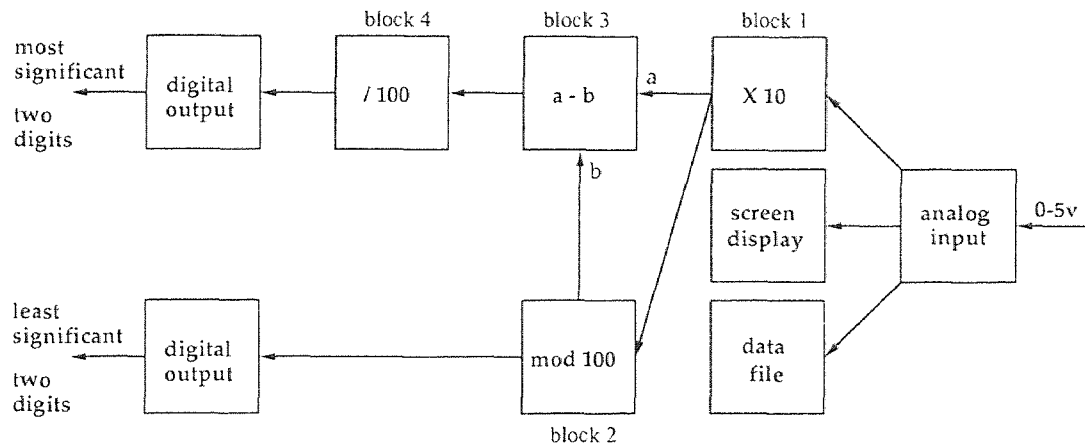
Figure 3.2 PC-to-SUN Communication Implementation

value) to block 3; block 3 subtracts the output of block 2 from the output of block 1, and block 4 divides the resultant number by 100 to obtain the two most significant digits of the scaled temperature value. Block 2 and block 4 then send their results to two separate 8-bit parallel digital I/O channels.

The data-file block and the screen-display block are used for data recording, display and analysis at the PC side.

Receiving the data from PC side, the host running the DATEL-660 boards obtains the two binary values from the two channels. At the host side, the number obtained from the most significant digit channel is multiplied by 10 and the number from the least significant digit channel is divided by 10. Sum the two rescaled numbers and the original temperature value is recovered.

3.2 Parallel Processing Subsystem

One of the bottlenecks in utilizing imaging pyrometers for real-time applications is the large computational requirement needed to accurately compute surface temperatures from thermal image. Fortunately, the computational algorithms can be parallelized and a parallel computer system can be used to reduce the computational time.

3.2.1   V-C40 Hydra Board

V-C40 Hydra, a multiple digital signal processor (DSP) board, is installed in the MAX-BOX.

- The V-C40 Hydra is a quad-DSP board which consists of a base card and a daughter card, each containing two Texas Instruments (TI) TMS320C40 floating-point DSP chips. The 50MHz TMS320C40, a 32-bit processor designed specially for parallel processing, is capable of 275 MOPS and 20 MB/sec independent inter-processor communication.

Each of the four TI TMS320C40 provides six 8-bit bi-directional half-duplex ports for high speed inter-processor communication, six-channel DMA co-processor for concurrent I/O and CPU operation, 4 KB on-chip dual-access single-cycle RAM, identical 32-bit external Global Bus [1] and Local Bus with 100 MB/sec transfer rate that are capable of addressing 8 GB in total, and a separate internal bus for massive concurrent I/O throughput. The four on-board DSPs are fully-connected, and there are three off-board communication ports for each DSP.

The V-C40 Hydra board supports up to 1 MB private SRAM for each DSP via both of their Global Bus and Local Bus, thus makes each of the DSPs an independent processing node. V-C40 Hydra has an Internal Shared Bus (ISB) to which the VME bus and the Global Bus of each DSP are attached. The ISB also supports up to 64MB shared DRAM or 4 MB shared SRAM. Figure 3.3 shows the block diagram of the Hydra board used in the SUN M-WIP.

3.2.2   Parallel Computing

Parallel processing systems are usually classified into two major categories, message-passing multicomputers and shared-memory multiprocessors, based on the way

---

[1]The nomenclature follows TI naming convention. The term "Global" does not imply that the bus is shared by more than one DSP.
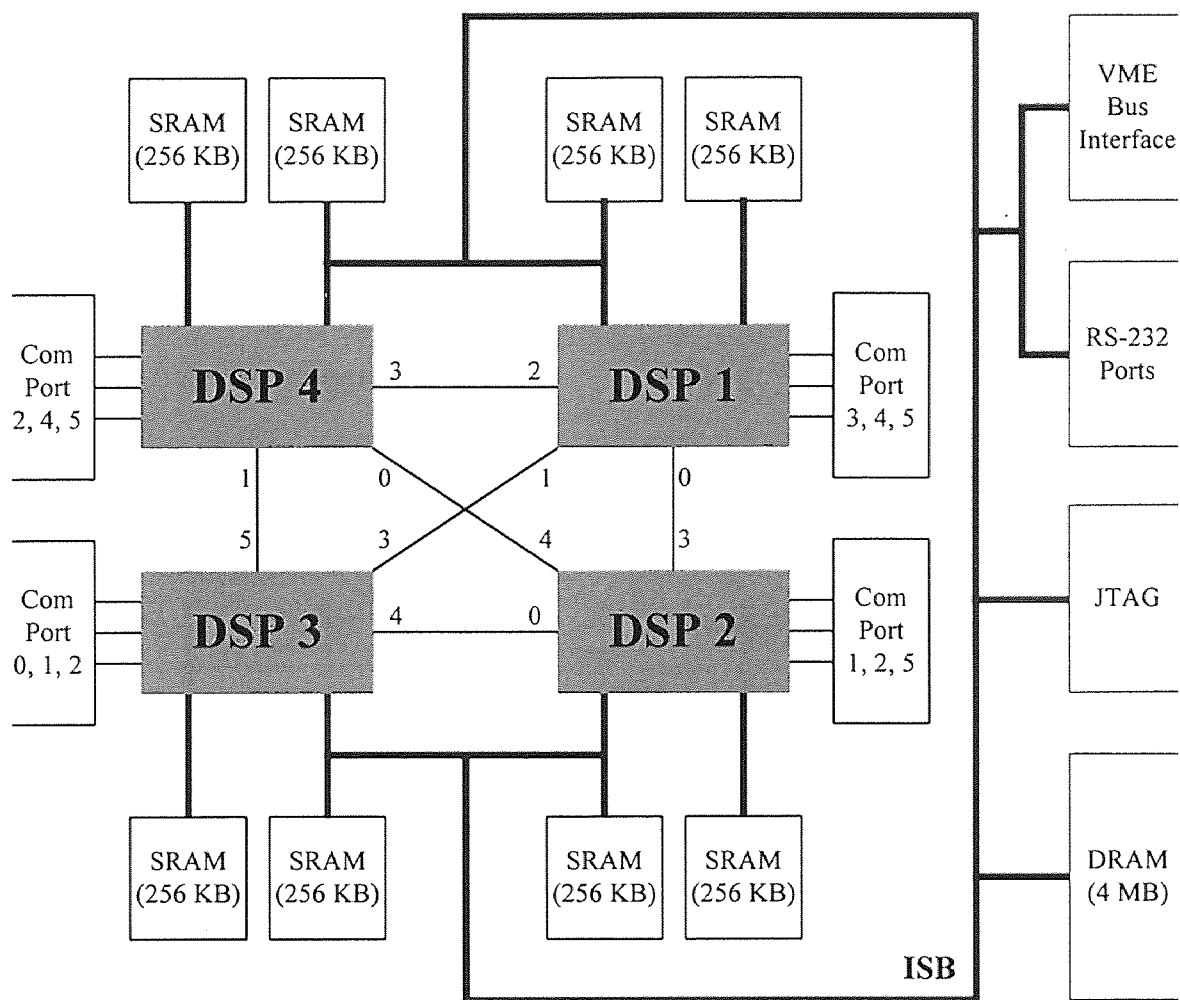
Figure 3.3 Block Diagram of V-C40 Hydra Board

communication is carried out. In *message-passing multicomputers*, the communication between the computers (nodes) is realized via an interconnection network which provides node-to-node communication. In *shared-memory multiprocessors*, all the communication tasks use a designated shared memory as the medium for information transactions.

Hydra board implements a hybrid architecture which supports both message-passing (via the communication ports which establish the complete connection) and shared-memory (via the ISB and the shared DRAM/SRAM) paradigms in a single parallel processing system. The complementary nature of the message-passing and shared-memory communication mechanisms and the advantage of the hybrid paradigm have been investigated [36].

In the M-WIP temperature measurements, temperature and emissivity are determined simultaneously by least-squares fitting of the measured data to the values given by the radiometric model of the IR camera system. Utilizing the V-C40 Hydra, the time consuming least-squares fitting computation is partitioned into several smaller pieces and then distributed to the DSPs.

There are two different methods in parallelizing the least-squares fitting procedure. The *multiple-program multiple-data* (MPMD) paradigm employs one DSP as the "root node" and makes it the only DSP that communicates with the host. Some software programming environment for parallel processing, including Parallel C (3L, Ltd.), uses this paradigm. The root node handles the task scheduling: it receives all the data needed for computation from the host; schedules tasks and distributes data to all the nodes; collects computation results from all the nodes; and then reports the final result to the host.

The *single-program multiple-data* (SPMD) paradigm considers all DSPs to be equal and executing an identical program. In addition, a supervisor/worker algorithm is used to coordinate the computations. The host (supervisor) divides the computa-

(a) MPMD Paradigm   (b) SPMD Paradigm
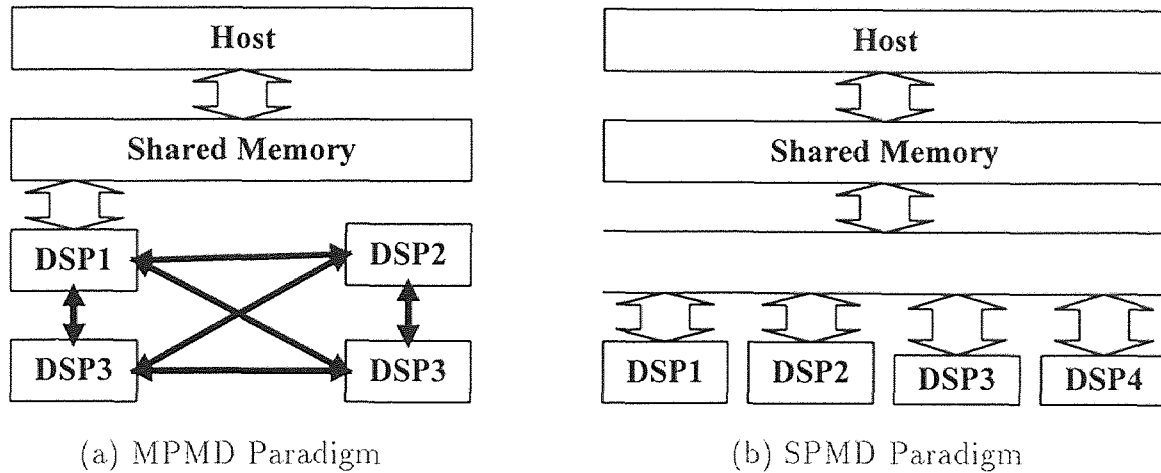
Figure 3.4 V-C40 Hydra Paradigms

tional work of the least-squares fitting into several equal-loaded independent parts, and subtasks each part to a different DSP (worker). In this way, the host controls all the task scheduling and data exchange so that node-to-node communication is not necessary. Figure 3.4 shows the two different paradigms that can be implemented in V-C40 Hydra.

SPMD and MPMD are not part of Flynn's hardware taxonomy [37] which includes SISD (Single-Instruction-Single-Data), SIMD (Single-Instruction-Multiple-Data), and MIMD (Multiple-Instruction-Multiple-Data). In fact, SPMD and MPMD are not hardware paradigms at all; rather, they are respectively, the software equivalent of SIMD and MIMD at procedure level. SPMD means running the same program but with separate data. Because the same program executed on different data can take different branches, the processors are no longer doing the same thing as in SIMD case where processors are tightly synchronized, and this leads to asynchronous parallelism. The processors execute asynchronously within a procedure that is duplicated on all processors, and they are globally synchronized only at the beginning and end of the procedure [38]. MPMD means simultaneously executing different programs on different data. Processors are globally asynchronized as in

MPMD case, and synchronization for data exchange between processors is achieved locally.

SPMD is actually a MIMD computer programmed in data parallel paradigm that comes from simultaneous operations across large sets of data, rather than from multiple threads of control. MPMD is usually used when the problem allows multiple heterogeneous tasks to be performed at the same time. Figure 3.5 shows the flowcharts of the two different M-WIP paradigms that can be implemented in V-C40 Hydra.

To take advantage of the V-C40 Hydra architecture and to reduce the communication overhead, the SPMD paradigm is used to implement the M-WIP temperature measurement. Its performance is compared with the MPMD approach and presented in Chapter 4.

3.3   Feedback Control Subsystems

The SUN M-WIP system is designed to be capable of controlling the RTP system through D/A ports and integration time control of the IR-CCD camera through digital I/O ports.

3.3.1   RTP Control

In the RTP system, the wafer is heated by the infrared radiation of tungsten-halogen lamps positioned above the quartz window of the reaction chamber. The lamps are arranged in three annular zones consisting of 1, 12, and 24 lamps from center to outer respectively. The central lamp zone consists of one 2 KW lamp, and the remaining two zones consists of 1 KW lamps. For RTP control, the electrical power supplied to each zone of lamps can be controlled independently.

A DATEL-624 D/A board (Datel, Inc.) is installed in the MAX-BOX which can send signals to the power supplies to close the loop of the entire system, and the

HOST   DSP1   DSP2-4

Host: Start DSPs

Host: Send data to DSPs

Host-DSP Communication

DSP1: Receive data from host

DSP1: Send data to other DSPs

DSP-DSP Communication

DSP2-4: Receive data from DSP1

Host: Acquire data for measurement

DSP1: Do least-square fitting

DSP2-4: Do least-square fitting

DSP-DSP Communication

DSP1: Collect results from other DSPs

DSP2-4: Send results to DSP1

Host-DSP Communication

Host: Receive results from DSPs

DSP1: Send results to host

(a) MPMD Paradigm for M-WIP

HOST   DSPs

Host: Start DSPs

Host: Acquire data for measurement

Host: Send data to DSPs

Host-DSP Communication

DSPs: Receive data from host

Host: Acquire data for measurement

DSPs: Do least-square fitting

Host-DSP Communication

Host: Collect results from DSPs

DSPs: Send results to host

(b) SPMD Paradigm for M-WIP

Figure 3.5 Paradigms for M-WIP

communication between the host computer and the process controllers is straight-forward.

- The DATEL-624 D/A board converts up to four channels of 16-bit to 0-5 V analog outputs that the lamp controllers needed.

Both open-loop control system and closed-loop control system can be realized. For the closed-loop control,either the information obtained by the IR-CCD camera or the data provided by the thermocouples can be used to construct the feedback control system.

3.3.2   Camera Control

Remote sensing of distant objects usually requires variable optical integration time. Adjust integration time according to the spatial statistics of input signal levels can improve the radiometric performance by accommodating a wide dynamic range and preserving a respectable signal to noise ratio.

Integration time control hardware is implemented in the camera headboard, and a digital input port is provided for the implementation of programmable automatic integration time control [18]. Currently, 256 different integration times are available, corresponding to 8-bit control code.

- Configuration

The IR-CCD camera integration time control system consists of the following major components:

1. SUN workstation host computer;

2. MaxVideo subsystem;

3. Camera drive subsystem;

4. PDIO control subsystem.
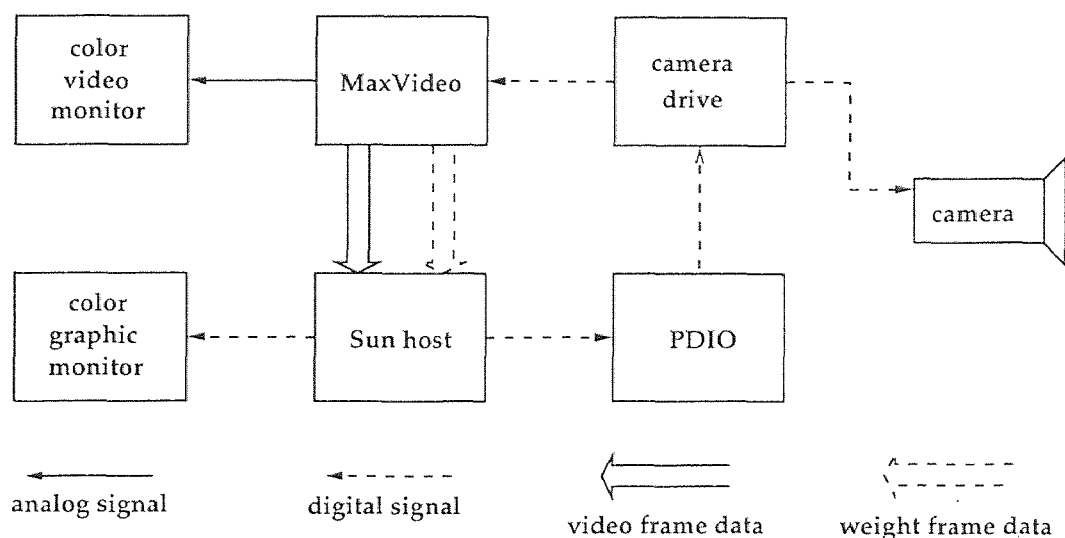
Figure 3.6 Integration Time Control System Configuration

Figure 3.6 shows a block diagram of the system.

The host computer is a SUN SPARC workstation. In the MaxVideo subsystem. 1 MAX-SCAN board (SC00), 1 MAX-SP boards (SP00), 2 ROI-STORE board (RS00 and RS01), and 1 MAX-GRAPH board (GH00) are needed. The camera drive subsystem is comprised of a Standard Clock Generater and a Variable Integration Sequencer [18]. The PDIO subsystem is a DATEL-660 which provides 8-bit integration time control code to the camera drive. Figure 3.7 sketches the arrangement of the MaxVideo boards in the MAX-BOX.

Programs were developed to setup and handle the pipeline in the real time image processing modules and device driver is developed to interface the I/O boards to the SUN operating system.

The video signal from the IR-CCD camera is fed into the special configured MaxVideo system for data acquisition. The HSync, VSync, and Pixel Clock signals can be either generated by he MaxVideo system or received from an external source, the camera drive subsystem.
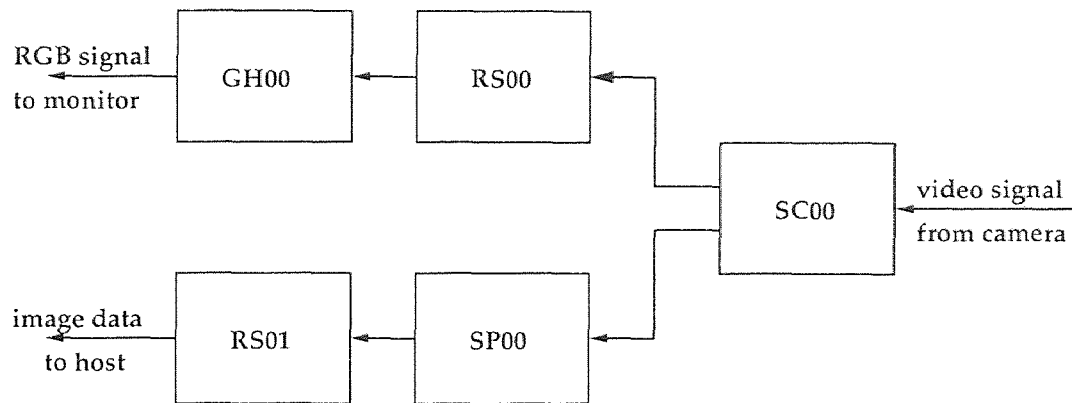
Figure 3.7 MaxVideo System for Integration Time Control

Currently, the Standard Clock Generator is used and the MaxVideo system is set to receive the synchronous signals from external source. If necessary, the Standard Clock Generator can be bypassed, and the MaxVideo can be set to transmit the synchronous signals generated by programmable internal source, and therefore simplify the camera drive circuitry.

● **Algorithms**

Algorithms are developed to perform the spatial statistics of the frame signal levels and to realize the reliable control of the camera integration time.

A look-up table can be set to obtain spatial statistics of signal levels in one frame. For each pixel, a weighted value can be assigned to it according to its signal level, and thus a weighted frame can be obtained. By processing the weighted values, it can be determined whether or not the integration time should be increased or decreased.

The look-up table can be performed by MAX-SP in real time, and the weighted frame can be transferred to host machine for further processing.

The latency of the control depends on not only the computational complexity of the statistics scheme and the control strategy, but also the speed and load of the host computer.

A threshold is set so that all pixels of signal level higher than the threshold are assigned with weight value 1, and others to 0. Spatially sum the binary weight values of the current frame, and assign the value to W, total weight value. If W is larger than a high water-mark T_h, it means the signal levels of a large percentage of pixels are saturated or near saturation, thus the integration time should be decreased; if W is smaller than a low water-mark T_l, this means the signal levels of almost all pixels are so low that the signal to noise ratio is poor, therefore, the integration time needs to be increased.

Different types of mapping scheme can be employed based on the specific application. For instance, in the case of line-scan M-WIP application, the sub-image corresponding to a certain bandpass filter at specified wavelength where the signal levels will saturate first and the sub-image where the signal levels are always of the lowest value are known. This prior knowledge provide the possibility of using much smaller reference regions to obtain the spatial statistics. This will speedup the computation procedure dramatically since the small reference regions can be used to realize real-time control of integration time.

The control of integration time is realized by adjusting the frequency of the transfer pulse signal. Different control strategies can be used to adjust the integration time of a camera based on the analysis of the spatial statistics.

Let W be the total weight value, and the current and previous integration time to be I_c and I_p, respectively.

For rapidly changing processes, let

$$I_c = I_p + F * W \qquad\qquad (3.1)$$

where F is a scale factor which transform the change in signal levels to the change in integration time.

For slower changing processes, let

$$I_c = I_p + C \qquad\qquad (3.2)$$

where C is a constant, or the control step. As discussed above, when $W > T_h$, $C = +1$; when $W < T_l$, $C = -1$.

More complicate control strategies can be used to obtain better control performance, and trade-off between the speed and accuracy should be considered.

CHAPTER 4

SUN M-WIP: SOFTWARE DEVELOPMENT

The software of the SUN M-WIP is developed mainly under UNIX and X Window. For the electronic imaging subsystem, ImageFlow is used in programming the real-time image capturing and pre-processing procedures. For the radiometric calibration subsystem, NoteBook visual programming tools are used in programming thermo-couple data acquisition and signal processing.

4.1   Graphical User Interface

The Graphical User Interface (GUI) on the SUN workstation side is programmed using Xlib (X library) which is the lowest X Window programming level and thus provides programmer with all the power of X Window. Higher level application development environment, such as OSF (Open Software Foundation) Motif Toolkit, is not chosen since it is a source code licensed software package. Xlib source codes are free but Motif source codes are not publically available.

4.1.1   Exclusive and Non-Exclusive Processes

The SunOS is not a real-time operating system. Due to its multi-task feature, the "continuous mode" operations of the SUN M-WIP system are divided into two categories: the exclusive processes and non-exclusive processes.

The *exclusive processes* are operations which must be performed alone, without any other time consuming process running at the same time. For example, during calibration or measurement procedures that request relatively precise [1] sampling rate, we should block the execution of other operations. The *non-exclusive processes* are those operations that can be performed concurrently. For example, while the system

---

[1] Since there are always some other processes, such as the system processes and the X server, we can never make the M-WIP operation the only one process which takes all the CPU time.

is reading and displaying thermocouple data, one can grab an image and process it, if the sampling time interval is not critical.

In the SUN M-WIP system, the event-driven loops are hierarchically assigned into two levels. The first level, or the top level, contains one loop which handles the events that start the operations when the buttons in the main menu are clicked. It also handles the non-exclusive process events which occur during the interactive dialog in the execution of a non-exclusive processes and the events to stop a non-exclusive processes. The second level, or the bottom level, contains one loop for each exclusive process. Whenever a second level loop is entered, it will never return the control to the first level loop until the corresponding operation is finished or stopped. Thus other processes are prevented from execution.

Non-exclusive processes are child processes generated by the *fork()* system call and they can be stopped by a first level event. During the execution of a non-exclusive processes, any other non-exclusive processes and/or an exclusive process can be started.

An exclusive process will block all the first level events. Although the running non-exclusive processes will not be stopped, no more non-exclusive processes can be started until the exclusive process is completed.

All the "one-shot mode" tasks are controlled by the first level events but would not return control until the operation is completed.

4.1.2 Xlib Menu-Driven Interface

The X Window System is a network-oriented graphics windowing system that was developed at MIT in 1984. Several versions of X have been developed since then, and the most recent of which is the popular X Version 11 (X11), first released in 1987. X11 has been adopted as an industry standard windowing system and supported by nearly every workstation manufacturers.

Using X11, applications can be written for an entire class of machines rather than for a single manufacturer's equipment. Applications can also run in a network of systems from different vendors.

X is a network-oriented system which employs the server-client model [39]. A *server* is a program that controls each *display*, which is defined as a workstation consisting of a keyboard, a pointing device such as a mouse, and one or more screens. It acts as an intermediary between user programs (called *clients*) running on either local or remote systems and the resources of the local system (display). Clients communicate with the server by means of calls to *Xlib*, a low-level library of C language routines. As an interface to the X protocol which makes up each packet of information that gets transferred between the server and clients in both direction, Xlib provides functions for connecting to a particular display server, creating windows, drawing graphics, responding to events, and so on.

X is an event-driven system which must be ready for any of the many different events at any time [40]. Events (such as key press, mouse click, window exposure, etc.) are received in order and then the program branches according to the type of the event and performs the appropriate response. Unlike traditional UNIX programs where the program is in control, the user is in control most of the time in X programs. This makes it natural to let user tell the program what to do instead of vice versa.

No other applications has higher priority than the SUN M-WIP due to the limited resources of the display, mainly screen space and colormaps. The final version of the SUN M-WIP operates like a stand-alone equipment which is controlled by an operator through the mouse. Thus the SUN M-WIP window-based interface occupies the whole screen, and specifies its own custom colormap that are not shared with any other applications.

The interface of the SUN M-WIP was designed to have fixed size and fixed position sub-windows so that window exposure events can be easily handled and

the requirement of the inefficient redrawing (when an obscured portion of a sub-window is exposed as another overlapping sub-window is moved, closed, or resized) is reduced to minimum. This also makes the window hierarchy and event selection simple. Based on this simplified window hierarchy, no event propagation is necessary in the SUN M-WIP application.

For example, in the SUN M-WIP application, a function is needed to allow operator to draw an arbitrary non-destructive overlapping line on the displayed image. The intensity profile along the line is then plotted automatically. To draw/redraw a line while making sure that the original image is recoverable, tricks such as rubber-banding technique are played. With the help of logical operation $GXxor$ and plane mask, the line, as a temporary graphics, can be erased without erasing other things already drawn in the image display sub-window. When drawn twice, the line disappears, and leaves the image as it was initially. For the 8-bit plane, ($Depth = 8$), plane mask takes 1 bit, and the other 7 bits are used to define custom colormap according to the pseudocoloring scheme.

4.1.3   NoteBook Iconic Interface

Computer-based data acquisition and control has made a historical progression from self-programmed systems to menu-driven software, and then to icon-based programs. NoteBook provides an easy-to-use visual context programming environment for application building [41]. It allows user to view, configure, and manipulate even the largest setups easily with a few clicks of a mouse. User can setup the system and program the interface without typing any commands. Instead, the programming procedure follows only three basic steps:

1. Click on the Command Menus to get ICONview, a graphical interface,

2. Drag-and-drop the icons and connect them to configure the system, and

3. Use the Setup Menus to specify the setup parameters for the functions corresponding to each icon [2].

ICONview gives user a picture of the application, showing the relationships and data flow between NoteBook functions.

NoteBook provides a Thermocouple Block which completes the following three steps when thermocouple measurement is performed:

1. Samples the low-level voltage created by the thermocouple,

2. Samples the cold junction reference on the hardware interface, and

3. Performs a polynomial linearization on the compensated thermocouple voltage and records the result in the temperature units specified in the setup menu.

Since NoteBook has to loop these steps for each reading, a Thermocouple Block cannot be sampled as quickly as an Analog Input Block. In the SUN M-WIP system, a linearized thermocouple input module is used to have the compensation and linearization done by hardware. The module filters, isolates, amplifies, linearizes the thermocouple input and converts it to a high-level analog voltage (0 V to 5 V). Therefore data can be collected from a thermocouple at higher sampling rates by using an Analog Input Block. The Scale Factor and Offset Constant options of the Analog Input Block allow us to convert data from voltage to temperature as the following

$$Temperature = (Voltage + OffsetConstant) * ScaleFactor \qquad (4.1)$$

where $OffsetConstant$ and $ScaleFactor$ can be obtained by calibration. A Calculated Block that performs polynomial $POLY(X)$ or calibration $CAL.E(X)$ can also be used to give better accuracy.

---

[2]Although setup parameters usually can be entered right on the Setup Menus, sometimes a disk file might be needed for some Calculated Blocks which requires many parameters, such as the coefficients for polynomial.

The highest sampling rate that NoteBook supports is determined by the maximum throughput of the PC and maximum sampling rate of the data acquisition board. When there are more than one function blocks in use, the highest sampling rate for a block in the setup is limited to the fastest sampling rate divided by the number of blocks. In the SUN M-WIP system's 386 PC-based LabTech subsystem, the setup has 32 function blocks, and the highest sampling rate is 70 Hz.

4.2 Special Hardware Interface

The SUN M-WIP has several special VME bus components in addition to the traditional SUN workstation devices. These hardware components must have their device drivers built into the kernel of the SunOS. The device drivers act as an interface programs. Utility and function libraries are also needed to setup and access these special hardware components.

4.2.1 MaxVideo Board Programming

Device drivers and utilities for MaxVideo board programming is included in Datacube's ImageFlow software package. When the ImageFlow is installed, system file which holds system configuration information is upgraded, and device driver is built into the kernel [42].

ImageFlow allows users to use a text file to describe the specific configuration of all MaxVideo IP devices in the application system. This configuration file documents which devices are in the system, what their based addresses are, how their jumpers are set, and the configuration of MAXbus cables which interconnect the devices.

In the application programming, the following basic steps should be taken.

1. Create the system according to the configuration file,

2. Get IP device handlers which is used to identify the particular IP in subsequent calls to ImageFlow functions,

3. Setup attributes of IP devices and configure the internal switches for each of the devices,

4. Define data surfaces which are objects where 2-D images input/output and storage performed,

5. Build, arm and fire pipeline which manages data stream,

6. Perform image processing functions where data surface accessing and pipe event handling may be necessary, and

7. Halt the pipeline, dispose the surfaces, and close the system before exit the application.

ImageFlow does not have development tools included. Run time debugging is performed using GNU tool **gdb** or **xxgdb** (a X Window graphical interface to the **gdb** debugger).

4.2.2 DATEL Board Programming

Both DVME-660 (48-line digital I/O board) and DVME-624 (4-channel 12-bit isolated D/A board) are used in the SUN M-WIP system. These DATEL boards are fully compatible with the VME bus and they are configured to appear as 256 bytes of location in the CPU's address space. They are short I/O devices which utilize the 16-bit addressing mode of the VME bus. The base address of the short I/O address space is typically mapped to addresses FFFF0000 to FFFFFFFF hex. Thus, base addresses of DATEL's boards are selectable only within the range of 0000 to FF00 hex. In the SUN M-WIP, base address of DVME-660's base address is C500 hex while DVME-624 is located at 7900 hex. DVME-624's output voltage range is set to 0-5 V.

Custom device drives for these boards are developed as they are not provided. From the device-independent view of the I/O hardware provided by SunOS, application programs see devices as if they were regular files, so that user processes can open, close, and manipulate devices by making *system calls*. The system calls provide the interface between user processes and the SunOS kernel, while the device drivers provide an interface between the kernel itself and its peripheral devices [43].

Devices are classified into several categories, and the DATEL boards are examples of so-called memory-mapped devices as they are mapped into user-process memory and then accessed directly. The DATEL boards were configured as *unstructured* or *character* I/O devices. DVME-660 is programmed as using all its 48-line as digital input channels by setting its Data Direction Register (based + 40 hex) as READ (all 0).

The device drivers should be built following the steps listed below.

1. Use mknod command to create a special file in /dev directory.

2. Put the register information for the device in the file /usr/include/sys/dxcmd.h,

3. Place actual C code for the driver in the file /usr/sys/sundev/dx.c,

4. Create a new config file in **/usr/sys/sun4/conf** by copying the current config file and add information about the addressing mode and base address of new device, (say dx), into the new file to reflect the presence of the new device.

5. Add entries to the end of the character device switch table *cdevsw* in file /usr/sys/sun/conf.c to specify the interface routines present for the device,

6. Run config and make to config and build the kernel, then substitute the old system with the new one, and

7. Reboot the system.

It is noteworthy that gcc compiler and cc compiler may have different macro _IOR and/or _IOW which are used in /usr/include/sys/dxcmd.h to define commands of ioctl. gcc's macro requires ioctl character to be used as 'd', while cc needs it to be d. Thus, conventional cc are used to make the kernel, and then compile the application with gcc, different "local" header file should be used.

4.2.3 Hydra Board Programming

The V-C40 Hydra is supplied with two independent "device drivers": VC40DSP and VC40MAP [44]. VC40DSP is a traditional UNIX device driver written for SunOS and it can be used as a "loadable" driver or directly configured into the SunOS kernel. VC40MAP is a library of routines that map the V-C40 Hydra's resources into a user program's address space. Since it does not provide the services of a traditional driver, such as handling interrupts generated by V-C40 Hydra, installation and configuration procedure is much simpler. In the SUN M-WIP system, the VC40DSP is installed as a configured device driver.

An utility library is provided that supports the SunOS device driver with functions for initialization, data transfer (between host and DSPs), and interruption. Data transfer between host and DSPs are performed by the V-C40 Hydra device driver on the host side and HydraMon (an EPROM-resident program that boots Hydra and allows it to interact with the host and the terminal) on Hydra side. When the host is reading/writing the local SRAM of a DSP, it requires HydraMon to transfer the data between the shared DRAM where the device driver can access it and the private SRAM where only the DSP can access it. Each DSP has a Command Parameter Block (16 Words) and a Data Transfer Area (1K Words) at fixed addresses in the global DRAM. When an access starts, the host

1. puts data into the DSP's Data Transfer Area if the request access is "write";

2. sets up the corresponding HydraMon command in the DSP's Command
   Parameter Block;

3. triggers the DSP's HydraMon interrupt; and then

4. polls the DSP's Command Parameter Block to wait for a return from the DSP.

   After HydraMon received the interrupt, it

1. reads the Command Parameter Block;

2. performs the requested operation (transfer data from DRAM to SRAM for
   "write" or vice versa for "read"), and then

3. overwrites the Command Parameter Block with a success, failure, or timeout
   code.

The host in turn acts according to the returned code from HydraMon and gets
the data from the DSP's Data Transfer Area if the request access is "read."

To perform data exchange between the host and DSPs, a communication
protocol is needed. When tasks share data, there are two kinds of synchronization,
cooperation and *competition* [45]. Cooperation is required between two tasks when
one of them must wait for the other to complete some specific activity before it can
continue its execution. Competition is needed between two tasks when both require
the use of certain resources that cannot be used simultaneously. In the SUN M-
WIP case, although host and DSPs share the same resource (Command Parameter
Block and Data Transfer Area), they have to wait for each other to exchange data.
Therefore, a cooperation synchronization is required, and a flag-based handshaking
approach is used to implement it.

Generally, a handshaking scheme has two nodes, a receiver and a sender. The
actual transmission, called *rendezvous*, can occur only if both the receiver and the
sender want it to happen. Two flags can be used to realize the scheme: one for

host to DSP transfer and another for DSP to host transfer. Each of the flags could have one of three states: "idle", "request", "acknowledge" and they are set to "idle" initially. In the flag-based handshaking scheme, it can always have one node, say the receiver, to start the transfer:

1. The receiver checks the flag and puts a "request" when it is "idle";

2. The sender checks the flag and waits until it gets the "request", puts the data in a buffer, and overwrites the flag with an "acknowledge";

3. The receiver waiting for the "acknowledge" then gets the data and resets the flag to "idle".

However, this simple approach can cause a problem. In the V-C40 Hydra, the address of a single buffer used for data transfer between the host and a DSP is assigned by the DSP, no matter which side is the receiver or the sender. When a host to DSP transfer occurs right after a DSP to host transfer starts, the host to DSP transfer (which assigns buffer address at the "request" step) may change the buffer address used by the DSP to host transfer (which assigns buffer address at the "acknowledge" step).

This problem can be solved by various methods, such as using a three-handshaking instead of two-handshaking, or using two common buffer pointers (one for host to DSP transfer and one for DSP to host transfer) instead of one. In the SUN M-WIP system, the problem is solved by modifying the handshaking scheme so that instead of having the receiver to start the transfer, the DSP will start the transfer no matter it is the receiver or the sender. Now the handshaking scheme becomes very similar to the one used between the host and HydraMon:

1. The DSP checks the flag, puts a "request" only when it is "idle", assigns the buffer address, and puts the data if it is the sender;

2. The host checks the flag and waits until it gets the "request", puts/gets the data into/from the buffer if it is the sender/receiver, and overwrites the flag with an "acknowledge";

3. The DSP waiting for the "acknowledge" then gets data if it is the receiver and resets the flag to "idle".

4.3 Functions and Experiments

A number of functions have been developed for the operation of the SUN M-WIP computer system. Using the procedures provided by the SUN M-WIP, experiments have been conducted for data acquisition, image processing, radiometric measurement, and process control.

4.3.1 Data Acquisition and Display

Real-time images from the IR-CCD camera can be acquired, corrected, and displayed in pseudocolor. Individual frame can be captured, stored, processed and displayed by the host computer. An arbitrary cross section of the image can be selected interactively and its profile displayed automatically for off-line radiation (temperature) distribution analysis. Figure 4.1 shows two ramp test patterns captured by the system.

A real-time implementation of a two-point non-uniformity correction algorithm for the IR-CCD camera was developed to compensate for the fixed pattern noise which limits camera sensitivity. The experimental results of this flat field correction procedure results in more than six fold spatial non-uniformity reduction [46].

A new scheme for thermal image pseudocoloring was proposed based on Bézier/Bernstein blending function [47]. Colormap bar-chart and cross-sectional (column-wise and row-wise) intensity plots of the image is displayed in real-time on the RGB color video monitor along with the pseudocolored live video.
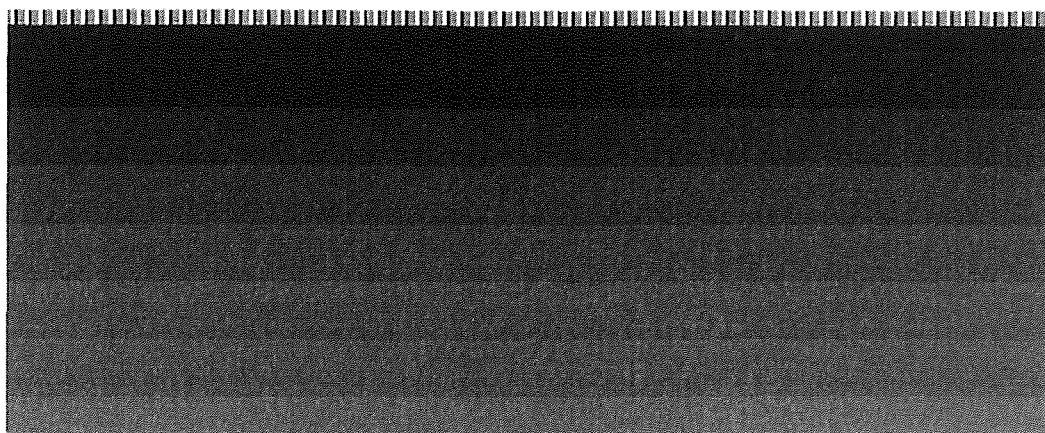
(a) Test Pattern 1
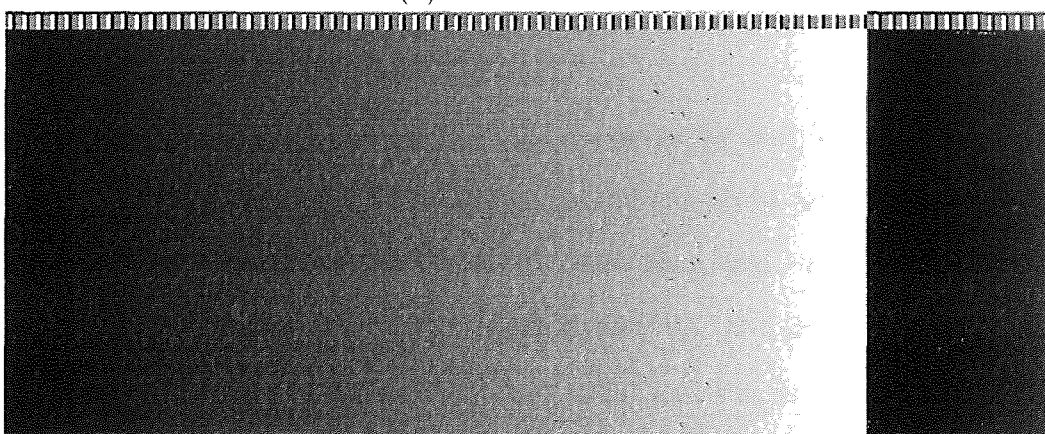
(b) Test Pattern 2

Figure 4.1 Test Patterns

Using techniques such as histogram equalization and histogram projection [48], a captured 12-bit intensity image can be converted to 8-bit image for display on the color graphics monitor of the host computer. The 3-D graphical representation of an image can also be plotted in either grayscale or pseudocolor to explore the global uniformity information. Figure 4.2 shows an example image and its corresponding 3-D graph. The object is a 6-inch silicon wafer illuminated by the tungsten-halogen lamp source at the center of the RTP chamber.

The system was calibrated against a commercial blackbody reference source. A set of pixels corresponding to the test points can be selected interactively by the system operator. Figure 4.3 is a blackbody image captured during calibration procedure with seven stripe filters assembled in front of the detector array.

Thermocouple values and profiles can be acquired, stored, and displayed by both the host computer and the PC.

4.3.2   Parallel Processing and Control

Based on the parallel processing facilities provided by the V-C40 Hydra, both SPMD and MPMD versions of the temperature and emissivity measurement software package were developed and their speedups were compared. Experimental results demonstrated that with the SPMD method and the V-C40 Hydra, 3.95 times speedup can be achieved over using a single DSP and this is close to the optimal speedup of four. In contrast, using four TMS320C40 DSPs and the MPMD method, approximately three times improvement in execution time can be achieved over using one DSP. The SPMD and MPMD speedup curves are shown in Figure 4.4.

Parallel least-squares fitting procedure for M-WIP temperature measurement is a data parallelism where the same operation is executed over a large array of operands. This is the reason that SPMD approach for M-WIP becomes possible and provides a higher speedup than the MPMD method.
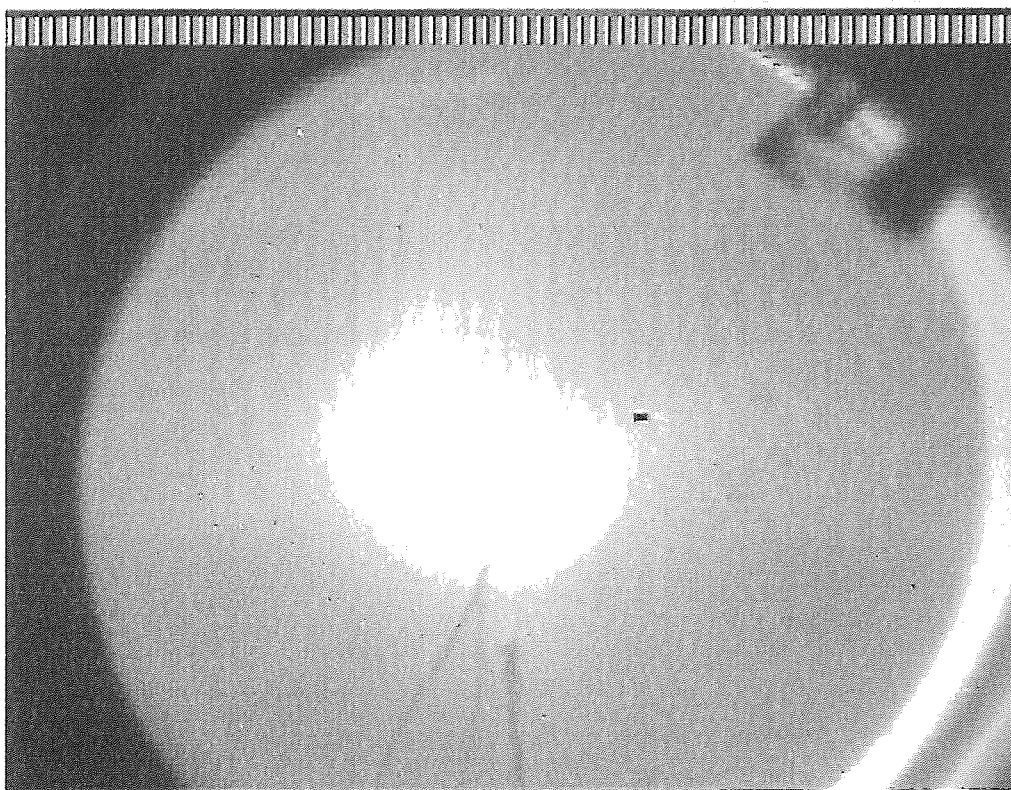
(a) Original Image
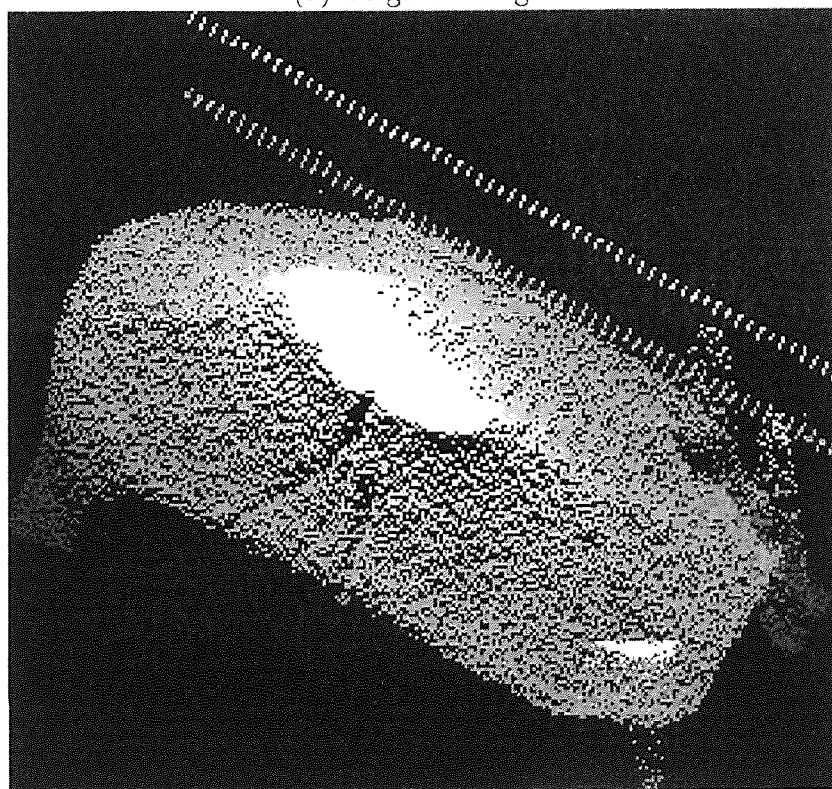
(b) 3-D Graph

Figure 4.2 Wafer Image and 3-D Graph
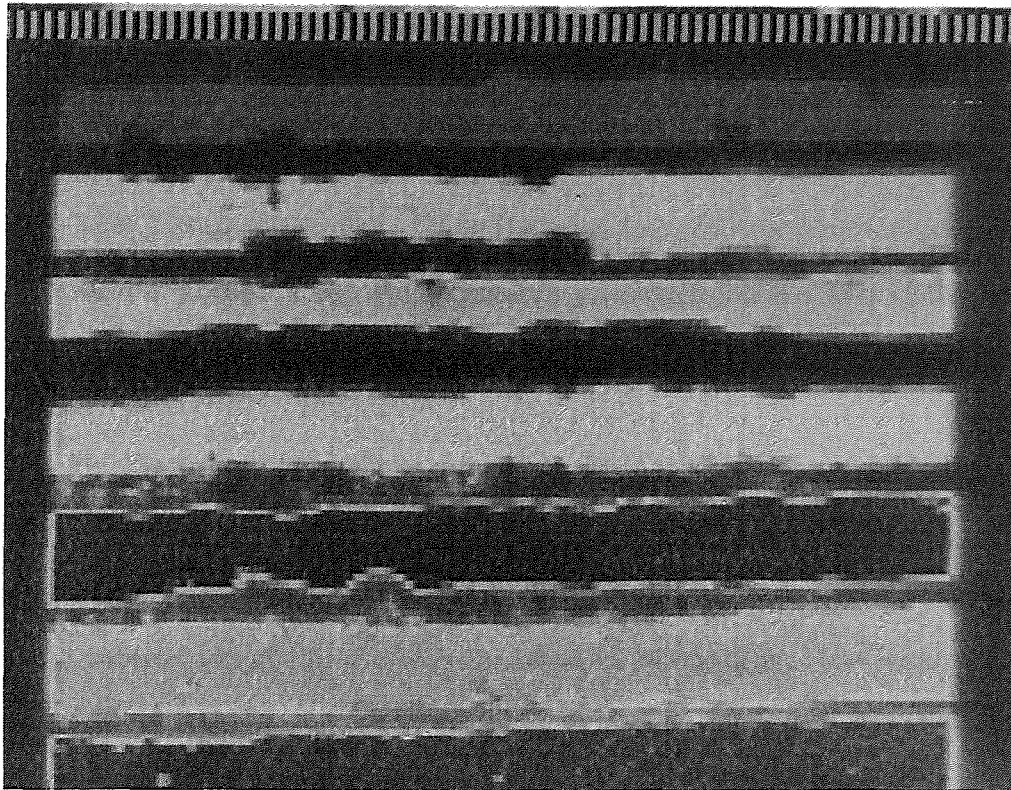
Figure 4.3 Stripe Filters
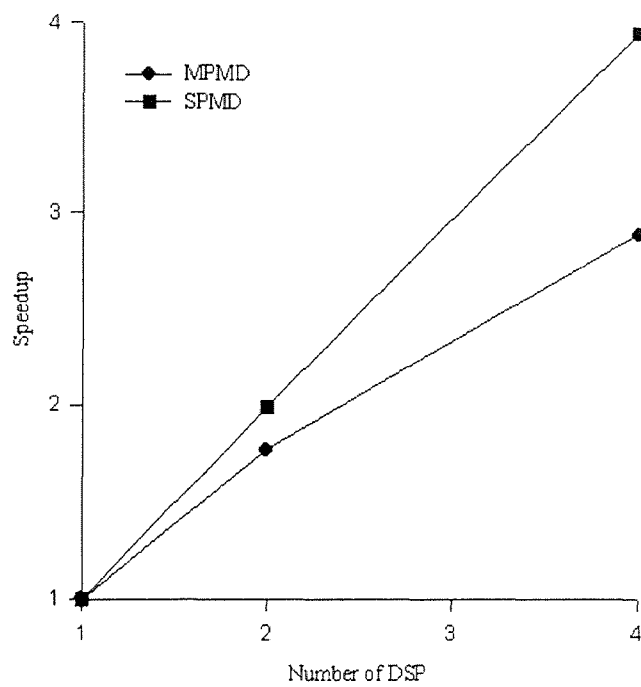
Figure 4.4 Speedup of SUN M-WIP

Experimental data obtained by the control subsystem have been used in RTP system modeling and design. To achieve adaptive multi-variable feedback control of the RTP system, real-time parameter estimation of the dynamic model for RTP radiation heat transfer is needed. Using the open-loop control function provided by the SUN M-WIP computer system, parameter estimation results were obtained [49].

4.3.3 SUN M-WIP Operations

The image processing procedures for SUN M-WIP operations include spatial averaging (typically, eight-neighbor averaging), temporal filtering (typically, sixteen frame averaging), subtraction of background corresponding to certain integration time, and subtraction of the overscan for offset compensation. The resultant pixel values can be recorded for different sampling time interval and duration, and their statistics are computed for further analysis.

Data from the electronic imaging subsystem were collected in experiments, and a kind of spark noise was found. It is a positive additive noise, and it occurs randomly in the time domain. The noise swings the signal toward the saturation by a large quantity as shown in the Figure 4.5 (a). The noise is about half of the background signal.

To remove the effect of the spark noise, median values are used instead of the mean values. The median filter is a signal pre-processing step before time domain averaging is used to reduce the shot noise. Figure 4.5 (b) shows the background data plot without the spark noise and the median value of all the data including the noise.

In the experimental SUN M-WIP, a square sheet of indium is placed over the photon-sensitive area to cover half of the imager. The original objective of placing the indium plate was to use data obtained from the covered part as dark current measurement. Figure 4.6 (a) and Figure 4.7 (a) show the signal data plots of a uncovered pixel and a covered pixel, respectively. Figure 4.6 (b) and Figure 4.7 (b)
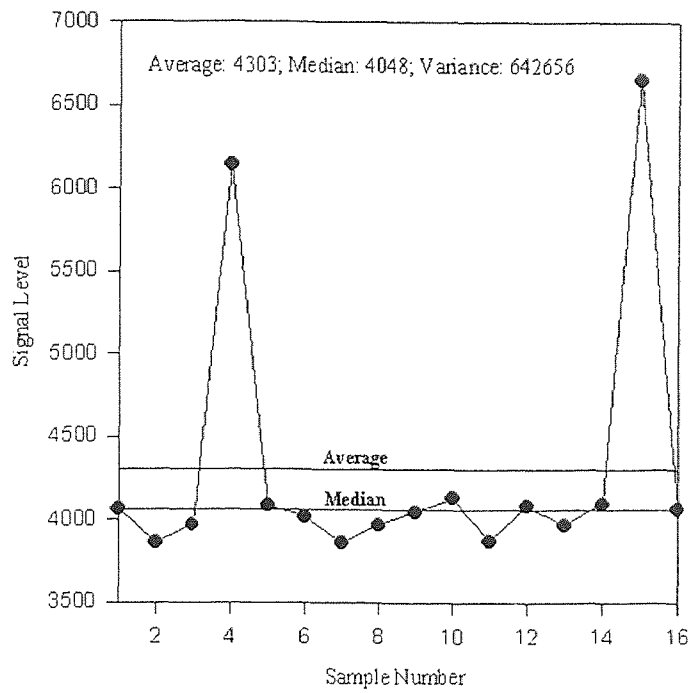
(a) Average or Mean Picks Up Spark Noise
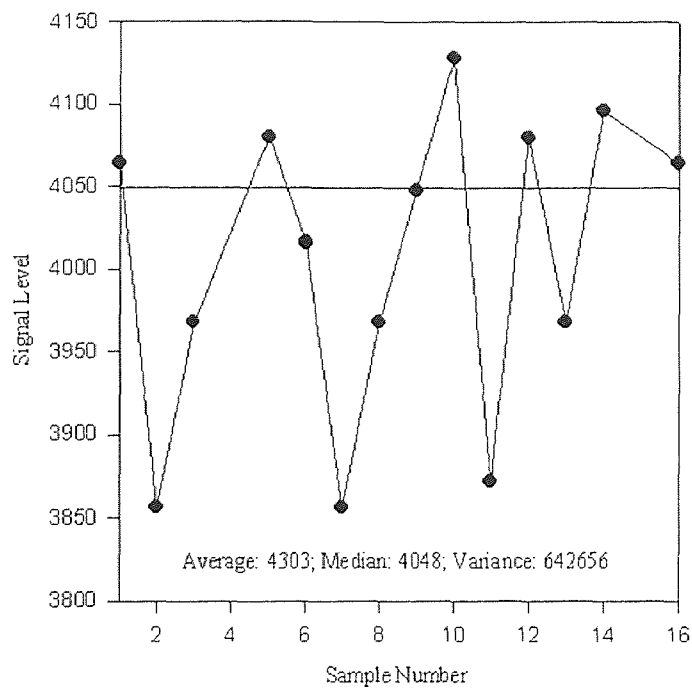
(b) Median Filter Removes Spark Noise

Figure 4.5 Background Data Plot

show the background data plots of the two pixels, respectively. Figure 4.6 (c) and Figure 4.7 (c) show the data plots of the results after background has been subtracted from the signal.

For the uncovered pixel, when the signal level is close to the saturation (at signal level 65535), the relationship between signal level and integration time shows irregular shape. To avoid curve fitting errors induced by the saturation, an upper limit to the signal level is used to cut off the undesired high signal level portion. Figure 4.6 (c) shows the result of using an upper limit at signal level 50000.

Ideally, the covered pixel should have a different characteristic from the uncovered pixel since it is not affected by temperature variation of the object under study. However, the resultant data plot of the covered pixel shows that the signal level increases as the target temperature goes up. This means that either the indium cover is not totally opaque to the infrared radiance or the whole imager is heated up by the incoming infrared flux from the uncovered part.

Figure 4.8 shows the data plots of a few pixels on one filter, and Figure 4.9 shows the data plots of one point on the scanning line. Both of these figures were obtained at integration time 16 (0.13312 sec). In Figure 4.8, it is clear that each pixel has to be calibrated separately because of the presence of the spatial non-uniformity unless non-uniformity correction is employed in the uncovered region of each filter stripe. In Figure 4.9, it can be seen that at room temperature background, spectral response increases along the filter number corresponding to increasing wavelength in the MWIR range.

Using the computer system, the relationship between the non-linearities and the integrated charge signal level was found during testing. This result allows us to model the dark current charge and charge trapping loss in the presence of optical signal. Also, subtracting black level measurements by using the output level during horizontal blanking (overscan) from input signal was found to be very effective in
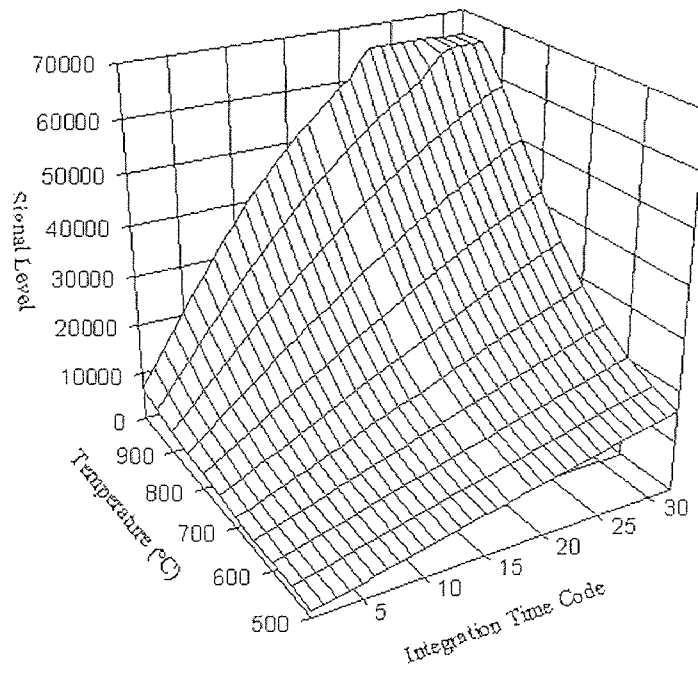
(a) Signal Data Plot
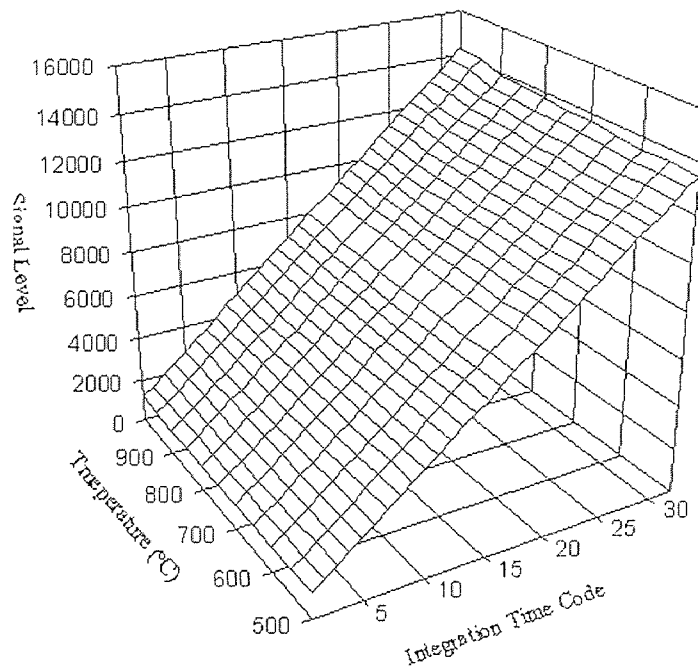
(b) Background Data Plot
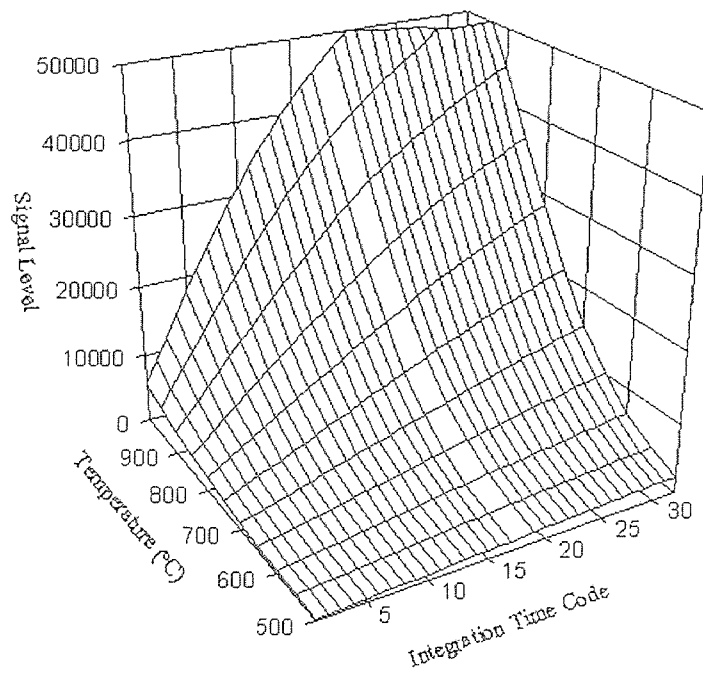
(c) Resultant Data Plot

Figure 4.6 Data Plots of Uncovered Pixel
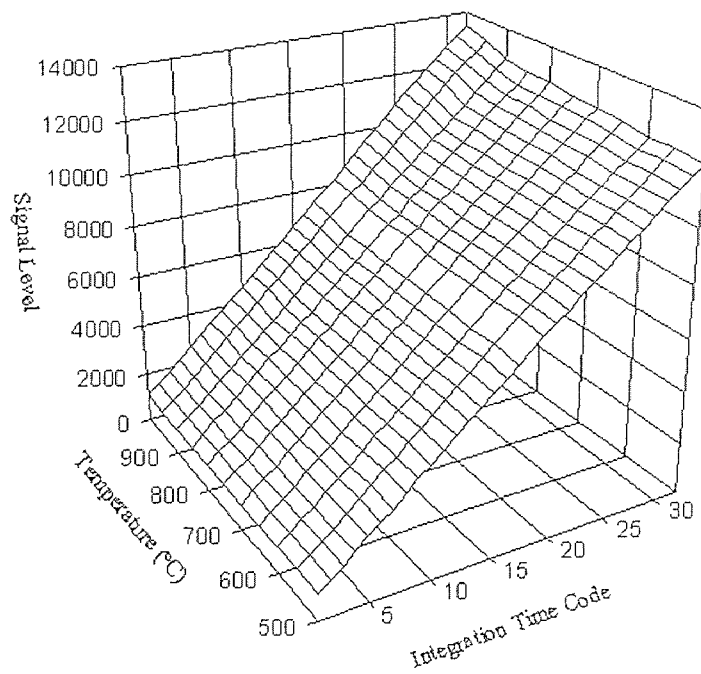
(a) Signal Data Plot
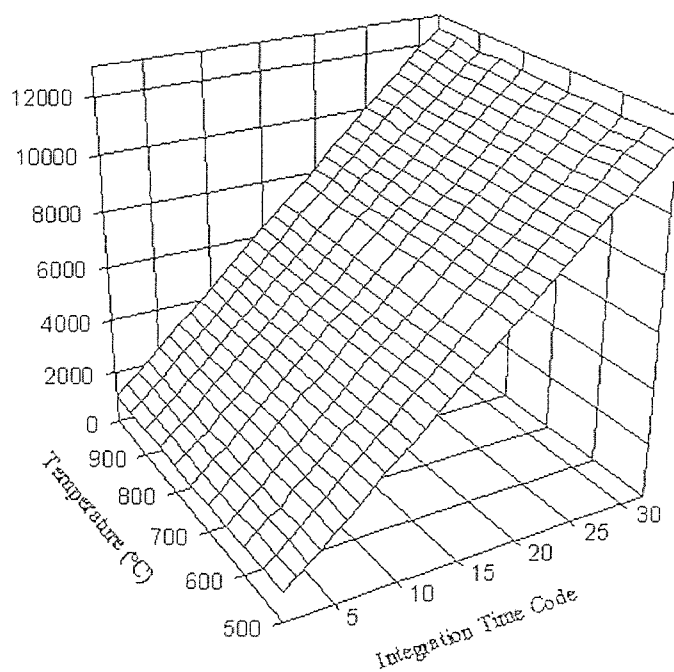
(b) Background Data Plot
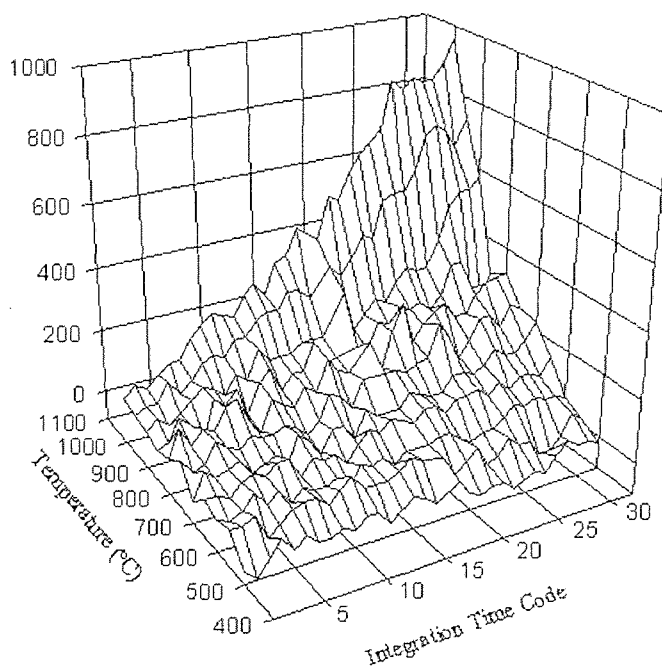
(c) Resultant Data Plot

Figure 4.7 Data Plots of Covered Pixel
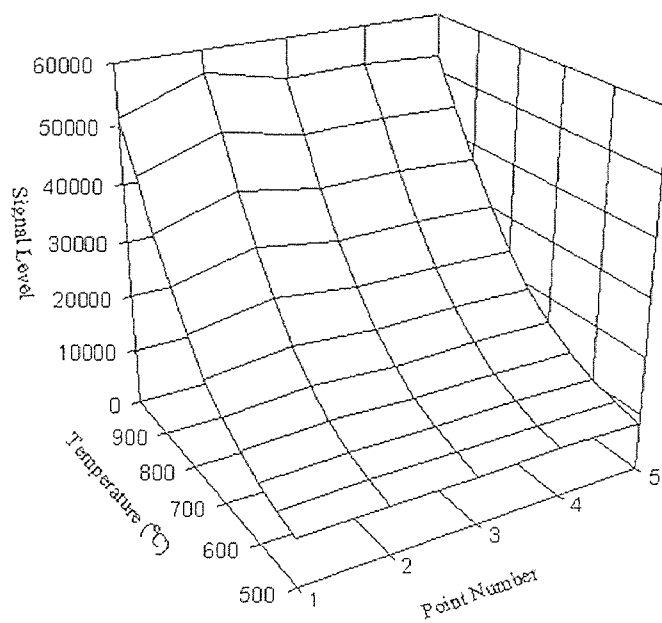
(a) Signal Data Plot
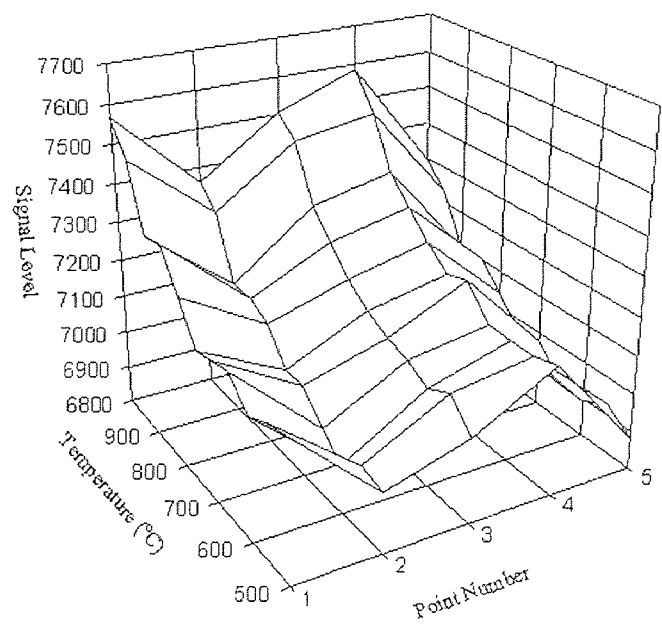
(b) Background Data Plot
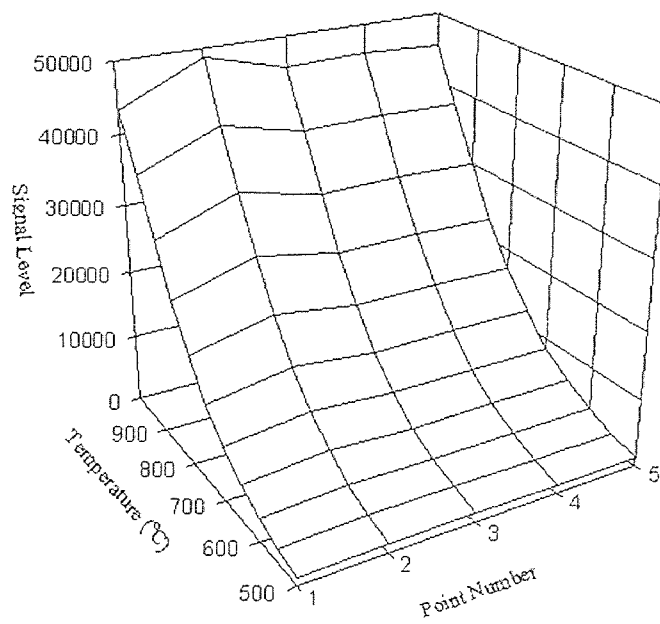
(c) Resultant Data Plot

Figure 4.8 Data Plots of Pixels on One Filter
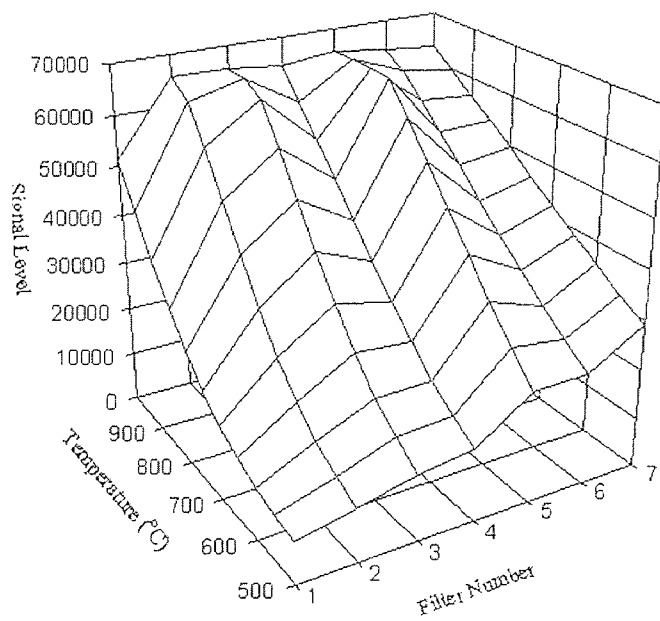
(a) Signal Data Plot
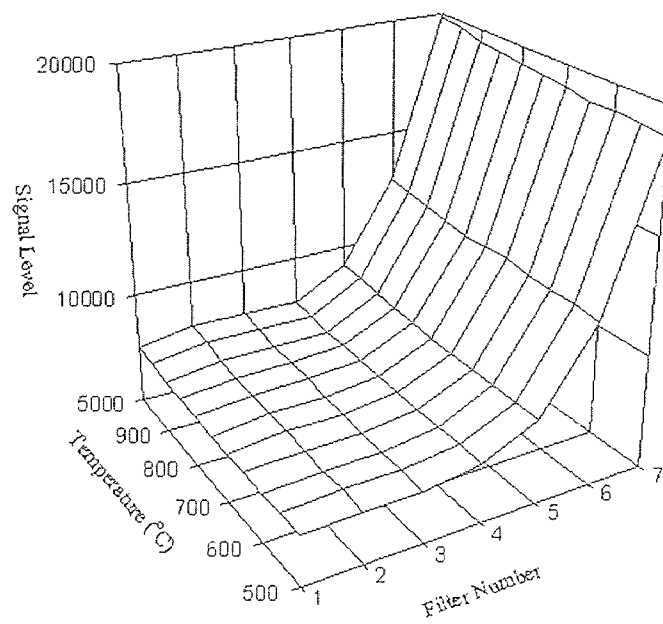
(b) Background Data Plot
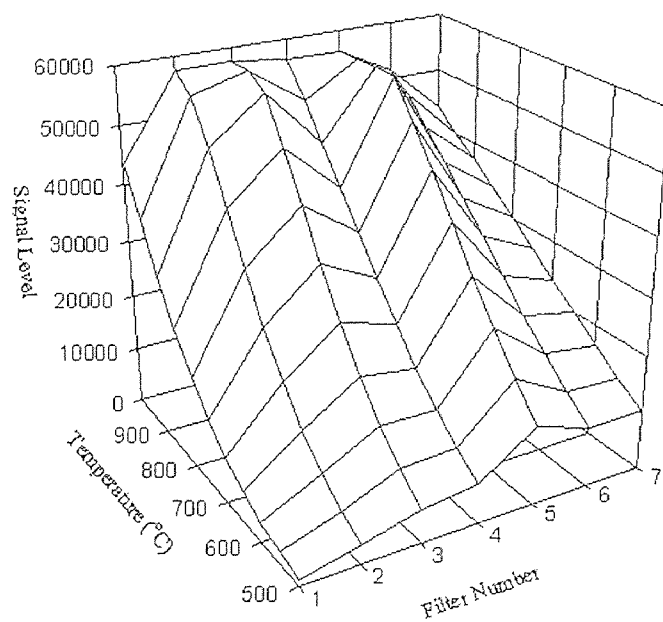
(c) Resultant Data Plot

Figure 4.9 Data Plots of Filters for One Point

reducing the effects of power supply fluctuations. After applying background and dark current correction, temperature measurement of the blackbody source demonstrated a temperature resolution of $\pm1°C$ [50]. Temperature measurement accuracy of $\pm4°C$ was achieved against simulated object with spectrally varying emissivity [51]. In this experiment, a double-polished silicon wafer with unknown spectral transmissivity was placed in the optical path between the blackbody source and the IR-CCD camera to simulate object with unknown spectrally varying emissivity.

CHAPTER 5

PC M-WIP: SYSTEM INTEGRATION

As described in Chapter 1, the PC M-WIP is designed to prototype a cost effective M-WIP with the $320X240$ uncooled microbolometer camera which is to be provided by Inframetrics, Inc. However, due to delay in the delivery of the camera, the PC M-WIP computer system is tested and demonstrated with a thermoelectric camera which has compatible capability.

5.1   Host PC

The host PC has a 166 MHz Pentium CPU and a Intel mother board with built-in sound blaster. The mother board has 3 PCI slots, 3 ISA slots and 1 PCI/ISA slot.

The PC M-WIP design is simplified mainly because of the newly developed PCI (Peripheral Component Interface) bus technology. The advantages of using devices on PCI bus in imaging include but are not limited to

- The PCI bus has a capacity of 132 MB/sec.

  This number is a theoretical rate derived from the bus running at 33MHz, and being 4 bytes wide. There is a difference between sustained and theoretical rates. Frame grabbers can sustain lower than 132 MB/sec, say 120 MB/sec. However, this is already much higher than the highest possible rates of the ISA (Industry Standard Architecture) bus (the original 16-bit PC/AT bus). This type of PCI bus based devices is also supplanting those based on EISA (Extended Industry Standard Architecture) or VESA (Video Electronics Standards Association) bus in machine vision applications.

  The PCI bus based image capturing board requires fewer expensive memory chips, thereby simplifying the circuitry and software protocols while expanding and accelerating data transfer rates.

84

- The PCI bus de-couples data transfer devices from the CPU and its memory. DMA bus master capabilities of the PCI bus based devices make it possible to have data transfer done simultaneously while the host is handling other processing tasks.

- The PCI bus supports plug-n-play (PnP).

  The PCI specification calls for add-on peripherals to automatically "announce" their presence during boot-up to the system, and the system "finds" a non-conflicting I/O address and IRQ for it. This process eliminates conflicts that previously prevented smooth integration of add-ins.

5.2 Thermal Imaging

This subsystem, or simply the frame grabber, performs thermal imaging in the PC M-WIP system. It plays a similar but simpler role comparing to the MaxVideo subsystem in the SUN M-WIP.

5.2.1 Requirements for Frame Grabber

For a system to have a good image capturing performance, the following should be provided by the frame grabber [52]:

- The frame grabber should be a PCI bus based equipment.

- The frame grabber should be programmable. Specifications such as data transfer rate (typically at least 12 MB/sec for high-bandwidth imaging applications), data resolution (usually 8-bit or 12-bit, barely 16-bit digital camera) should be software setable to allow possible changes in bandwidth.

- The frame grabber should be memory mapped. In the case of real-time application, memory mapped board is probably faster than DMA. If using on-board
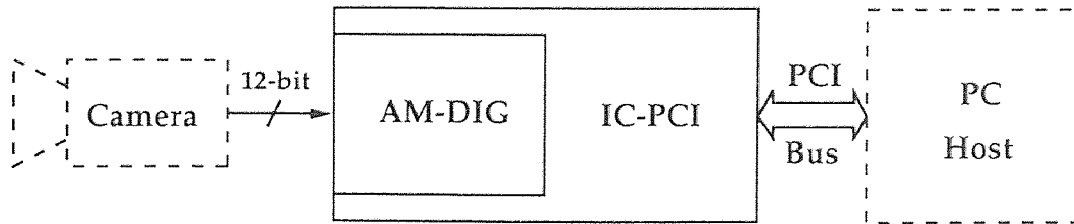
Figure 5.1 Frame Grabber Configuration

memory, dual-ported memory is preferred since it enables the simultaneous streaming feature.

- There should be a complete software package which provides user the ability of setting and accessing the board under the operating system which is being used in the software development.

- Other features that are useful if available, such as tools for image processing and analysis.

5.2.2 Frame Grabber Specifications

The frame grabber used in the PC M-WIP system is an Image Capture PCI (IC-PCI) board which has up to 4 MB high speed dual ported linear mapped video memory [53]. The IC-PCI can act as a PCI bus master, and its features include integration control, clock I/O control, and $16X16$ LUT. Image capturing is done by the DIGital Acquisition Module (AM-DIG) which can handle 16-bit differential RS-422 video input up to 20 MB/sec effective throughput. Its programmable window generator allows acquisition of the valid video portions of the camera image. During the acquisition, an image is captured and loaded into AM-DIG's line FIFOs at the frame rate of the camera. The IC-PCI receives the data unloaded from the FIFOs and puts the image in its frame memory at a rate up to 20 MB/sec. Figure 5.1 is a block diagram of the frame grabber configuration.

IC-PCI frame grabber has a memory system running at 120 MB/sec. Its bus interface is capable of interfacing to the frame grabber memory at 120 MB/sec, and to the PCI bus at the full theoretical rate of 132 MB/sec. This allows the IC-PCI to sustain 120 MB/sec transfer rate on to the PCI bus.

Special circuitry of IC-PCI automatically de-interlaces the image on-the-fly. In this manner, data can be direct memory accessed one frame at a time, instead of one line at a time. This greatly reduces the overhead of the CPU for each transfer. Special circuitry in the address generator allows AOI (area of interest) to be transferred out of memory at full speed, without the need to write any special code.

IC-PCI conforms to the PCI PnP specification. Display is done completely by the host display processor. Data is transferred out of the IC-PCI over the PCI bus to the memory on the display card or to the host memory.

IC-PCI and AM-DIG are programmable for acquisition control. Video format (such as pixel size, image size, interlaced/non-interlaced, etc.) must be set up prior to image acquisition.

5.3 Data Acquisition

Real-time systems are characterized by their ability to perform data acquisition and/or control task within an appropriate time window. How fast such a system must respond depends upon the speed and accuracy requirements of the given application. Since the analog input channels for the thermocouple measurement and the digital output channels for camera control require no faster than frame rate, and the response time of thermocouples is generally slow, a low speed data acquisition board is sufficient for the PC M-WIP. Also, because the goal of the M-WIP system is to measure object surface temperature at an accuracy of $\pm 1°C$, inexpensive termination board can be employed.
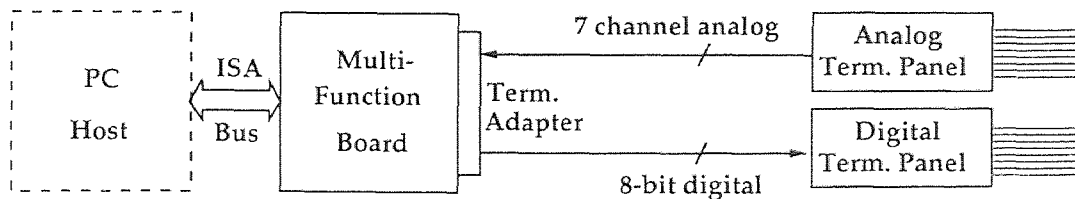
Figure 5.2 Multifunction Board Configuration

The data acquisition subsystem of the PC M-WIP replaces both the thermo-couple temperature value input system and integration time code output system in the SUN M-WIP, and thus reduce the cost of the system drastically.

5.3.1 Multifunction Board Description

Based on the requirements of the PC M-WIP system, the PCI-20428W-1 (Intelligent Instrumentation, Inc.) was chosen for data acquisition. Figure 5.2 is a block diagram of the multifunction board configuration.

PCI-20428W-1 is a low cost multifunction board on ISA bus [54]. It supports 16 single-ended or 8 differential analog input channels with software programmable gains 1, 10, or 100, and 12-bit A/D with up to 100 KHz throughput. It also provides 2 analog voltage output channels with 12-bit resolution and up to 100 KHz throughput. An 8-bit digital input channel, an 8-bit digital output channel, and a 16-bit counter are available for general use.

The multifunction board is an I/O mapped peripheral which occupies one 16 byte section of the host PC's I/O space. In PC M-WIP, the base I/O address of the PCI-20428W-1 is set to 0x0320. To make all the connections easy, a termination panel adapter PCI-20430A-1 is plugged directly into the back of the PCI-20428W-1 board.

5.3.2 Analog Input Channels

For the system calibration and performance evaluation of the PC M-WIP system, thermocouple readout is collected through the analog input channels which are set to

differential. Although PCI-20428W-1 provides 8 differential analog input channels, the first channel is occupied by cold-junction compensation (CJC). Therefore 7 channels are available for thermocouple temperature measurement.

A PCI-20303T-2 analog termination panel is connected to the PCI-20430A-1 via shielded analog cable assembly (PCI-20310A-1). The analog termination panel has a built-in CJC circuit connected to the first channel to support thermocouple inputs. There is a 0.8"X1.1" area for each of the remaining 7 channels to introduce additional thermocouple signal conditioning circuitry if necessary.

Most A/D converters perform best when their inputs are in the range of 1 to 10V. Therefore, many data acquisition products include an amplifier to boost low-level signals to the desired amplitude. Adding a fixed-gain amplifier increases sensitivity, but does not increase dynamic range. While it extends low-level sensitivity, it reduces the maximum allowable input level proportionally. PGA (Programmable Gain Amplifier) has several choices of gain, all under software control. It can increase the effective dynamic range of the system, but this technique is restricted to applications where the sample rate is slow enough to permit the time required for the auto-ranging function. In the case of PC M-WIP, auto-ranging is not necessary, but different gains for different channels are required.

Thermocouples (TC) are transducers used widely in industry and science to measure temperatures in the range of $-200°C$ to $+4000°C$. The output voltage is usually in the range of -10 to +50 mV and has an average sensitivity of 10 to 50 $\mu V/C$, depending upon the metals used. However, the output voltage is very nonlinear with respect to temperature. The CJC used on PCI-20303T-2 is LM335 (National Semiconductor, Co.). Its output voltage V (mV) is

$$V = T \pm 1K \qquad (5.1)$$

where T (K) is the room temperature, $273K < T < 298K$.

In the PC M-WIP, the input voltage range is set to $\pm 5V$ for all 8 channels. The gain for the seven TC channels is set to 100, and the gain for the CJC channel is set to 10. The non-linearity and other noise of the temperature reading can be corrected by the host PC using conventional signal processing algorithms. PC M-WIP uses a piecewise linear approximation which conforms to the NIST tables within $0.05°C$.

5.3.3 Digital Output Channels

The 8 digital output channels of the PCI-20428W-1 board are used in camera control. Integration time code (8-bit for 256 different integration time) can be sent to the camera via a PCI-20305T-1 digital termination panel which is connected to the PCI-20430A-1 by a ground-plane digital cable assembly (PCI-20311A-1).

The output digital signals are buffered TTL-level voltages. There is a 0.8"X1.1" area for each of the 8 channels to add custom signal conditioning circuitry when needed. Examples are optical isolation, control device, etc.

5.4 Parallel Processing

In the PC M-WIP system, PC-Hydra is used instead of the V-C40 Hydra employed in the SUN M-WIP system. The PC-Hydra board (Ariel, Inc.) is an ISA bus product which has four 50 MHz TMS320C40 Floating-Point DSPs on it [55].

5.4.1 PC-Hydra Description

PC-Hydra is a single ISA slot board with up to 2 MB of private SRAM or 8 MB of private DRAM for each DSP and 32 KB of dual-port RAM between host PC and DSPs. It supports up to 2.5 MB/sec high-speed block transfer. Host interrupt and flexible DSP communication port configuration are also supported. Figure 5.3 is a block diagram of the PC-Hydra structure.

As a quad-processor system, the PC-Hydra used in the PC M-WIP comprises a TMC-4 carrier card fitted with four identical TIM-40 modules. The TMC-4 provides
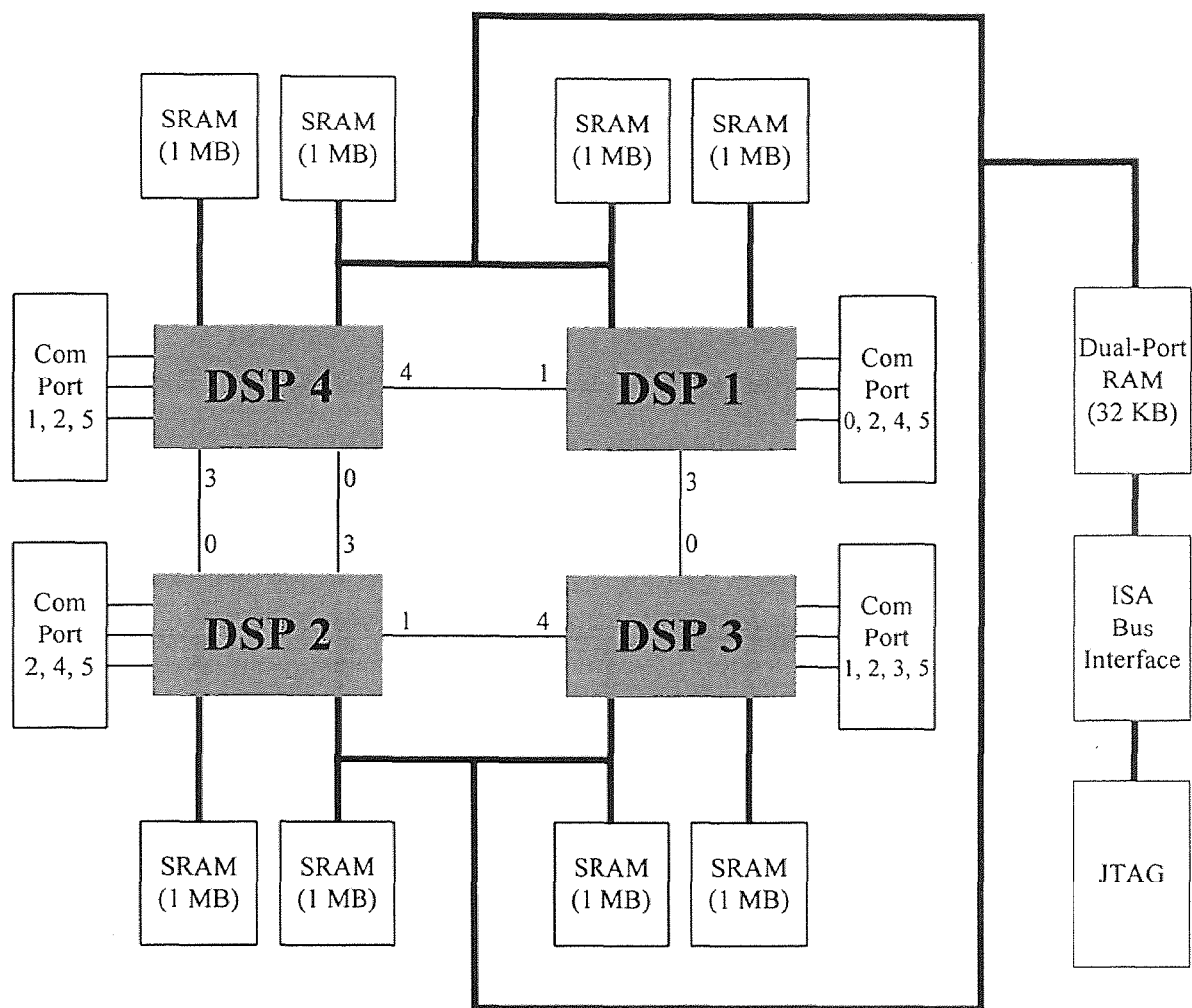
Figure 5.3 Block Diagram of PC-Hydra Board

ISA Bus Interface
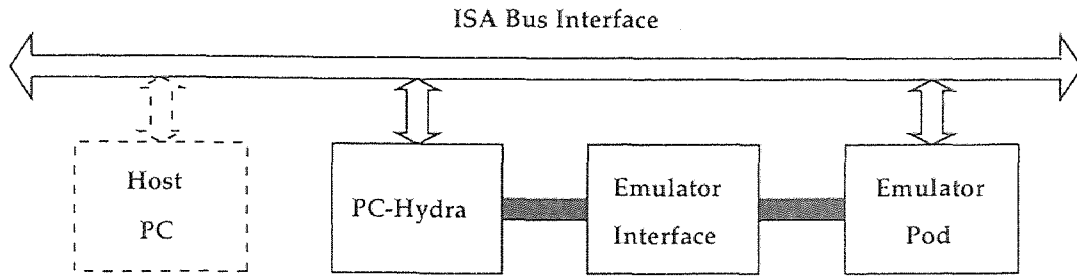
Figure 5.4 UXDS-PC System Configuration

resources including a bank of 8 Kwords (32 KB) of one wait-state dual-port SRAM for shared memory interface to the PC host, flexible local and non-local interconnection between module sites, and 128 KB Flush EEPROM for stand-alone applications. Each TIM-40SG module used in the PC M-WIP has a 50 MFLOPS TMS320C40 CPU, 2 MB zero wait-state SRAM configured as equal banks on the DSP's two memory buses, six 20 MB/sec byte-wide interprocessor communication ports, etc.

To provide programmer a powerful debugging aid, TI dedicated a portion of the TMS320C40 chip's silicon to debug circuitry and therefore gave TMS320C40 an innovative feature of JTAG SCAN Path port facility. There are basically two debugger alternatives available to the PC-Hydra: hardware/software debuggers (such as Ariel's UXDS-PC) that have their hardware emulators installed between an ISA bus interface board and the **JTAG in** header on the PC-Hydra board; software-only debuggers (such as Ariel's AXDS-PC) which access PC-Hydra's on-board JTAG Test Bus Controller over the ISA bus. In the PC M-WIP, an Ariel's UXDS-PC system is installed to support debugging. Figure 5.4 shows the diagram of the UXDS-PC system. Its hardware components includes an ISA bus emulator interface board, a JTAG interface cable and a emulator "pod". An AXDS-PC debugger is also installed, and both the UXDS-PC and AXDS-PC support multiple processor debugging.

Figure 5.5 PC-Hydra Inter-Processor Connection

5.4.2 PC-Hydra Configuration

The PC-Hydra is an I/O mapped peripheral and its base I/O address is set to 0x0340. Each inter-processor communication port of the DSPs can be either set to as an input port or an output port. Unlike the V-C40 Hydra used in the SUN M-WIP, the four DSPs of the PC-Hydra is not fully connected. Figure 5.5 is a block diagram of the PC-Hydra structure. The topology shown in the block diagram is set for the flood-fill bootstrapping. Obviously, a complete-connection can be easily made when its necessary.

5.5 Filter-Wheel Control

The PC M-WIP has an optical filter-wheel assembly to achieve area temperature profiling instead of the line-sensing approach implemented in the SUN M-WIP. The filter-wheel is developed by Dr. Timothy Chang and his students.

5.5.1 Filter-Wheel Description

The current filter-wheel has 12 filters. Shown in Figure 5.6, each filter is attached to the end of a graphite rod, and a round aluminium ring holds the rods which are evenly separated by 30 degrees. The ring is mounted on the axis of a rotary motor.

Figure 5.6 Filter-Wheel Configuration

The motor is controlled by an indexer and an encoder is used to acknowledge the actual motor position back to the indexer.

The P315X-H indexer [56] (American Precision Industries, Inc.) used in the PC M-WIP is a microprocessor based motion controller which has its own operating system, data storage and manipulation capabilities, and an interface for data communication with external computers. The stepper motor, 42D112-12C (American Precision Industries, Inc.) is an electromagnetic incremental actuator which converts digital pulses into mechanical rotation. The amount of rotation is directly proportional to the number of input pulses from the indexer, and the speed of rotation is relative to the frequency of the pulses. The encoder, Dynapar M20100003331 (Danaher Controls, Inc.), provides the indexer with position feedback.

5.5.2 Serial Port Communication

The indexer has a serial port for the communication with a PC using RS232 interface. The default baud rate is preset to 9600, no parity, 8 data bit, and 1 stop bit.

5.6 IR SnapShot Camera Interface

The IR SnapShot camera [57] is a commercial product of Infrared Solutions, Inc. The camera used in PC M-WIP system testing is a prototype of the IR SnapShot obtained from Honeywell Technology Center. Honeywell Technology Center originally developed the uncooled sensor and the prototype camera. Infrared
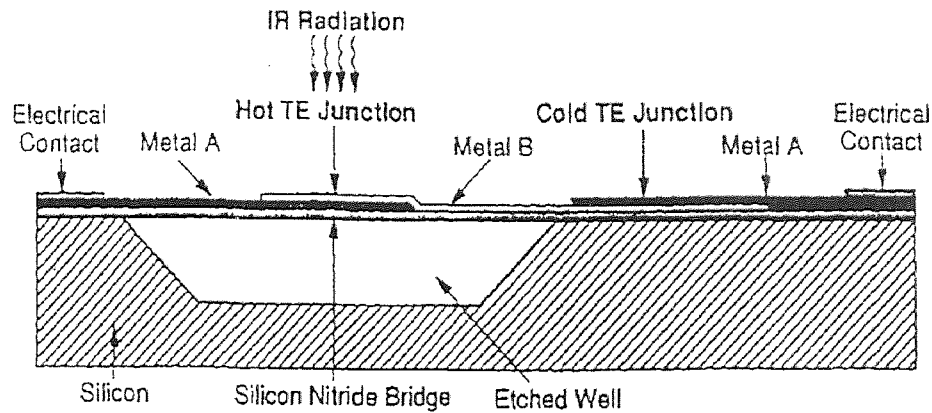
Figure 5.7 Thermoelectric Pixel Structure

Solutions optimized the camera and is commercializing the product using the sensors provided by Honeywell Technology Center.

5.6.1 Thermoelectric Line-Sensing Array

The IR SnapShot camera has a 96 pixel linear thermoelectric array as its imager. The array is manufactured based upon silicon microstructure technology [58].

Each pixel of size $150 X 150$ μm^2 and silicon nitride membrane extends across an etch pit in a silicon substrate. On the thermal isolation membrane structure, two metals are deposited in thin film form, providing the "hot" junction. A second junction on the silicon substrate and thereby heat sunk to the substrate provides the reference or "cold" junction. The pixel structure of a thermoelectric detector is shown as Figure 5.7 [58].

Each pixel consists of 30 series-connected chromel-constantan thermoelectric junctions. The pixel thermal response time, the ratio of pixel heat capacity to the thermal conductance of the pixel legs, is designed to be 0.75 msec.
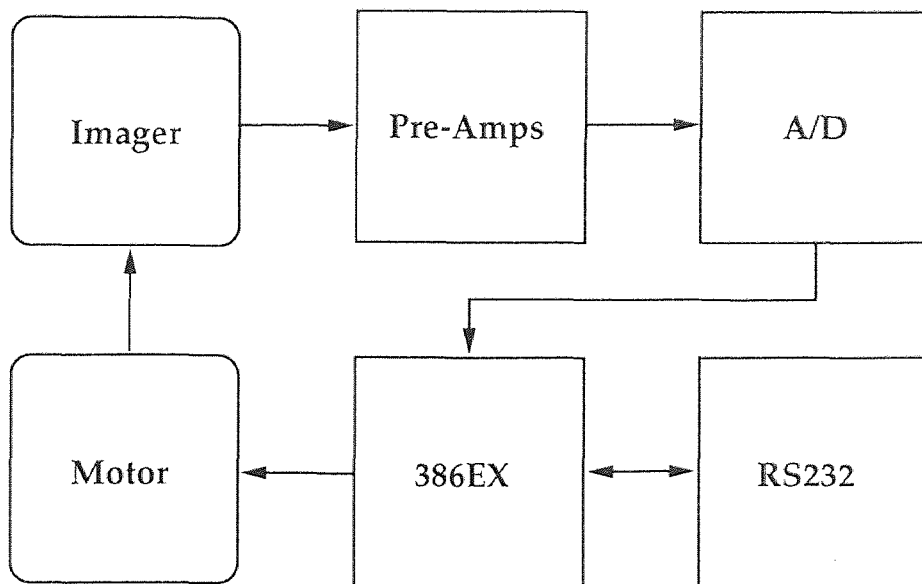
Figure 5.8 IR SnapShot Camera Configuration

5.6.2 IR SnapShot Camera

The IR SnapShot camera is an uncooled, handheld imaging radiometer designed primarily for the predictive and preventive maintenance market.

To reduce the system noise by limiting the system bandwidth [59], each pixel has its own pre-amplifier providing a gain of 4000. The output from a pre-amplifier is followed by an integrate and dump filter which integrates the signal for 0.8 msec. Each pixel is scanned for 1 msec.

The signals from the pixels are multiplexed and fed to a 16-bit A/D converter for digitization. The digital signals are processed by a 386EX microprocessor that in turn transfers the data out of the camera via a RS232 serial communication port on the camera. Figure 5.8 sketches the configuration of the SnapShot camera.

Due to the parallel nature of the pixel readout, the scan time of an entire array of 96 pixels is 1 msec for a stand-alone camera. However, communicating to the PC slows down the effective scan rate. Although the data transfer speed between camera and PC allows selection of standard baud rates up to 115.2 Kbps, the default baud

rate is only 38400. The serial port settings for the camera are no parity, 8 data bit, and 1 stop bit.

The prototype camera has a motor inside which horizontally moves the vertically positioned linear imager to obtain an 2-D image. The scan time is 1.44 sec plus 0.5 sec activation time. For the purposes of eliminating vibration induced by the mechanical motion and achieving fast scan. only the line scan mode of the camera is employed in the PC M-WIP system testing.

CHAPTER 6

PC M-WIP: SOFTWARE DEVELOPMENT

To convert the SUN M-WIP into a more cost effective PC M-WIP, hardware interface programs must be rewritten, user interface has to be reprogrammed, and parallel processing design modified.

6.1   Operating System

At the beginning stage of the PC M-WIP design, Linux was considered as the operating system since this will make it easier to port user interface software from the SUN M-WIP to the PC M-WIP. However, MS-DOS/Windows was selected eventually.

6.1.1   Linux

Linux runs mainly on 386+ PCs, using the hardware facilities of the 386 processor family to implement features like task-switching and memory management [60, 61].

- Linux has an advanced storage management paradigm.

  The Linux kernel supports demand-paged loaded executables therefore only those segments of a program which are actually used are read into memory from disk. Also, copy-on-write pages are shared among executables so that if several instances of a program are running at once, they will share pages in physical memory, reducing overall memory usage.

  In order to increase the amount of available memory, Linux also implements disk paging: that is, up to 256 MB of "swap space" [1] can be allocated on disk. When the system requires more physical memory, it will swap out inactive

---

[1] Swap space is inappropriately named: entire processes are not swapped, but rather individual pages. Of course, in many cases entire processes will be swapped out, but this is not necessarily always the case.

pages to disk, thus allowing user to run larger applications and support more users at once.

The kernel also implements a unified memory pool for user programs and disk cache. In this way, all free memory is used for caching, and the cache is reduced when running large programs.

- Linux can coexist with other operating systems.

Linux uses the standard PC partitioning scheme, so it can share disk with other operating systems. It provides a seamless interface for transferring files between Linux and MS-DOS, and MS-DOS can always run as well as Linux on the same system. There is also an MS-DOS emulator available, which allows users to run many popular MS-DOS applications.

MS Windows can share the same swap partition with Linux. Currently under development is a project known as WINE — a Microsoft Windows emulator for the X Window System under Linux. Once WINE is complete, users will be able to run MS-Windows applications directly from Linux.

- There is a complete distribution of the X Window software, XFree86, containing the X server itself, many applications and utilities, programming libraries, and documentation. The XFree86 distribution contains programming libraries and include files for those wily programmers who wish to develop X applications. With sufficient hardware, running X and Linux is as fast, or faster, than running X on UNIX workstations.

Several relational databases and client/server database applications as well as many scientific computing applications are also available for Linux.

Linux is covered by what is known as the GNU, or GPL (General Public License). The GPL allows people to take and modify free software, and distribute

their own versions of the software. However, if any software is derived from Linux, that software must be covered by the GPL as well. Many companies have decided to keep the hardware interface proprietary. This means volunteer Linux developers simply cannot write drivers for those devices (if they do, those drivers would be owned by the company that owned the interface, which would violate the GPL). There is very little that can be done about the situation. In some cases, programmers have attempted to write hackish drivers based on assumptions about the interface. In other cases, developers will work with the company in question and attempt to obtain information about the device interface, with varying degrees of success.

For the PC M-WIP development, the drawback of using Linux is the hardware information has to be obtained from the board manufacturing companies and the device drivers for some special boards have to be developed to establish hardware support under Linux. No drivers of suitable frame grabber, data acquisition board or parallel processing board for the project was found at the time when the work started.

6.1.2 MS-DOS/Windows

MS-DOS/Windows are the most familiar operating software to PC end-users. By choosing MS-DOS/Windows as the operating system for the PC M-WIP, better software development support can be obtained. However, MS-DOS/Window is reported slower than Linux [62], and the disadvantages of using MS-DOS/Windows in the PC M-WIP development are

- Windows uses extended memory which is organized (as descriptors) somewhat differently than conventional base memory below the 1 MB address. Users must access the extended memory through BIOS calls that take extra time because the CPU must be in a protected mode and because of descriptor overhead.

- Multitasking in Windows is realized by running each program by itself for some time, then returns control to Windows, which then runs the next program on its list. The sequential multitasking in this round robin mode means that one cannot say for sure when Windows will run a certain program again.

- Windows also uses the disk as virtual memory if it cannot find real physical memory. Since disk is much slower than memory, extraordinary delays can be generated, but Windows does not tell it is doing this. With these probabilistic or nondeterministic characteristics combined in random ways, one cannot predict the speed of data collection with absolute certainty.

Windows NT and Windows 95 are preemptive operating systems which provide a known, predictable and faster response time. However, since most of the special hardware devices used in PC M-WIP are not supported by 32-bit software development environment for Windows NT and Windows 95, MS-DOS and Windows 3.1 were chosen.

6.2   User Interface Programming

In the development of PC M-WIP software, Microsoft's 16-bit Visual Basic (VB Pro 3.0) and Visual C++ (VC++ 1.52) is used for GUI prototyping. The GUI was developed in conventional Windows style.

6.2.1   Visual Basic

Visual Basic is recognized as one of the best highly accessible and productive software development programming environments for rapid application development [63]. Its fundamental philosophy of pre-built functionality, program reuseability, and powerful debugging tools dramatically reduces the time to create and modify custom applications comparing to programming in C/C++. This makes VB a powerful tool

for prototype system software development which features rapidly and constantly changing requirements.

Using VB, GUI can be created for the application by drawing objects in a visual and graphical way and then set properties of these objects to refine their appearance and behaviour. Code that responds to events can be written to make the interface react to the user. However, the most notable negatives of using VB are the expenses of speed and size that ease of use comes at.

6.2.2 Visual C/C++

The most popular C/C++ compilers now available for Windows programming are Microsoft C++ and Borland C++. They all feature Windows-hosted IDEs (Integrated Development Environments) with syntax highlighting, and both of them offer Windows-based debuggers and resource editors. Also, they can create C and C++ programs for Windows and DOS, and they are compliant with C++ version 2.1.

However, Microsoft C++ and Borland C++ has different Windows application frameworks. Microsoft C++ uses MFC (Microsoft Foundation Classes) and Borland C++ uses OWL (Object Windows Library). MFC has received more third-party support and it is more likely to become a standard. Microsoft C++ also has a resource editor, and App Studio that features a drag-and-drop interface. These makes it much easier to program GUI [64].

6.3 Frame Grabber

The programming of the frame grabber system is supported by ITEX-IC, a driver level comprehensive camera interface software library. It provides C-callable function library and software development environment for the frame grabber and its acquisition module. 16-bit DLLs for MS-DOS/Windows programming are also included.

6.3.1 Frame Grabber Programming

Basically, a program which performs the frame grabber operations has the following steps.

1. Load the configuration file. The frame grabber system requires a binary configuration file to build the necessary data structures accordingly. The configuration file contains the information about each component in the system, such as scanning mode. It can be created and edited as a text file, and the text version can be converted to its binary version using a utility program.

2. Initialize the frame grabber system.

3. Obtain pointers to frame grabber and acquisition module. Each of IC-PCI and AM-DIG has its own data structure which initially inherited the component information from the configuration file. The pointer to the data structure of a component can be obtained and then used later in data access and acquisition control.

4. Set up pixel size and image size. In PC M-WIP, pixel size is set to 16-bit so that the AM-DIG's input multiplexers are configured to store 16-bit image data in frame memory. Pixel size can also be set via the configuration file. Up to 16 frames can be created, each with its specified size. The frame memory is located and a frame ID can be obtained to access and delete the frame.

5. Access data by frame or by pixel. Data can be read from or written to defined frame memory. ROI can also be created/deleted, and it is allowed to read/write from/to ROI by area or by pixel.

6. Display image in grab or snap mode. Images can be captured either in a single shot mode (referred as "snap"), or a continuous mode (referred as "grab").

Windows DIB is used in the PC M-WIP raw image (snap mode) and live video (grab mode) display.

7. Change acquisition control setup when necessary. For a certain camera, settings as acquisition mode, clock frequency and sync signal polarity are usually not adjusted at run time. However, to meet the special requirements such as variable integration time control, some FIFO window settings may need to be changed accordingly.

6.4   Multifunction Board

A software library named as Master Link is used in the programming of the multifunction board. It provides import library and DLLs for MS-DOS/Windows programming.

6.4.1   Multifunction Board Programming

Programming of the multifunction board is fairly easy. The following basic steps are necessary for driving the board, reading in thermocouple data, and sending out integration time code.

1. Initialize the system. Several functions are used in the initialization and they must be called in the right order: software initialization first and hardware initialization last. (a) Prior to any other function call, SWinit() must be called first to initialize the software and to perform system timer calibration; (b) then Include428W() and IncludeTC() should be called to link software support for PCI-20428W and thermocouple temperature measurement; SlotAssignIO() must also be called to assign a slot number to the PCI-20428W; (c) and finally, HWInit() should be called to establish software configuration and initialize the hardware components.

2. Read in temperature measurement. The room temperature measured by the CJC and the temperatures measured by the thermocouples are read in using different functions. There is no dedicated functions for CJC readout, AIRead() is used to read in data in common analog data format and CountsToVolts() is used to convert the readout to voltage value. The voltage to temperature conversion formula (Eq 5.1) for the LM335 CJC is then used in the program to obtain room temperature reading. On the other hand, Master Link provides functions for thermocouple measurement, including CJC compensation, data conversion, and linearization for J, K, T type of thermocouples. TCMeasure() is used in PC M-WIP program for thermocouple temperature measurement.

3. Send out integration time code. Digital output for integration time control is straightforward. Just call DIOWrite() with the desired integration time code as the input data, it will be used to switch the TTL levels of the digital output channels.

6.4.2 Analog Input Testing

The analog input channels for thermocouple reading have been tested using type K thermocouples. According to the specification of the thermocouples, their accuracy is $2.2°C$ or 0.75%. To precisely calibrate the thermocouple reading channels, a reference with temperature measurement accuracy better than $1.1°C$ or 0.375% is needed.

In the initial experiment, the readout of a thermometer using the same kind of thermocouple was compared to the data acquisition system readout in order to prove the system is working properly. The microprocessor thermometer HH22 (Omega Engineering, Inc.) has an temperature measurement accuracy of $±0.1\%$ of reading temperature plus $±0.8°C$. System readout is the average of every four original samples.

Figure 6.1 shows an example of the testing results obtained using a magnetic stirrer hot plate GYRATHERM IIa (VWM Scientific, Inc.) which was heated up first and then allowed to cool down naturally. The measurement was conducted during hot plate cooling, and four system temperature measurements were acquired at each time so that a temporal noise could be figured out, and the average value of the four readouts (effectively sixteen time averaging of the original samples) is used to compare the results of readings of thermometer and the system.

Data plotted as dots in Figure 6.1 (a) shows the correspondence of temperature measurements of thermometer and the system, the straight line shown is the ideal correspondence. Figure 6.1 (b) shows the actual temperature measurement difference between thermometer and the system, and the error bars in the plot show the noise (standard error) of the system measurements.

Comparison of readings from thermometer and the system at room temperature was also performed. Figure 6.2 (a) shows several samples of temperature measurement of thermometer and the system, and Figure 6.2 (b) shows the measurement difference obtained by subtracting thermometer measurement from the system measurement.

In both of the hot plate and room temperature experiments, the differences between the system measurements and thermometer readings are within the accuracy of the thermometer. This demonstrated that the system measurement is working properly. Precise calibration can be performed using reference more accurate than the thermometer, and circuitry can be added to the termination panel for desired signal conditioning.

6.4.3 Digital Output Testing

The digital output for integration time control is tested in two ways. First, the digital output channels are connected to the multifunction board's digital input channels
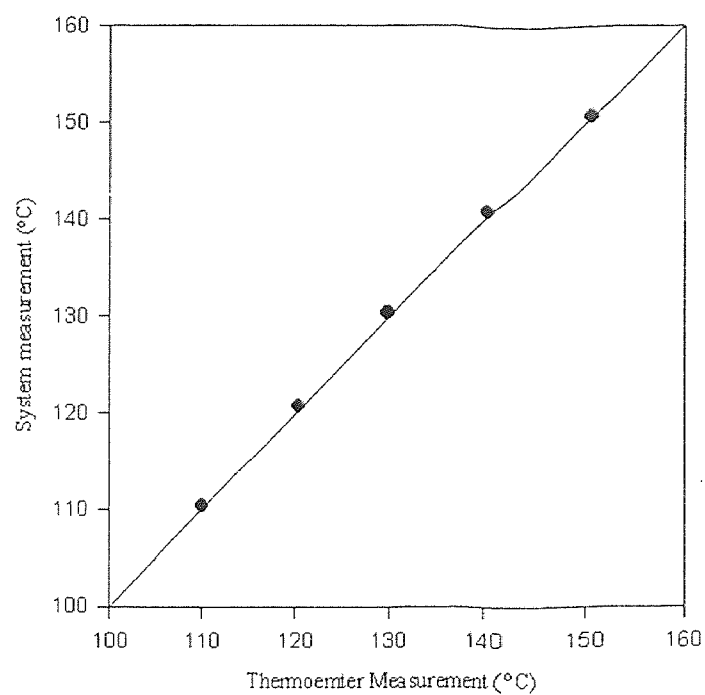
(a) Measurement Correspondence
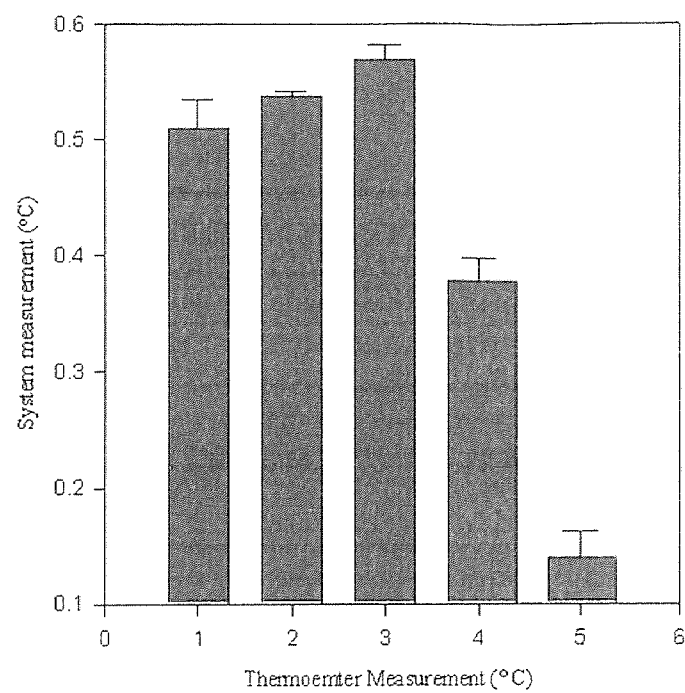
(b) System Measurement Noise

Figure 6.1 Hot Plat Temperature Data Plot
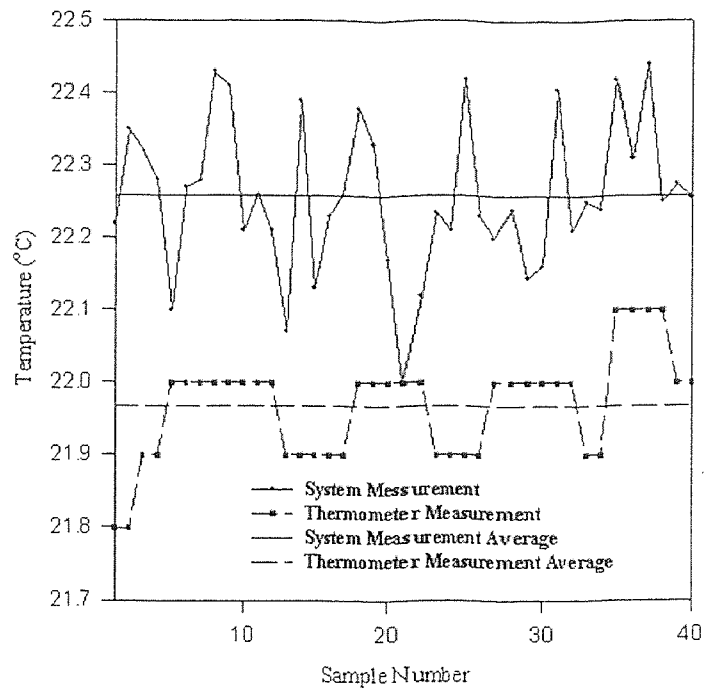
(a) Room Temperature
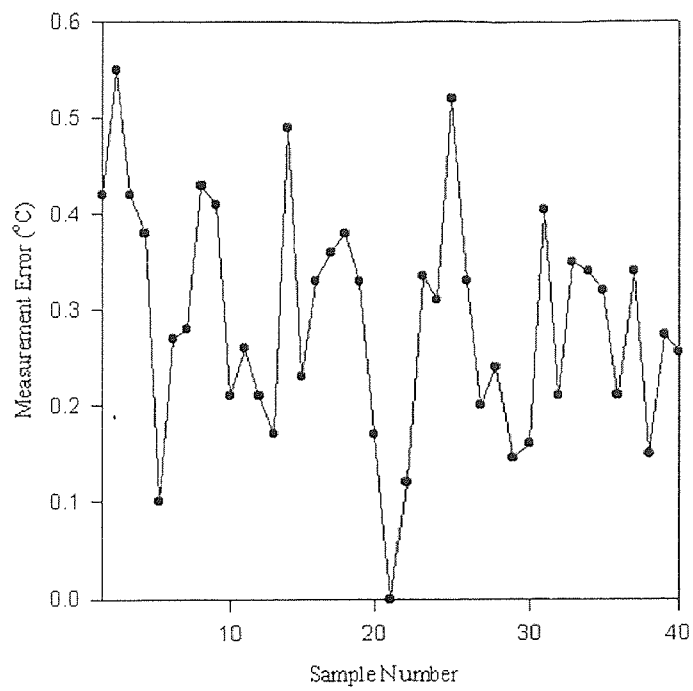
(b) Measurement Difference

Figure 6.2 Room Temperature Data Plot
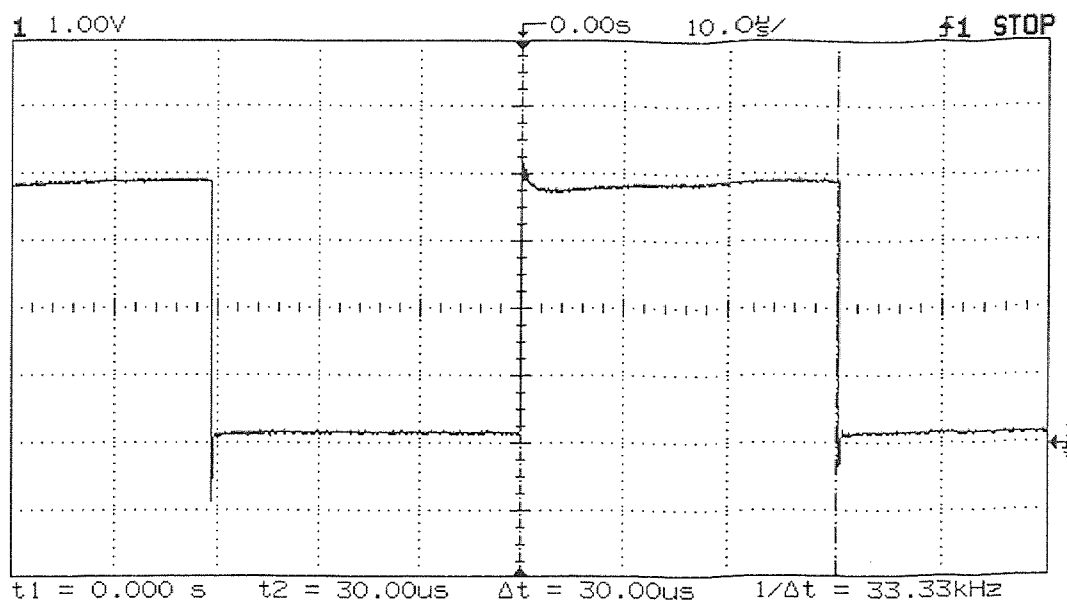
Figure 6.3 Digital Output Testing Waveform

and each channel was checked by comparing the output bit with the corresponding input bit. The test result proved the logical correctness.

Then a HP 54602B oscilloscope (Hewlett Parkard, Co.) was used in testing the waveform of the digital output channels to ensure the signal is acceptable by the integration time control circuitry of the camera. Figure 6.3 shows a testing waveform recorded by the scope. The waveform was generated by one of the digital output channel and the channel is programmed to output 0 and 1 after each other as soon as possible. The result shows the delay time of the channel is only 30 μsec, much less than the possible frame rate. Considering all the 8 channels are parallel and the raising/falling time is very short, the camera should not be confused about the desired integration time.

6.5   PC-Hydra Board

Programming of the PC-Hydra can be done in two different ways by using either the Standard Host Interface or Parallel C. Parallel C is at a higher level than the Standard Host Interface for PC-Hydra. It provides a unified environment for creating

the overall parallel program. The disadvantage of using Parallel C is that it uses a model with a root processor, thus it adapts a MPMD paradigm. Although application development using the Standard Host Interface will be more difficult than using Parallel C, the Standard Host Interface allows SPMD implementation which is proved to be more efficient than its counterpart, the MPMD paradigm. In PC M-WIP software development, both of the above two approaches are implemented for comparison.

6.5.1   Standard Host Interface

The PC-Hydra software release includes a complete interface driver, the Standard Host Interface (callable from C language program), which provides the interface between the host PC and the PC-Hydra. These drivers isolated the programmer from the low-level hardware details of the PC-Hydra's ISA interface. The driver has a function library designed to be linked with various PC programming tools. On the host side, the Standard Host Interface is compatible with Microsoft C/C++, so that user interface can be programmed in C/C++ without any problem. On the DSP side, TI C compiler can be used, which has the advantage of the TMS320C40 processor's parallelism as well as providing a runtime support library.

The disadvantage of using the Standard Host Interface is that its functions are all host-side only. The way to program the DSP side is to directly manipulate the memory map by use of pointers. The user accessible memory resource for each DSP on the PC-Hydra used in PC M-WIP is summerized in Appendix B.

The Standard Host Interface provides eight system semaphores implemented by eight Host Interface Semaphore Registers designed to allow DSPs and host to control access to shared locations in the dual-port memory or any other shared resources where arbitration is required between the host and any one of the four DSPs. A device requesting the use of a dual-port memory location must first request

the resource via a semaphore by writing a "0" to the semaphore register. The device then reads back the value of the semaphore register to determine whether the submitted request for the resource has been granted. If the result is "0", it means the device "owns" the semaphore now and may use the relevant shared resource exclusively; otherwise, a "1" indicates another device currently owns the semaphore and its associated resource. A device that owns a semaphore must write a "1" to the corresponding semaphore to relinquish ownership of the semaphore as soon as it no longer needs the access the shared resource. In case that the semaphore is not available, the device can either continue polling the semaphore until it get "0" or just write a "1" to the semaphore register to nullify its request.

There are also two general purpose handshaking flags available: HostFlag and C40Flag. HostFlag, implemented by the HFLAG bit in the Global Status Register, is used to acknowledge the host that one of the DSP has stored information to a predetermined dual-port memory location. It is set by the DSP whenever it writes to a fixed dual-port memory location (0xC000 1FFF). The flag is then cleared whenever the host reads this dual-port location (0x1FFF). C40Flag, implemented by the C40FLAG bit in the Global Status Register, is used to tell a DSP that the host has written data to a predetermined dual-port memory location. It is set by the host whenever it writes to a fixed dual-port memory location (0xC000 1FFE). The flag is then cleared whenever the DSP reads the dual-port location (0x1FFE).

Although the system semaphores and handshaking flags can be used to establish a protocol for data transfer between the host and the DSPs, restrictions on the usefulness of the flags in a multiprocessor system makes it complicated comparing to just user defined handshaking flags. Since there is only one single flag shared between multiple DSPs in each direction (DSP to host, or host to DSP), a separate semaphore and a DSP identification tag (user defined dual-port memory location) have to be used to identify which of the four DSPs is responsible for the flag. For this

reason, user defined software handshaking flags are used in the PC M-WIP system instead of the hardware semaphores and flags. For each DSP, a flag is defined at a predetermined dual-port memory byte.

6.5.2 Parallel C

There are several software packages which support high level PC-Hydra programming. Since Microsoft Windows is used in PC M-WIP, the only choice (not including all the mathematics libraries) is Parallel C (3L, Ltd.), which is a parallel programming environment based on TI's C compiler [65]. It supports multi-processor systems including PC-Hydra. It also supports user interface programming in VB and VC++ via a server program [66].

Parallel C is built on an abstract parallel processing model *communicating sequential processes* (CSP) [67]. In this model, a computing system is a collection of concurrently active sequential processes which can only communicate with each other over channels. A channel connects exactly one process to exactly one other process and can only carry messages in one direction. Each process can have any number of input and output channels, but channels in a system are fixed, and new channels cannot be created during the operation. Communication via channels are synchronized message passing. Two communicating processes can be on the same processors (multi-tasking) or on distant processor (multi-processor). Parallel C provides virtual channels that automatically carry messages between distant processes via intermediate network nodes; physical channels which map directly to physical links are also provided for fast data transfer.

Processor farm is also an advantage of Parallel C. Applications created using processor farm technique will automatically configure themselves to run on any network of processors. This means the applications will automatically run faster when more processors are added to the network, without recompilation or recon-

figuration. In the processor farm technique, a *master* task must be written for the application which will split the job up into small, independent *work packets* which the *worker* tasks can handle without communicating with other tasks. All of the worker tasks must run the same code, and they are just simple sequential loops: read a packet; process it; send back a result packet; repeat. Work packets are automatically distributed across an arbitrary network of processors by routing software, and result packets are sent back via the same routing software. Fortunately, M-WIP's least-squares fitting can be implemented by processor farm.

6.5.3 Experimental Results

The data transfer protocol used in the SPMD implementation for PC M-WIP is different from what is used in the SPMD implementation for SUN M-WIP. In PC M-WIP, for each DSP there is a single shared memory address used for flag, and a single starting address for data block. The flag can be assigned to five states, "idle", "host request", "dsp request", "host acknowledge", and "dsp acknowledge". The flag based handshaking scheme for host to DSP or DSP to host is:

1. The sender checks the flag. When it is "idle", it puts the data and sets the flag to "request";

2. The receiver checks the flag and waits until it gets the "request", then gets the data and overwrites the flag with an "acknowledge";

3. The sender waiting for the "acknowledge" then resets the flag to "idle".

The MPMD implementation for PC M-WIP is programmed using Parallel C and its Windows Server. Running on the host side, the Windows Server is the front end of the application. It takes charge of the GUI, monitors the status of the DSP board, and acts on service requests from the DSP board. Programs running in the DSPs are the back ends of the application. They take care of the computational
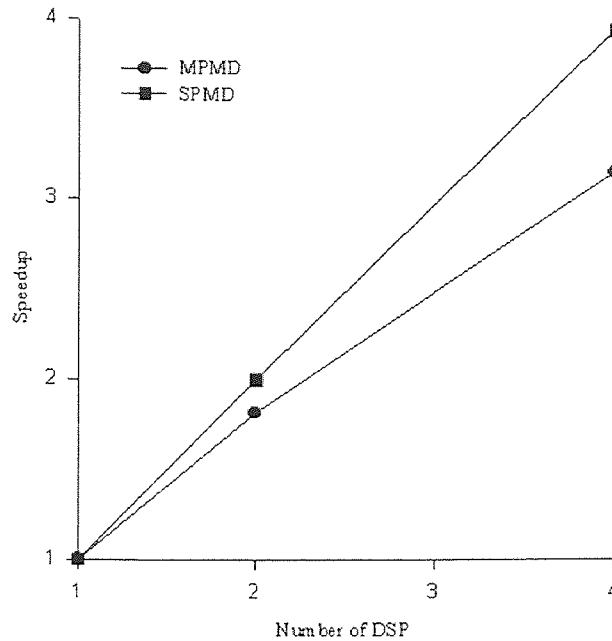
Figure 6.4 Speedup of PC M-WIP

intensive real-time tasks. The executable files of the DSP programs are downloaded to the DSP hardware by the Windows Server. The I/O requests from the DSP board is handled by the Windows Server during the front end idle time (whenever there are no Windows messages to be processed). In the PC M-WIP system, three back end service function and front end service handler pairs are established for passing input signal and integration time to the DSPs, and collecting the results from the DSPs, respectively.

The resultant speedup values from PC-Hydra are very similar to those from V-C40 Hydra. However, more efficient code produces less overhead and thus a higher speedup in both SPMD and MPMD cases may be achieved. The SPMD and MPMD speedup curves obtained from PC M-WIP are shown in Figure 6.4.

6.6   SnapShot and Filter-Wheel

Both the SnapShot camera and the filter-wheel are interfaced to the host PC via RS-232 serial communication ports (COM ports).

RS-232 serial port is used by the PC to exchange information with peripheral by means of bit flow [68]. Most PCs have only two physical COM ports (COM1 and COM2), and the PC M-WIP's host machine is not an exception. Since the mouse is also a serial peripheral, the system must have at least three COM ports. A high speed serial board DSerial-550 (Lava Computer MFG, Inc.) is installed in the system which provides two more COM ports (COM3 and COM4). In the PC M-WIP system, the mouse is connected to COM1, SnapShot to COM2, and filter-wheel to COM3.

6.6.1   SnapShot Camera Programming

Since VB's MSComm serial communication control supports baud rate only up to 19200, to operate the SnapShot camera at the default baud rate 38400, the PDQComm for Windows [69] is installed to enhance the COM port control capacity. The PDQComm control, heart of the PDQComm for Windows, is an enhanced version of Microsoft's MSComm control that comes with VB 3.0 Pro. It supports up to 230400 baud rate with the appropriate Windows driver and provides many other enhancements in file transfer and terminal emulation features.

The SnapShot camera has its built-in processor which receives commands from the host PC, performs the required functions, and returns image data and camera status to the host PC. Basic operations for camera control in line-sensing mode are summarized in the following steps.

1. Initialize the camera. Assign on-board frame memory location for data collection, and move the linear array to the center of the scanning area (horizontal center of the lens).

2. Acquire images. To compensate the spatial non-uniformity, a few reference images should be acquired first for non-uniformity correction. Generally, both offset and gain correction are necessary.

3. Reformat data. Pixels have to be organized into correct order and the two separate bytes (MSB and LSB) of each pixel must be merged to one signal value. Bad pixels are replaced by interpolation.

4. Reset the camera. Camera should be reset after all the tasks are finished.

6.6.2 SnapShot Camera Testing

The SnapShot camera comes with a DOS version software which allows user to operate the camera through a menu-driven interface. Without the source code and necessary document, it is impossible to use the program in the PC M-WIP software. However, the program is still useful for the system setup. The focus function and scan function are used in getting the object into the FOV and focussed. Since the SnapShot program works only for COM1 or COM2, the SnapShot camera is interfaced to COM2 in the PC M-WIP system. Fortunately, the APICOM program for filter-wheel programming works for all the COM ports, so the filter-wheel is interfaced to COM3 in the PC M-WIP system.

The SnapShot camera was tested against a commercial calibration source, Temperature Source 1805D and Temperature Controller TH2450E-2302B (Electro Optical Industries, Inc.),which has a blackbody (with emissivity of 0.99 ± 0.01) temperature range from $15°C$ to $180°C$ (with an accuracy of $\pm 0.05°C$ or 0.5%).

Figure 6.5 shows a picture obtained using SnapShot's software in a scan mode.

Figure 6.6 shows a plot obtained using PC M-WIP software which programs the SnapShot in a line sensing mode. This program moves the imager to the center and takes snap shots without having the mechanical movement to prevent camera vibration. The plot shows the signal level changes against temperature variation
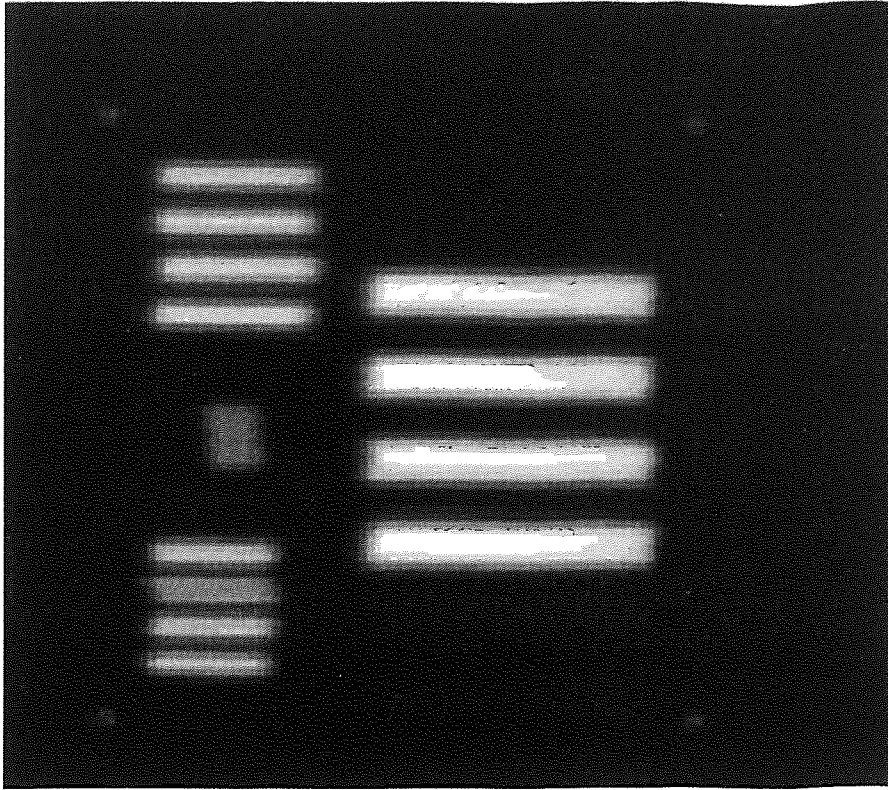
Figure 6.5 Test Pattern Image Taken by SnapShot

for each of the 60 center pixels staring at the blackbody. Spatial non-uniformity is obvious, and the actual non-uniformity value is less than 0.1, calculated from the data obtained in blackbody temperature range 50°C to 150°C.

Spatial averaged values were taken from the same test data set to plot the correspondence between temperature and signal level as shown in Figure 6.7. It can be observed that the correspondence is not a very smooth curve. This suggests a fine calibration is needed for temperature measurement.

6.6.3 Filter-Wheel Programming

The motion control indexer has its own dedicated operating system [70]. It provides two modes to the user to enter and manipulate data to perform motion: (1) immediate mode allows user to command the indexer via the communication port one command at a time; (2) stored program mode let user create and store programs
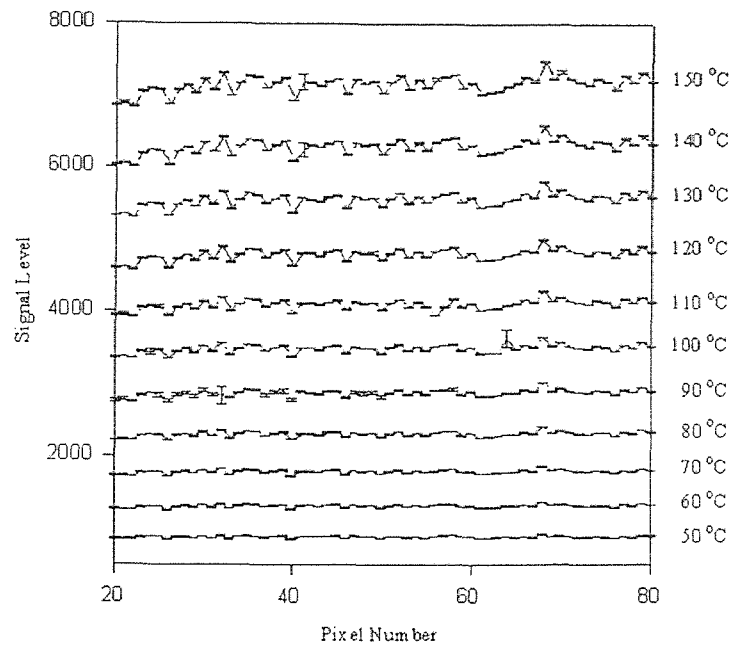
Figure 6.6 SnapShot Temperature Response Curve 1
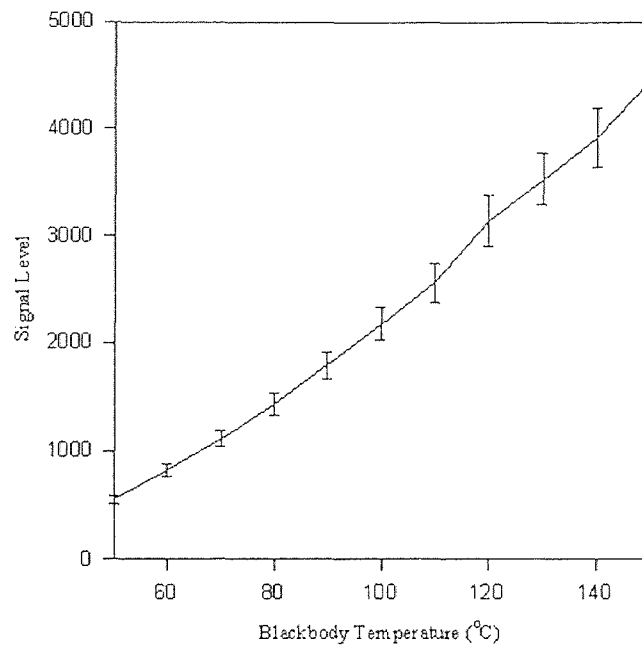
Figure 6.7 SnapShot Temperature Response Curve 2

in the ICL system and execute them when required. The stored programs can be initiated through the communication port or triggered by an input.

The indexer itself is programmed in Intelli-Command Language (ICL). ICL has three parts: ICL parameters, ICL variables, and ICL commands. The ICL commands tell the indexer "what to do", and the ICL parameters and variables instruct the indexer "how to do it". Once entered, the parameters and variables will be maintained in non-volatile battery backed memory until cleared. ICL system has its own editor for program creation, modification and deletion.

Since all the programming should be done in ICL system via the COM port of the host PC, a stand-alone software is needed to provide a simple interface for the programming and debugging. APICOM is the one provided by the vendor. Other public domain software packages, such as PROCOM or KERMIT, can also be used for the same purpose.

The ICL programs for PC M-WIP are simply three programs corresponding to the three steps of operation listed below:

1. Initialize parameters and variables. The parameters and variables used by both of the next two steps should be initialized first before performing any motion. This is necessary to minimize the overhead so that a required motion can be started with minimum response time.

2. Initialize the filter-wheel position. The position parameters for each filter on the filter-wheel at correct location in the optical path can be obtained by calibration.

3. Switch to next filter. The "next filter" can be any filter, depending on the filter sequence set by the user. Generally, the next filter can be obtained by rotating the filter by a certain degrees. For example, the next filter would be the adjacent filter 30 degree clockwise or counter-clockwise from the current

one. If an irregular order is used, the previous step can be used to achieve the special sequence.

CHAPTER 7

3-COLOR InGaAs FPA DEMONSTRATION SYSTEM

In recent years, the demand for near infrared (NIR) detectors is growing rapidly. More and more applications require NIR detectors with high sensitivity and fast response. This chapter presents an imaging computer developed for the demonstration of a novel three wavelength InGaAs focal plane array (FPA) with detection wavelength range of 0.9 - 2.5 μm. The special multi-wavelength imaging system can be used in many applications, such as temperature measurement, gas spectroscopy, and blood-flow inspection.

7.1 Imager Description

The 3-color FPA consists of three interleaved $32X32$ InGaAs diode arrays [71]. Each of them is sensitive to a certain region of the near infrared spectrum. The detectors responding to wavelength ranging from 0.9 to 1.7 μm are referred as "blue" (B), 1.2 to 2.1 μm as "green" (G), and 1.6 to 2.5 μm as "red" (R), respectively. Figure 7.1 shows the schematic structure of a 3-color pixel element. Detectors for each color reside at a different level with blue being at the bottom and red on the top. In the back illumination mode with light incident upon the substrate side, the epitaxial layer stack's filtering effect provides excellent optical isolation between each color.

The three sets of detectors make up an $96X96$ array and the array is indium-bumped to a switched FET $128X128$ CMOS readout multiplexer [72]. Figure 7.2 illustrates two different pixel readout arrangement of the 3-color FPA. In the case of column mode, the 32 BGR detector triplets correspond to 32 active FPA columns and each of them is followed by two blank columns. In the case of row mode, there are 96 active rows in the form of 32 active triplets and each row corresponds to 32 single-color detectors that are separated by two blank pixels.
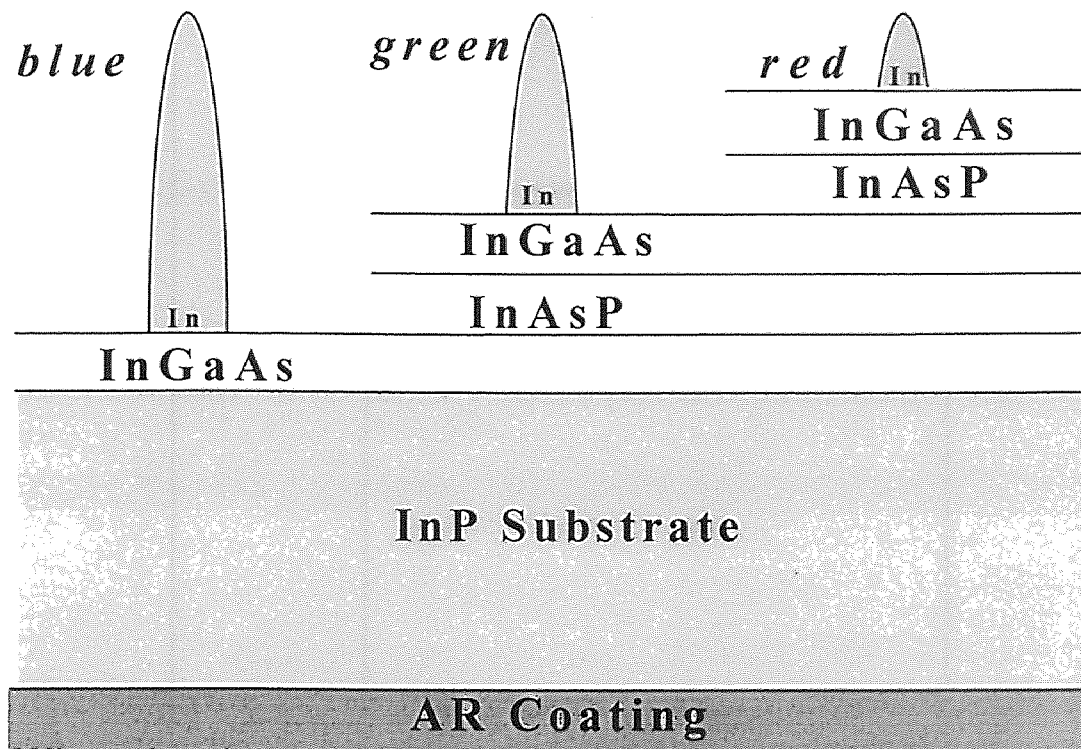
Figure 7.1 3-Color FPA Pixel Structure

To operate the FPA, three timing pulses are required to produce the video output: PCLK (pixel clock), LSYNC (line synchronization), and FSYNC (frame synchronization).

1. Pixels are clocked at both the rising and falling edges of the PCLK.

2. LSYNC starts at the raising edge of PCLK and should have a duration of one PCLK period.

3. Exposure is initiated by the rising edge of the FSYNC signal, and the length of FSYNC determines the optical integration time in integer line-times. After the falling edge of FSYNC and a delay of 2 line-times, the first video line is clocked out from the FPA.

Figure 7.3 sketches the waveform for the operation of the readout multiplexer.

128X128

96X96

BGRBGR...
        (blank row)
        (blank row)
BGRBGR...

(a) Row Mode Arrangement

...RGBRGB   ...RGBRGB
(blank column) (blank column)

96X96

128X128
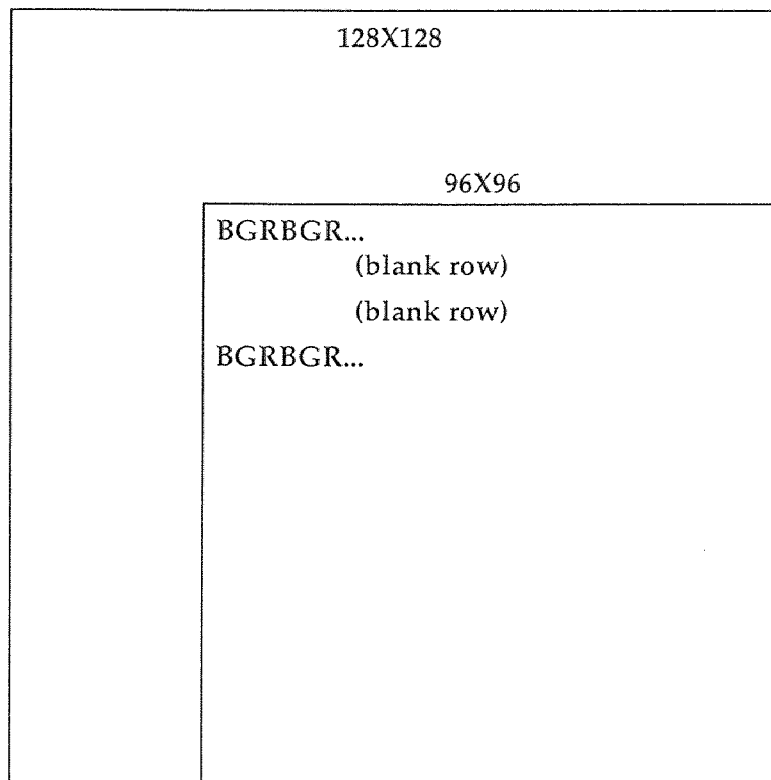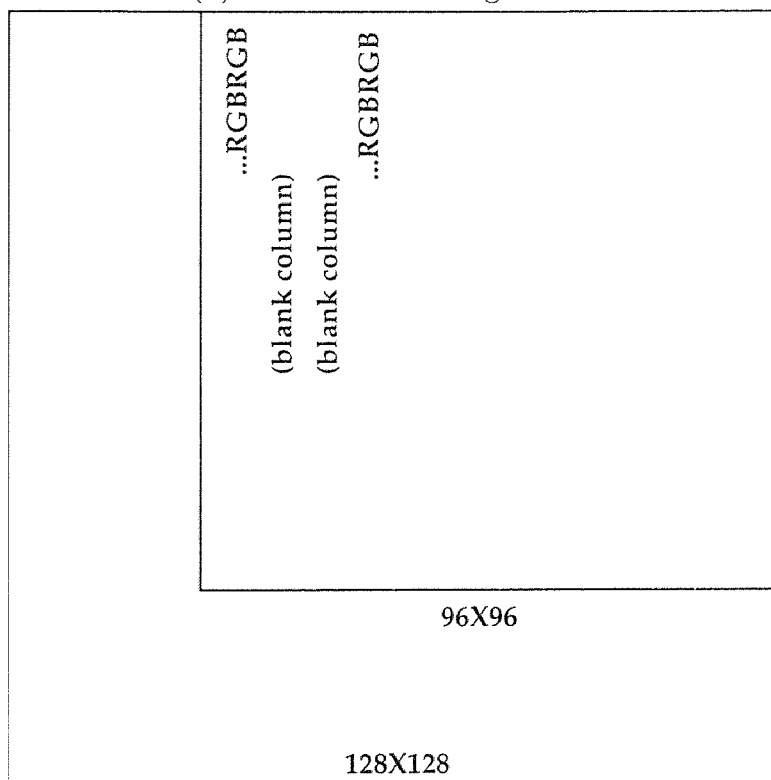
(b) Column Mode Arrangement

Figure 7.2 3-Color FPA Pixel Arrangement
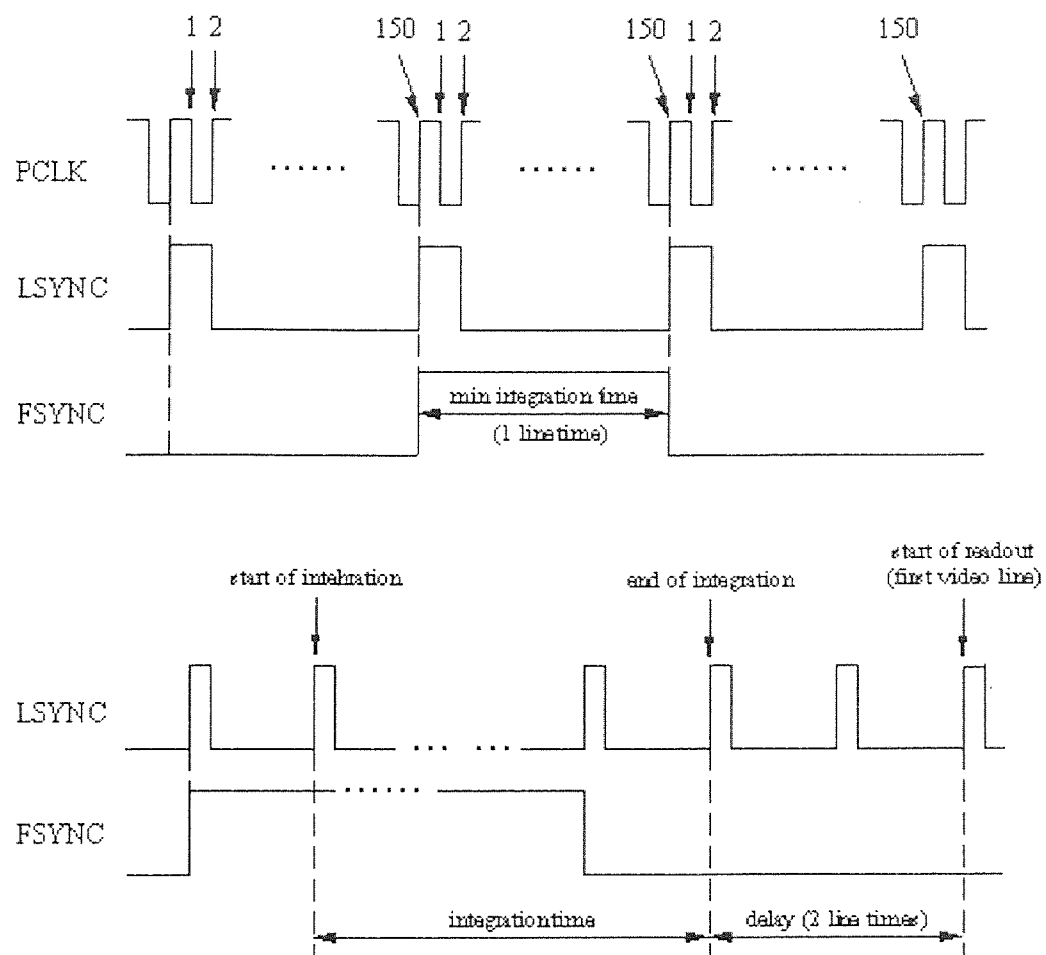
Figure 7.3 Waveform for Operating the 3-Color FPA
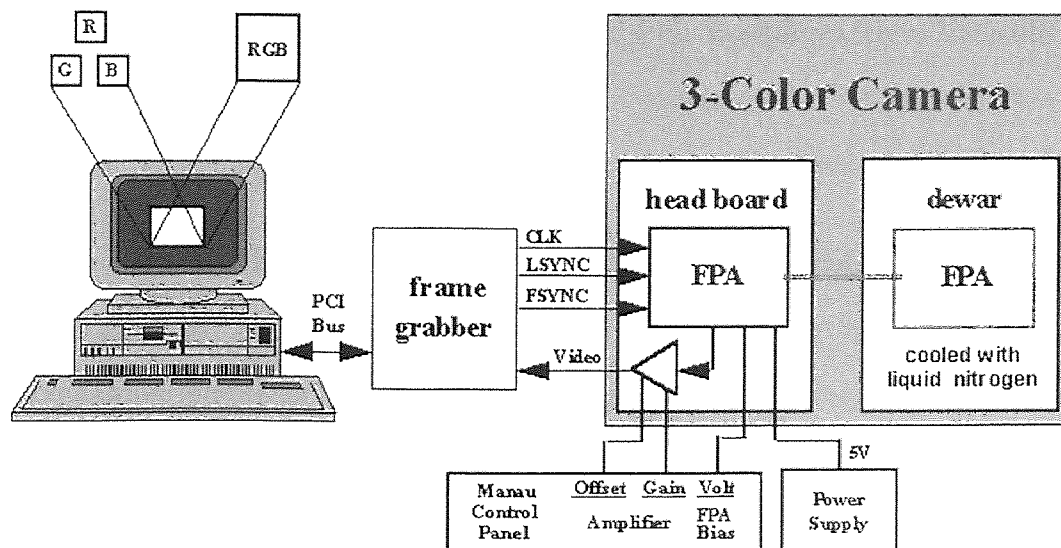
Figure 7.4 3-Color System Configuration

7.2 System Configuration

The system was developed for the demonstration and evaluation of the 3-color InGaAs FPAs. The major components of the system are a host PC, a prototyping camera, and a frame grabber. The block diagram of the system is shown in Figure 7.4.

- The host computer is a Pentium PC with 100 MHz CPU, 16 MB RAM, 1.2 GB hard drive, and a 4X speed CD-ROM drive. The mother board has the Intel chipset for compatibility with the frame grabber. Microsoft's Visual Basic (VB 3.0 Pro) is installed for programming.

- The test camera built at NJIT supplies power, bias and all the necessary timing pulses to run the FPA which is cooled in the test Dewar. It also provides analog video and all the necessary synchronization signals to the frame grabber for digitizing. The optical integration time can be set manually to 8 different values between 1 and 256 line-times which correspond to 244 μsec through 62.5 $msec$. Manual gain and offset adjustments are also available.

- The frame grabber is comprised of an IC-PCI together with a Variable Scan Acquisition Module (AM-VS). The IC-PCI hosted in the Pentium PC has been discussed in Chapter 5. The AM-VS supports non-standard analog video input.

Video and synchronization signals feed into the frame grabber from the camera can be either single-ended or differential. To interface frame grabber with the camera, the acquisition module is programmed to receive external timing. The voltage range of the video signal before ADC should be between 0.8 and 1.5 V. Since the voltage range of the video signal from the camera is 2.0 V, the programmable pre-scale factor is set to 1, and the positive reference (PREF) and negative reference (NREF) are set to 1.2 V and 0.0 V, respectively.

A video line is in the form of 128 active pixels and 22 blank pixels. Horizontal offset (HOffset) and horizontal active (HActive) are set corresponding to these numbers. A video frame is in the form of 128 active lines and certain number of blank lines. The number of blank lines depends on the integration time setting of the camera. It can be calculated as current integration line-time plus 10. Vertical offset (VActive) and vertical offset (VOffset) are set according to these numbers.

7.3   Software Development

The 3-Color FPA Demonstration System was programmed in VB. The GUI for the 3-color system is designed as a virtual-instrument which uses PC's bit-mapped screen to simulate a physical instrument so that the display of the PC looks like the front panel of a traditional instrument with buttons, dials, etc.

The frame captured by the frame grabber is kept in IC-PCI's 4 MB memory. There are two different ways to transfer data from the on-board memory to the host memory:

n: total number of pixels						4thByte	3rdByte	2ndByte	1stByte
Pixel#n	Pixel#n-1	Pixel#n-2	Pixel#n-3		//	Pixel#4	Pixel#3	Pixel#2	Pixel#1
Last DWORD					//			**First DWORD**	
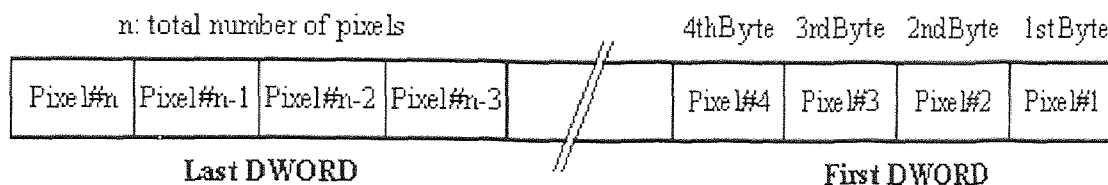
Figure 7.5 3-Color FPA Pixel Packing Scheme

- In bus master operation, the IC-PCI is granted control of the PCI bus and becomes the source of both address and data to some other target location within the system. Live video display works in this fastest data transfer mode.

- In bus slave operation, the host processor does all the work involved in accessing the frame area on the IC-PCI board. Obviously, this pass-through mode is much slower than bus master mode.

ITEX-IC, the development supporting software for the frame grabber, provides function calls, icp_read_area() and icp_write_area(), for the host to access the data in a certain frame area, and icp_rpix() and icp_wpix() for the host to access the data of a single pixel. Icp_read_area() and icp_write_area() perform bus master transfer when it is enabled, and icp_rpix() and icp_wpix() perform bus slave transfer. Obviously, accessing an area using pixel by pixel bus slave transfer is much slower than transferring the same area in bus master mode.

The access to the on-board frame memory is always on DWORD (32-bit unsigned double-word) boundaries, and each DWORD packs four 8-bit pixels. Figure 7.5 shows the pixel packing scheme in a frame.

The functions of the 3-color system are listed below. In the following descriptions, "current image" indicates the current image on the screen. It can be an image captured by Snap or Grab, or a resultant image of Average, Correction, or Database/Load, whichever is the latest. The resultant image of Reformat, Zoom, or Defect is not referred as "current image".

- Snap

This function captures one-shot image and displays the still image on the screen. Image processing and analysis can then be applied to the image. The image can also be stored as a disk file.

- Grab

This function grabs images in real-time and displays the live video on the PC screen. Data is transferred out of the IC-PCI over the PCI bus to the memory on the display card and display is done completely by the host display processor. When the procedure is stopped, the last frame is displayed on the screen as a still image that can be processed and stored as a one-shot image.

- Average

This function averages 16 consecutive frames to reduce temporal noise and displays the resultant image on the screen.

- Reformat

The camera treats the imager as a pure $128X128$ FPA without extracting the 3 color information. This Reformat function rearranges the current image into three $32X32$ images corresponding to each wavelength and displays them along with a fourth image which is the composite image of the three. The image corresponding to the detectors of 1.7 μm cutoff wavelength is displayed in blue (B), 2.1 μm in green (G), and 2.5 μm in red (R). The composite image is displayed in RGB false color with the three images of R, G, B being primary components.

This function also save the three images into files named as RED.BMP, GREEN.BMP, and BLUE.BMP. Note that every time the function is executed, the files will be overwritten.

- Zoom

  This function allows the user to zoom the current image. A dialog window pops up to prompt user for input of the zoom percentage.

  When the cursor is on the zoomed image and the left button on the mouse is pressed down, a small window pops up and shows the position of the pixel pointed by the cursor.

- Background

  This function reads in the current image and keeps it as the offset image for one-point non-uniformity correction.

- Non-uniformity

  This function calculates and displays the histogram of pixel value distribution over the current image.

- Correction

  This function performs one-point non-uniformity correction. It subtracts the offset image from the current image and displays the resultant image on the screen (see Background also).

- Integration Time

  This function allows the user to set integration time by changing vertical offset according to the change of integration time setting on the front panel of the camera. Integration time can be selected from a pop-up dialog window.

- Defect

  This function displays the current image in a way that red represents white (or hot) defect pixels that always saturate or give abnormal high response to the incoming flux, and blue represents black (or cold) defect pixels that always give

no responds or very low response to the incoming flux. Two threshold values are used in the determination of bad pixels, and a pop-up dialog window allows user to enter the values.

- Database

This function allows the user to save the current image into a disk file (using the Save button), or retrieve a disk file (using the Load button) and displays it on the screen. A pop-up screen lets the user change current drive, directory interactively, and shows a file list of certain user-determined type.

- Test

This function shows the average values of pre-selected R, G, B pixels respectively in a pop-up window. It is currently used in some special pixel-based testings, such as spectral response measurement and integration time response test. A file named TESTDATA is overwritten or created when the operation is performed. It stores the date, time, and all samples of R, G, B values in order.

When the function is executed, a display window pops up and shows the averaged R, G, B values for the pre-selected pixels and the default sampling rate is set to 1 minute. Each time when a new sample is displayed, the bell will ring once. The sampling time interval can be changed. Clicking on the display window, a dialog window will show up to prompt input for sampling time interval and duration. Clicking on the dialog window, the display window will show up again and the testing starts again from the beginning.

- Exit

Quit the program.
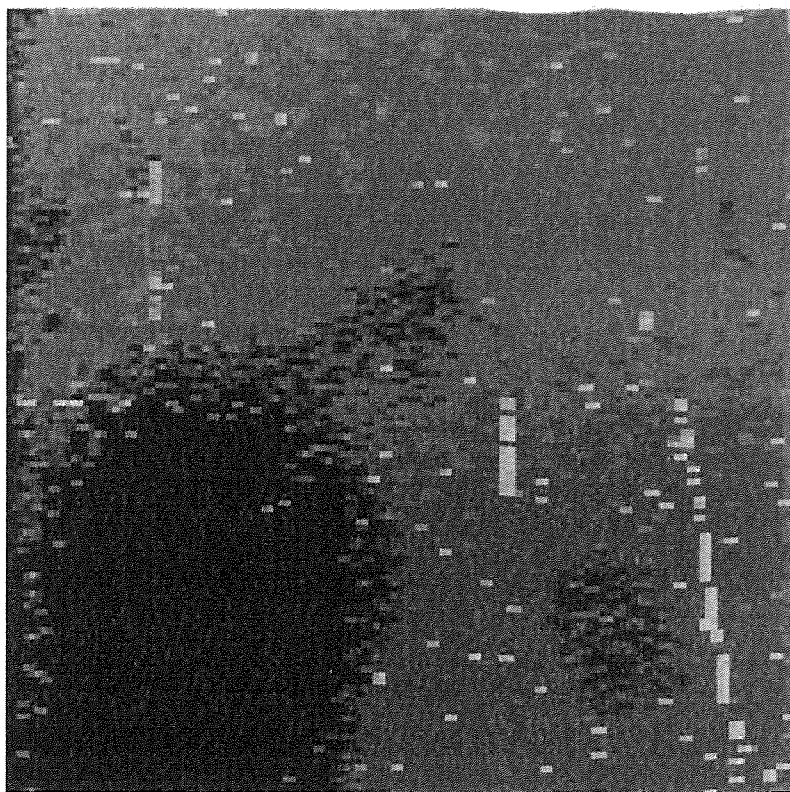
Figure 7.6 Dark Current Image from the General InGaAs Imager

7.4 Testing and Evaluation

During system integration and software development, a single color $128 X 128$ InGaAs FPA with cutoff wavelength at 1.7 μm was tested at room temperature. Figure 7.6 shows a dark current image taken by the system with the 1.7 μm InGaAs FPA.

Two 3-color InGaAs FPAs were tested at 77 K in a Dewar cooled with liquid nitrogen. To have the FPA working properly, FPA bias voltage, offset voltage, and gain voltage were adjusted to the appropriate levels, and the position of the A/D converter sampling pulse was tuned for the alignment of the FPA and the frame grabber. Figure 7.7 contains images taken by the camera system with the 3-color InGaAs imagers packaged in the row mode and the column mode, respectively.

Preliminary experiment has been performed for measuring the spectral response of the FPAs. The results are shown in Figure 7.8. The operating temperature for this test was 140 K and integration time was 244 μsec.
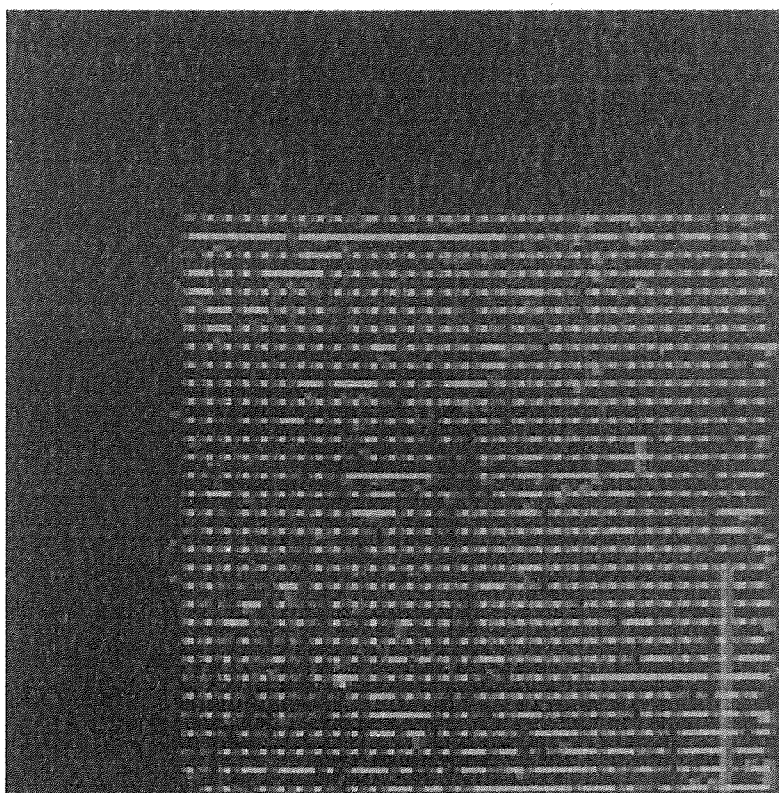
(a) Row Mode Image
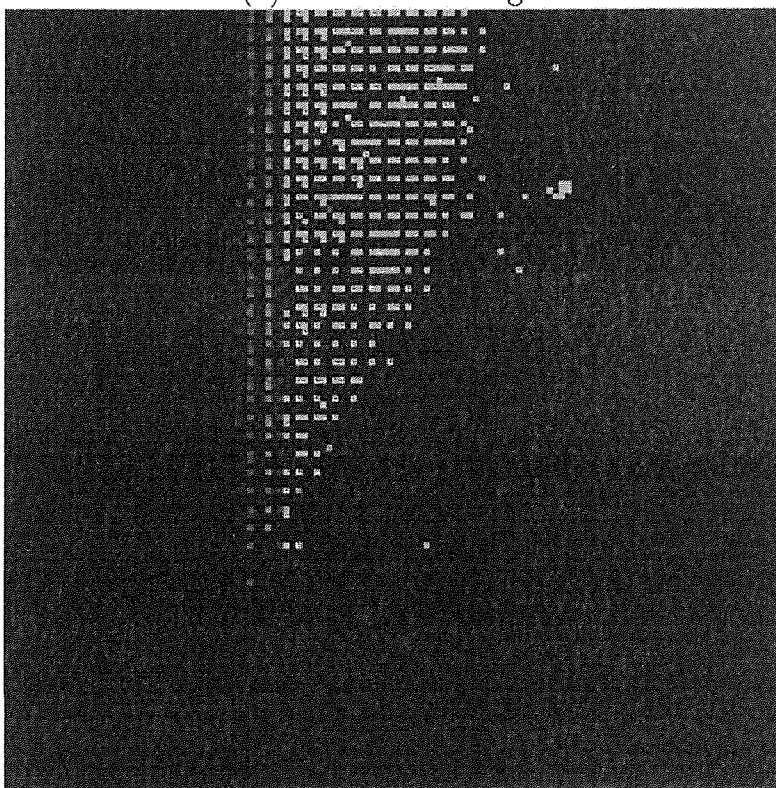
(b) Column Mode Image

Figure 7.7 Images from 3-Color InGaAs Imagers
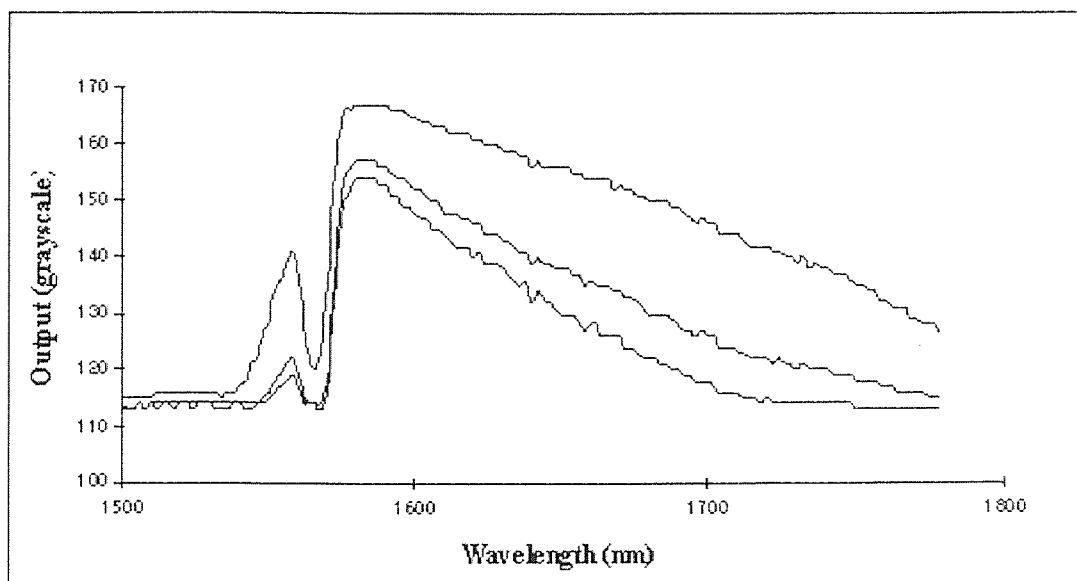
(a) Row Mode Response
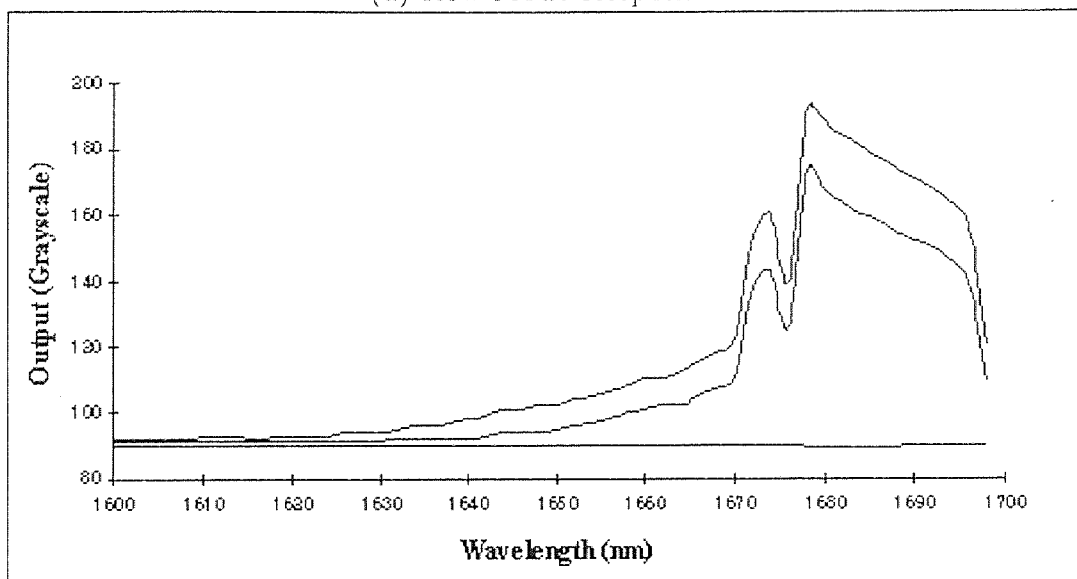
(b) Column Mode Response

Figure 7.8 Spectral Response of 3-Color InGaAs Imagers
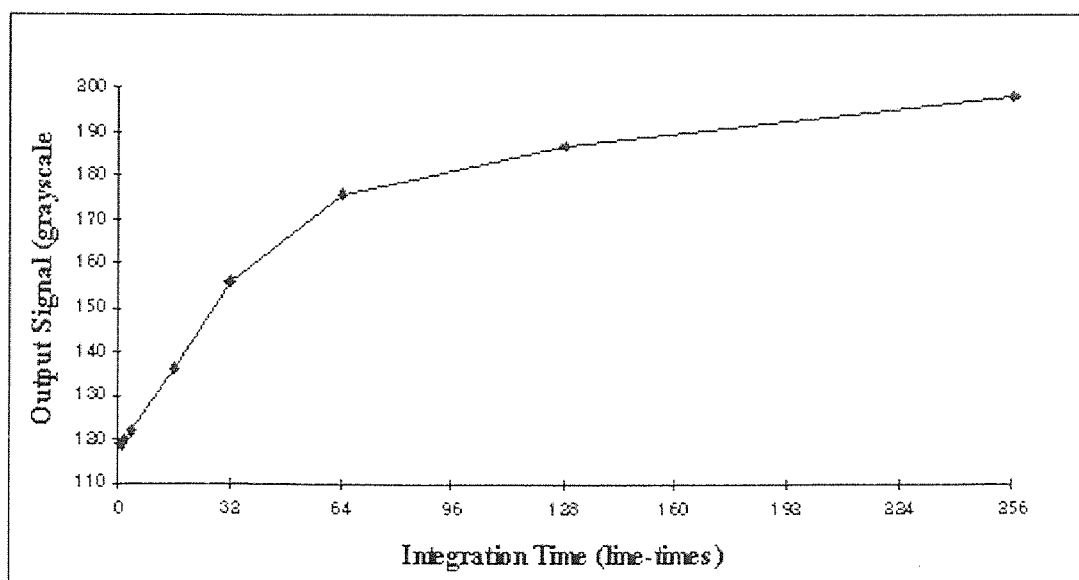
Figure 7.9 Time Response of 3-Color InGaAs Imagers

The integration time control was also tested. Figure 7.9 shows the signal level changes along integration time.

CHAPTER 8

CONCLUSIONS

In this dissertation research, three computer systems were developed for multi-wavelength infrared imaging applications. Various image processing, system calibration, and real-time temperature measurement algorithms were developed and implemented for these systems. The dissertation summarizes the integration and application of the systems, and demonstrates the advantages of the newly developed algorithms. Experimental results were illustrated for the evaluation of the systems and the algorithms.

8.1 System Development

The M-WIP computer systems represent the state-of-art development in remote temperature measurement system based on the multi-wavelength approach.

- A general purpose multi-wavelength infrared imaging computer system was developed and with M-WIP software embedded. This system consists of a SUN workstation as host machine, a MaxVideo real-time image processing subsystem for thermal imaging, a LabTech data acquisition subsystem for thermocouple reading, a V-C40 Hydra parallel processing subsystem for fast computation, and also devices for data communication, camera control, and process control.

  Graphical interface was developed in C and Xlib. Software were developed to interface and operate the subsystems and other devices. The system is capable of (1) real-time image capturing, processing, and display, (2) data acquisition and communication, (3) multi-processor parallel processing, (4) camera integration time control, and (5) feedback process control.

M-WIP application of the system demonstrated temperature measurement accuracy of $\pm 1°C$ against blackbody and $\pm 4°C$ for colorbody objects.

- A cost effective multi-wavelength infrared imaging computer system was developed. This system consists of a Pentium PC as host machine, a digital frame grabber for infrared image capturing, a data acquisition board for thermocouple reading and integration time control, a parallel processing board for data processing, and device for filter-wheel rotation and positioning control.

  Graphical interface was developed in Visual Basic. Software were developed in Visual Basic, Visual C++, and Parallel C to interface and operate the devices. The system is capable of (1) real-time image capturing and display, (2) data acquisition and analysis, (3) multi-processor parallel processing, (4) camera integration time control, and (5) filter-wheel control.

- A PC-based computer system was developed for the demonstration and characterization of 3-color InGaAs FPAs. It consists of a Pentium PC as host machine and an analog frame grabber for infrared image capturing.

  Graphical interface was developed in Visual Basic. Software were developed in Visual Basic to interface the camera and to operate the system. The system is capable of (1) real-time image capturing and display, (2) off-line image analysis, (3) image reformatting, (4) defect detection, and (5) integration time control.

  The system was delivered to the FPA manufacturer.

8.2 Algorithm Development

Various algorithms were developed for image processing tasks, system calibration, and interfacing with subsystems. They include real-time two-point non-uniformity correction, thermal image pseudocoloring, PC to SUN workstation data transfer,

automatic IR camera integration time control, and radiometric measurement parallel processing.

- A real-time implementation of the two-point non-uniformity correction algorithm was developed. The experimental result demonstrated more than six fold non-uniformity reduction by using the algorithm.

- Three pseudocoloring schemes were developed and implemented for thermal image enhancement. The theoretical analysis and experimental result showed the unique features of the schemes and the improvement to the conventional scheme.

- A split-and-merge procedure was designed and implemented for the data transfer from ISA bus LabTech system to VME bus SUN host.

- SPMD paradigm for M-WIP computation were developed and implemented in both V-C40 Hydra and PC-Hydra. The experimental results illustrated that SPMD approach achieves higher speedup than MPMD method.

- Algorithms were developed for automatic camera integration time control. Procedures were implemented for embedded information retrieval from the smart frame.

APPENDIX A

MAX-SCAN CONFIGURATION

A.1   Hardware Settings for MAX-SCAN

The IACKIN/IACKOUT jumper associated with the VME bus chassis slot which holds the MAX-SCAN is removed, since MAX-SCAN is a VME bus interrupter device.

Other hardware settings for the MAX-SCAN are listed in Table A.1

A.2   Programmable Settings

Polarity switches (SC_PS1, SC_PS3, and SC_PS5 to SC_PS8):   These switches determine whether or not the incoming signal will be inverted. In the M-WIP case, SC_PS7 is set to INVERT (invert external Vsync input to use low resets counter) and others are NOINVERT.

Programmable signal switches (SC_S1 to SC_S23):   These 2 or 3 position switches are used to select a signal to be passed on or turned off. In M-WIP, we set SC_S6 is set to 1 (receive external pixel clock from the camera), SC_S9 is 1, SC_S14 is 1 (receive external Vsync from the camera), and SC_S17 is 2 (receive external Hsync from the camera). Others are set to 0.

The ImageFlow's dqSpecVideoSync() is useful in setting the timing switches. After the execution of this function, with DQ_VIDSYNC_SEP_HV (camera sends Hsync and Vsync on separate cables) and DQ_PIXELCLOCK_XMT (camera sends pixel clock signal to acquisition device) plugged in, SC_PS1 and SC_PS7 are set to NOINVERT and INVERT, respectively, to fit the specification of the camera.

Table A.1 MaxScan Setup

Items	*Settings*	*Descriptions*
JW1-JW8	W3, W8 removed, others installed	Base Address at 840000
A45	removed	Pixel Clock Role is slave
SW1	all ON	terminator
J1	removed	100 Ohm impedance is not provided
J2	2-3 installed	sync separator is selected
J3	2-3 installed	DC restore on the raising edge of the incoming composite sync
J13	installed	5 to 10 MHz VCO range
J17-J22, J27, and J30-J33	J18-J20 and J32 1-2 installed, others removed	receive timing pulse from external source with single ended, variable threshold, and high impedance
J28, J29	A-C installed	P5, P6 output always enabled
J48	installed	enable interrupts
J50, J51	J50 installed, and J51 removed	bypass the low-pass filter
J52	1-2 installed	phase lock loop filter
W1-W7	installed	nominal voltage level 1.0 to 4.0 V; DC coupling; DC restoration

APPENDIX B

SUPPORTING SOFTWARE NOTES

B.1 MaxVideo

To interface the IR digital camera to MAX-SCAN, a surface on the SC_ADC needs to be created even though the input data will come from DQ_DP11. Without the surface, requirements of ImageFlow's Data Stream Manager will not be satisfied since the MAX-SCAN model does not include a surface element representing the digital input.

The MAX-SCAN requires 8 to 12 pixel clock between Hsync and valid data transfer for each line, 4 Hsync between Vsync and valid data transfer for each field. However, the IR camera does not provide the extra sync signals. This causes the first 3 rows and first 12 columns missing in the captured images. To display the image without overscan, the (x, y) coordinates (12, 3) of the alignment point are specified for the data surface.

B.2 NoteBook

Calculated Block X can be used not only to change the data rate as described by NoteBook's reference manual, but also to align the data flows. In the SUN M-WIP system, when the 4-digit numbers are split to two 2-digit numbers, a X identical function block is added between block 2 and the digital output block to ensure that the two data flow between "split point" and "output point" to have the same number of calculated blocks.

B.3 ITEX-IC

Some of the global constants needed for function calls are not declared in the VB files provided by the vendor. User has to figure it out from head-files for C.

Table B.1 PC-Hydra Memory Resource

Start Address	Capacity (Word)	Descriptions
0x002FF800	0x400 (1 K)	RAM block 0 [73]
0x002FC000	0x400 (1 K)	RAM block 1 [73]
0x00300000	0x40000 (256 K)	SRAM on Local Bus [74]
0x80000000	0x40000 (256 K)	SRAM on Global Bus [74]
0xC0000000	0x2000 (8 K)	Host Interface Dual-Port RAM [75]
0xC8000000	0x20000 (128 K)	Flash EEPROM [75]

B.4   Master Link

In Master Link PCI-203698S-1 V2.40, the VB example project AO_BW has a bug. User has to change SEGMENTIO to ADDRESSIO in the SlotAssignIO() function call.

To make all the example projects work, user has to modify the programs according to the "Quick Tip for Master Link Software Library BASIC sample programs" which can be obtained from the vendor. Basically it tells a user to remove codes related to other boards which is not used. User also has to copy the file PCIDATAW.BAS from the *source* directory to the *sample* directory.

If a program calls TCLinearize() or TCMeasure(), thermocouple files type*.tc must be copied from home directory into the working directory of the project.

B.5   Standard Host Interface

User accessible memory resource for each DSP of the PC-Hydra is described in Table B.1.

In addition to the memory resources listed in Table B.1, there are also memory locations for flag register, semaphore register, global status register, etc.

B.6   Parallel C

The DSP numbering scheme that Parallel C uses is arbitrary and dependent only on the order in which it finds the DSPs.

Parallel C derives its DSP numbering results purely from the connections between DSPs. It finds out what DSPs are in the system by first probing the host link to find the root DSP. From there it then probes all other links, finds out which DSPs are connected to which, and numbers the DSPs in the order it reaches them. Therefore, the number of a DSP used in the configuration file is not necessary identical to its physical site number. c40worm, an utility program, can be used to explore a DSP network and to report back its topology information.

The physical path that Parallel C takes to realize a communication link between two DSPs is determined automatically and is transparent to the application programmer. If the network is simply connected with no loops, such as pipeline or spanning tree, then the shortest path will be used. Otherwise, the shortest path will be used unless this will cause deadlock. Parallel C's routing program tries to produce the best load balancing of traffic over the links, but will sacrifice this to avoid deadlock.

REFERENCES

1. H. Kaplan, "Commercial Applications for Thermal Imaging Instruments, An Update," *SPIE Proceedings*, Vol. 2269, 1994.

2. W. L. Wolfe, "Radiation Theory," *Sources of Radiation, G. J. Zissis, ed., The Infrared and Electro-Optical Systems Handbook, Vol. 1, J. S. Accetta, and D. L. Shumaker, eds.*, SPIE Optical Engineering Press, Bellingham, WA, 1993.

3. T. L. Williams, "Industrial and Civil Applications of Thermography," *Applications of Thermal Imaging, S. G. Burnay, T. L. Williams, and C. H. Johns, eds.*, Adam Hilger, Philadelphia, PA, 1988.

4. P. W. Kruse, "Uncooled IR Focal Plane Arrays," *SPIE Proceedings*, Vol. 2552, 1993.

5. S. Hejazi, D. C. Wobschall, R. A. Spangler, and M. Anbar, "Scope and Limitations of Thermal Imaging Using Multiwavelength Infrared Detection," *Optical Engineering*, Vol. 31, No. 11, 1992.

6. K. Watson, "Spectral Ratio Method for Measuring Emissivity," *Remote Sensing of Environment*, Vol. 42, No. 2, 1992.

7. M. A. Khan, C. Allemand, and T. W. Eagar, "Noncontact Temperature Measurement I," *Review of Scientific Instrument*, Vol. 62, No. 2, 1991.

8. S. Jaggi, D. Quattrochi, and B. Baskin, "An Algorithm for the Estimation of upper and lower bounds of the Emissivity and Temperature of a Target from Thermal Multispectral Airborne Remotely Sensed Data," *SPIE Proceedings*, Vol. 1699, 1992.

9. M. A. Khan, C. Allemand, and T. W. Eagar, "Noncontact Temperature Measurement II," *Review of Scientific Instrument*, Vol. 62, No. 2, 1991.

10. G. B. Hunter, C. D. Allemand, and T. W. Eagar, "Multiwavelength Pyrometry: An Improved Method," *Optical Engineering*, Vol. 24, No. 6, 1985.

11. R. M. Spitzberg, "Parameter Estimation for Gray and Nongray Targets: Theory and Data Analysis," *Optical Engineering*, Vol. 33, No. 7, 1994.

12. P. R. Bevington, *Data Reduction and Error Analysis for the Physical Science*, McGraw-Hill, New York, NY, 1969.

13. R. M. Spitzberg, "Parameter Estimation for Gray and Nongray Targets: Theory and Data Analysis," *Optical Engineering*, Vol. 33, No. 7, 1994.

14. N. J. McCaffrey, M. Kaplinsky, B. Esposito, and W. F. Kosonocky, "Radiometric Performance of 640X480 and 320X244 *PtSi* IR Camera," *SPIE Proceedings*, Vol. 2225, 1994.

15. T. S. Villani, W. F. Kosonocky, F. V. Shallcross, J. V. Groppe, G. M. Merey, J. J. O'Neill III, and B. J. Esposito, "Construction and Performance of a 320X244-Element IR-CCD Imager with PtSi Schottky-Barrier Detectors," *SPIE Proceedings*, Vol. 1107, 1988.

16. W. F. Kosonocky, "Review of Infrared Image Sensors with Schottky Barrier Detectors," *Optoelectronic – Devices and Technologies*, Vol. 6, No. 2, 1991.

17. E. H. Rhoderick, *Metal-Semiconductor Contacts*, Clarendon Press, Oxford, UK, 1978.

18. N. J. McCaffrey, "Design of a 320X122 MWIR-CCD *PtSi:Si* Imaging Radiometer with Automatic Optical Integration Time Control," *Master Thesis*, Department of Electrical and Computer Engineering. New Jersey Institute of Technology, Newark, NJ, 1993.

19. M. Kaplinsky, W. F. Kosonocky, N. J. McCaffrey, J. Li, E. S. Hou, C. N. Manikopoulos, N. M. Ravindra, "Multi-Wavelength Imaging Pyrometer for Non-Contact Temperature Sensing," *Proceedings of the IEEE International Symposium on Industrial Electronics*, 1995.

20. R. A. Wood, "Uncooled Thermal Imaging with Monolithic Silicon Focal Plans," *SPIE Proceedings* Vol. 2020, 1994.

21. P. E. Howard, C. J. Han, J. Stevens, E. J. Clarke, E. C. Whitcomb, T. A. Hartwick, E. T. Fitzgibbons, "GENII 320X240 TV Compatible VOx Microbolometer UFPA," 1996.

22. S. Horn, and R. Buser, "Uncooled Sensor Technology," *SPIE Proceedings*, Vol. 2020, 1994.

23. M. A. Gallo, D. S. Willits, R. A. Lubke, E. C. Thiede, "Low Cost Uncooled IR Sensors for Battlefield Surveillance," *SPIE Proceedings*, Vol. 2020, 1994.

24. R. J. Herring, P. E. Howard, "Design and Performance of the ULTRA 320X240 uncooled focal plane array and sensor," *SPIE Proceedings*, Vol. 2746, 1996.

25. *Datacube Image Processing Manual*, Datacube, Inc., 1993.

26. D. L. Perry, and E. L. Dereniak, "Linear Theory of Nonuniformity Correction in Infrared Staring Sensors," *Optical Engineering*, Vol. 32, No. 8, 1993.

27. V. Dhar, and R. Ashokan, "Computer Simulation of Fixed-Pattern-Noise-Limited Noise-Equivalent-Temperature Differences in Mercury Cadmium Telluride Focal-Plane Arrays," *Optical Engineering,* Vol. 34, No. 5, 1995.

28. J. M. Mooney, F. D. Shepherd, W. S. Ewing, J. E. Murguia, and J. Silverman, "Responsivity Nonuniformity Limited Performance of Infrared Staring Cameras," *Optical Engineering,* Vol. 28, No. 11, 1989.

29. J. E. Murguia, and W. S. Ewing, "Statistical Characterization of a Large PtSi Focal Plane Array," *SPIE Proceedings,* Vol. 782, 1987.

30. J. E. Murguia, J. M. Mooney, and W. S. Ewing, "Evaluation of a PtSi Infrared Camera," *Optical Engineering,* Vol. 29, No. 7, 1990.

31. R. J. Hanisch, "Image Processing, Data Analysis Software, and Computer Systems for CCD Data Reduction and Analysis," *Astronomical CCD Observing and Reduction Techniques,* ASP Conference Series, Vol. 23, 1992.

32. W. S. Ewing, "Silicide Mosaic Array Compensation," *SPIE Proceedings,* Vol. 409, 1983.

33. H. C. Andrews, A. G. Tescher, and R. P. Kruger, "Image Processing by Digital Computer," *IEEE Spectrum,* Vol. 9, No. 7, 1972.

34. R. C. Gonzalez, and R. E. Woods, "Chapter 4: Image Enhancement," *Digital Image Processing,* Addison-Wesley, Reading, MA, 1983.

35. D. F. Rogers, and J. A. Adams, "Chapter 5: Space Curves," *Mathematical Elements for Computer Graphics,* McGraw-Hill, New York, NY, 1992.

36. X. Li, "Parallel DSP Algorithms on TurboNet," *Ph.D Dissertation,* Department of Electrical and Computer Engineering, New Jersey Institute of Technology, Newark, NJ, 1995.

37. K. Hwang, *Advanced Computer Architecture with Parallel Programming,* McGraw-Hill, New York, NY, 1993.

38. T. G. Lewis, and H. El-Rewini, *Introduction to Parallel Computing,* Prentice Hall, Englewood Cliffs, NJ, 1992.

39. V. Quercia, and T. O'Reilly, *X Window System User's Guide,* 4th Ed., O'Reilly & Associates, Sebastopol, CA, 1993.

40. A. Nye, *Xlib Programming Manual,* 3rd Ed., O'Reilly & Associates, Sebastopol, CA, 1992.

41. *LABTECH NOTEBOOK Reference Manual*, Laboratory Technologies, Co., 1992.

42. *ImageFlow System Manual*, Datacube, Inc., 1993.

43. *Writing Device Drivers*, Sun Microsystems, Inc., 1988.

44. *User's Manual for the V-C40 Hydra*, Ariel, Co., 1994.

45. R. W. Sebesta, *Concepts of Programming Languages*, Addison-Wesley, Reading, MA, 1996.

46. E. Hou, J. Li, and W. F. Kosonocky, "A Real-Time Implementation of Two Point Non-Uniformity Correction for IR-CCD Camera," *SPIE Proceedings*, Vol. 2598, 1995.

47. J. Li, and E. Hou, "Pseudocoloring Schemes for Thermal Imaging," *SPIE Proceedings*, Vol. 1656, 1995.

48. J. Silver, J. M. Mooney, and V. E. Vickers, "Display of Wide Dynamic Range Infrared Images from PtSi Schottky Barrier Camera," *Optical Engineering*, Vol. 29, No. 2, 1990.

49. S. Belikov, M. Kaplinsky, and B. Friedland, "Parameter Estimation in a Dynamic Model of Rapid Thermal Processing: Theory and Experimental Results," *Proceedings of 1995 American Control Conference*, 1995.

50. W. F. Kosonocky, M. Kaplinsky, N. J. McCaffrey, E. S. Hou, C. N. Manikopoulos, N. M. Ravindra, S. Belikov, J. Li, and P. Vapel, "Multi-Wavelength Imaging Pyrometer," *SPIE Proceedings*, Vol. 2225, 1994.

51. M. B. Kaplinsky, J. Li, N. J. McCaffrey, E. S. H. Hou, and W. F. Kosonocky, "Progress on the Development of Multi-Wavelength Imaging Pyrometer," *SPIE Proceedings*, Vol. 2746, 1996.

52. J. R. Hobbs, "Ways to Meet Your Image-Processing Needs," *Laser Focus World*, February, 1995.

53. *Modular Vision Computer Product Line Guide*, Imaging Technology, Inc., 1995

54. *PCI-20428W Series Multifunction Boards and Master Link Software Libraries Manual*, Intelligent Instrumentation, Inc., 1994

55. *User's Manual for the PC-Hydra*, Ariel, Co., 1995

56. *P315X User Guide*, American Precision Industries, Inc.

57. R. A. Wood, T. M. Rezachek, P. W. Kruse, and R. N. Schmidt, "IR SnapShot Camera," *SPIE Proceedings*, Vol. 2552, 1995.

58. R. E. Higashi, and R. G. Johnson, "Micromechanical Thermoelectric Sensor Element," U.S. Patent 5,220,189, June 15, 1993.

59. P. W. Kruse, "Uncooled IR Focal Plane Arrays," *SPIE Proceedings*, Vol. 2552, 1995.

60. M. Welsh, *Linux Installation and Getting Started.*

61. I. Jackson, *Frequently Asked Questions about Linux*, Version 2.6.

62. L. Copeland, "Performance Considerations for High-End PC A/D Boards," *EE-Evaluation Engineering*, February, 1995.

63. P. Feldman, R. Jennings, B. Seymour, B. Eidson, P. Palmer, S. Gillmor, and J. Pesso, *Using Visual Basic 3.0*, Que, Indianapolis, IN, 1993.

64. D. J. Kruglinski, *Inside Visual C++*, 2nd Ed., Microsoft Press, Redmond, WA, 1994.

65. *Parallel C User Guide*, 3L, Ltd., 1995.

66. *Windows Server User Guide*, 3L, Ltd., 1996.

67. C. A. Hoare, *Communicating Sequential Processes*, Prentice Hall, Englewood Cliffs, NJ, 1985.

68. H. S. Stone, "Chapter 5: Serial Interfacing," *Microcomputer Interfacing*, Addison-Wesley, Reading, MA, 1983.

69. *PDQComm for Windows Owner's Manual*, Crescent Software, Inc., 1995.

70. *ICL User Guide*, American Precision Industries, Inc.

71. D.-S. Kim, S. R. Forrest, M. J. Lange, G. H. Olsen, and M. J. Cohen, "A Three Wavelength Infrared Focal Plane Array Detector Element," *IEEE International Photonics Technology Letters*, Vol. 6, No. 2, 1994.

72. D.-S. Kim, S. R. Forrest, M. J. Lange, G. H. Olsen, and W. F. Kosonocky, "A Monolithically Integrated InGaAs-InP p-i-n/JFET Focal Plane Array," *IEEE International Photonics Technology Letters*, Vol. 8, No. 4, 1996.

73. *TMS320C4x User's Guide*, Texas Instruments, Inc., 1993.

74. *Hardware Reference Manual for the TIM40-SG*, Ariel, Co., 1995.

75. *PC-Hydra Series Software Reference Manual*, Ariel, Co., 1995.